DISSERTATION

THE USE OF MODEL MEMBRANE TECHNIQUES FOR THE ANALYSIS OF INTERACTIONS, CONFORMATION AND REDOX PROPERTIES OF MENAQUINONES AND OTHER SMALL MOLECULES

Submitted by

Kaitlin A. Doucette

Graduate Degree Program in Cell and Molecular Biology

In partial fulfillment of the requirements

For the Degree of Doctor of Philosophy

Colorado State University

Fort Collins, Colorado

Spring 2021

Doctoral Committee:

Advisor: Debbie Crans

Dean Crick
Deborah Roess
Carmen Menoni

ABSTRACT

THE USE OF MODEL MEMBRANE TECHNIQUES FOR THE ANALYSIS OF INTERACTIONS, CONFORMATION AND REDOX PROPERTIES OF MENAQUINONES AND OTHER SMALL MOLECULES

This thesis explores the use of model membranes to solve complex problems in determining the placement, conformation, and electrochemical properties of hydrophobic compounds as they interact with a model membrane. Menaquinone, an electron transporter commonly found in Gram-positive and Gram-negative obligate anaerobes, consists of a naphthoquinone head group and isoprene tail of variable length and saturation. Chapter two shows the use of liposomal model membranes to solubilize menaquinone analogues of variable length and saturation for aqueous electrochemical studies characterizing half-wave potentials, reversibility, and diffusion coefficients to examine its redox properties in connection to its role as an electron transporter. This work shows a distinct odd-even effect with respect to the isoprene chain length of the compound and its electrochemical properties. In chapter 3, the conformation and placement of menaquinone-2 is determined in the context of a phosphatidylcholine liposome using 1D and 2D ^{1}H NMR. Finally, chapter four explores the use of a reverse micellar model membrane for determining the placement of glycine and short glycine peptides to explore its placement near a membrane. The experiments contained herein show that model membranes are a useful tool for the study of hydrophobic compounds and molecules commonly found within a cellular membrane.

ACKNOWLEDGEMENTS

I would like to acknowledge friends in the lab for pointing me in the right direction on projects, the undergraduate and graduate students I have mentored who have helped extensively in my data collection, my advisor Dr. Crans for invaluable advice as well as Dr. Crick, and my committee for taking the time to work with me on this project.

DEDICATION

For Tippy.

TABLE OF CONTENTS

Chapter 1: Model Membranes and Their Utility for Studying Hydrophobic Compounds and Membrane Interactions

1.1 Composition of the Cellular Membrane and Model Membranes That Can Be Used to Study It

1.1.1. Composition of the Cellular Membrane and Factors Lending to its Complexity

The cellular membrane is a complex barrier that surrounds the cytoplasm of all cells. It is crucial for the life of the cell due to its main role in maintaining cell boundaries and the essential differences between intracellular and extracellular environments.[1-2] The base, fundamental foundation of a cellular membrane for most living organisms is the lipid bilayer, which consists of lipids arranged such that the polar heads point outwards toward the outside of the cell in the outer leaflet, and towards the cytoplasm on the inner leaflet.[3] With the hydrophobic tails pointing inwards towards each other, the lipid bilayer provides cells a semipermeable barrier from their surroundings consisting of two charged polar regions and a hydrophobic region.[4] There are numerous lipids that are present in the cellular membrane; different species, even different cells within the same species and organelles within the same cell, will consist of a different lipid profile based on their biological function as lipids participate in a broad range of cellular processes.[5-7] One of the most notable examples of this is in the human nervous system, which has a rich lipid composition with both high lipid content and diversity in the human brain. Lipids found predominantly in the brain are sphingolipids, glycerophospholipids and cholesterol, and interestingly, they are considered to be present roughly in equal ratios and their functions include acting as signaling molecules, impulse conduction, as well contributing to neurogenesis.[8-9] Sphingolipids are especially abundant in the brain as they play a role in the myelination process, which is closely associated with cognitive maturation.[10] By contrast, the

lipid composition of human lungs is roughly 80% phospholipids, with phosphatidylcholine being the major lung surfactant constituent in the alveolar region of the lungs as it reduces the surface tension at the air-liquid interface of alveolar spaces.[11] Bacterial membrane lipids also display diversity and complexity in their composition, with many bacterial membranes composed of lipids such as phosphatidylinositol, phosphatidylethanolamine, and phosphatidylserine, and many bacteria even have a cell wall, which further increases the complexity of the membrane enveloping the cytoplasm.[12-13]

In addition to complexities in the types of lipids which are present in the cell membrane depending on what type of cell is being studied, there are a number of other components in the plasma membrane that further lend to the overall complexity of the cellular membrane components. Besides lipids, proteins also play a significant role in the cellular membrane, with membrane proteins comprising about a third of the proteins in living organisms.[14-15] Some of the most notable examples of protein types associated with the membrane are integral membrane proteins, such as G protein-coupled receptors, which are central to transmitting signals from the extracellular matrix to the cellular interior, peripheral membrane proteins, which interact with the surface of the bilayer rather than in the hydrophobic space within the cell membrane.[15-16] Examples of peripheral membrane proteins are the all-important proteins that are involved in electron transport chains such as cytochrome c, cupredoxins, flavoproteins, and others.[17] Besides the presence of varying proteins and lipids, depending on the biological function of the cell in question, plasma membranes also contain cholesterol, which can affect the rigidity or fluidity of the bilayer, as well as carbohydrates.[18-20]

The many components of the cellular membrane, which includes lipids, proteins, carbohydrates, and in the case of eukaryotic membranes, the lipid cholesterol, do not remain

static with regards to their position on the cell membrane. Rather, according to the fluid mosaic model of a cell membrane, the molecules which comprise the cell membrane are able to laterally diffuse across the surface of the bilayer.[21-22] This means that the components that comprise the cell membrane being studied may be able to laterally diffuse near to one another, which could potentially affect the function of the study of membrane components within an endogenous cell membrane.

As a result of all the different complexities present within the cell membrane: differing lipid composition, protein composition and the types of proteins present, as well as the presence of carbohydrates and the fluid manner in which all of these components move, the cellular membrane and its constituent components can prove difficult to study. Increasing this difficulty, compounds and membrane components found within the plasma membrane, despite being in a largely aqueous environment as required for life, can be quite hydrophobic and therefore immensely difficult to study. For example, the study of integral membrane proteins and indeed, even peripheral membrane proteins or membrane-associated proteins, are difficult to study in standard aqueous enzyme activity assays due both to their hydrophobicity as well as potential dependence on the membrane to provide favorable electrostatic interactions with the protein, making it possible for it to perform its function.[23-24] In addition to proteins, many membrane components themselves are quite hydrophobic, including of course the lipids of which the membrane is composed as well as cholesterol, electron transporters and other important biological molecules.

1.1.2. Model Membranes Commonly Used to Facilitate the Study of Cellular Membranes and Membrane Components

Because of the difficulty in studying molecules in a wild-type plasma membrane, it

becomes prudent to mimic a cell membrane rather than try to study it in its entirety, or to try to study one of its components with a variety of other variables present, making any real observation impossible. In order to simplify the components of a plasma membrane such that experiments can be performed on any of its constituents or processes, model membranes are used. Model membranes are a useful tool for studying cellular membranes by allowing researchers to probe the behavior of proteins and lipids in a membrane by isolating different aspects of membrane function to study them in detail and gain insight about their function and the larger impact they may have on the cell.[25]

There are a number of different model membrane systems which are used for studying membrane components and processes, the three main model membranes are lipid monolayers, micelles, and lipid vesicles. Briefly, lipid monolayers consist of half a bilayer, formed by spreading amphipathic molecules on an aqueous surface which may contain only water or buffer, and may also contain a molecule of interest added either in the hydrophobic phase with the lipids that are spread over the aqueous subphase or within the aqueous subphase itself.[26-27] They provide a way to examine lipid-lipid interactions and even protein-lipid interactions by changing parameters such as the composition of the subphase and temperature, and can be used to obtain information about the nature of lipid mixtures by measuring the surface pressure of the interfacial film as a function of the mean molecular area (Figure 1.1).[27]

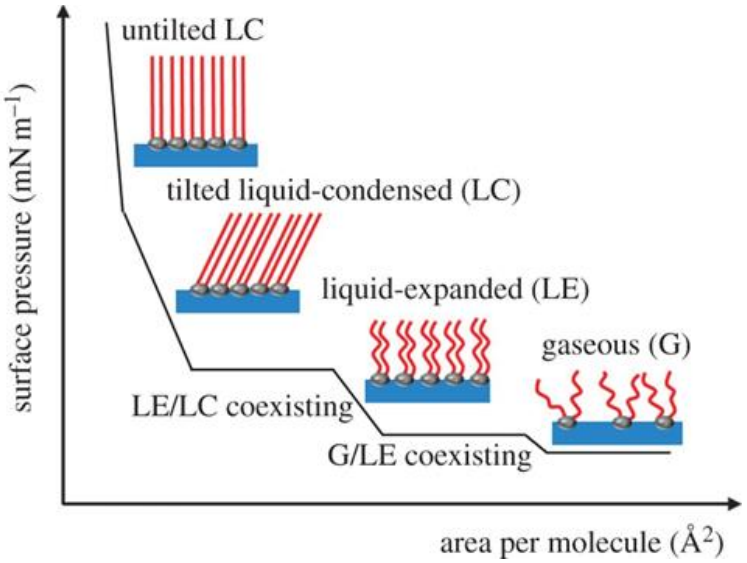

Figure 1.1. Simplified illustration of a lipid monolayer used for a surface pressure-area isotherm for low molecular weight surfactants and possible phase states, including gaseous (G), liquid expanded (LE), and tilted and untilted liquid condensed (LC). This figure was published by Schöne et al.[28]

While lipid monolayers are a good way of studying the effects of low molecular weight compounds on lipid interactions and behavior and work has been performed with monolayers in the Crans lab previously, the main model membrane systems which will be focused on are liposomes and reverse micelles.[29-30]

Reverse micelles consist of nanometer sized water droplets dispersed in organic solvent with surfactant molecules organized with the polar heads pointed inward toward the water droplet, and the hydrophobic tails pointed outward towards the organic solvent.[31-32] While the structure of reverse micelles is not as analogous to the structure of a membrane bilayer as, for example, a liposome, which will be discussed later, it is still able to give information about the interactions of compounds with spherical lipid mimetic monolayer.[31] The components used to create reverse micelles in this thesis consist of 2,2,4-trimethylpentane, or isooctane, as the organic solvent that the reverse micelles are dispersed in, and the surfactant used to form the vesicles is dioctyl sodium sulfosuccinate, or aerosol-OT (Figure 1.2).

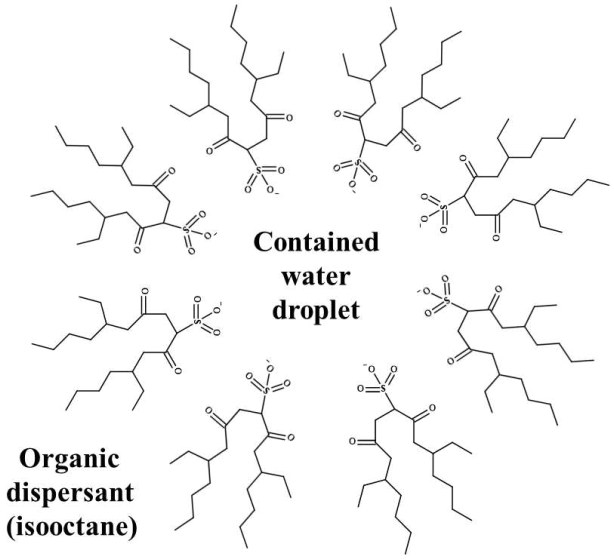

Figure 1.2. Structure of the reverse micelle used for experiments contained in this thesis. The surfactant used to form the vesicle is aerosol-OT, shown with the polar sulfonate head groups pointed towards the contained water droplet, and the hydrophobic tails pointing outwards towards the organic dispersant, in this case, isooctane.

By probing the location of molecules confined in reverse micelles, we can roughly determine placement of probe molecules relative to the structure of the vesicle through spectroscopic techniques such as nuclear magnetic resonance (NMR). It is also possible to determine how this placement or interaction with the lipid-like AOT changes with changing conditions of the water pool, such as pH, ionic strength and probe concentration.[30, 33]

While reverse micelles are a useful tool for probing membrane interactions or behavior of low-molecular weight molecules in a membrane-like setting, their biological relevance is decreased by the surfactant used as well as the environment they are formed in. While the surfactant AOT is able to mimic the overall behavior of an amphipathic molecule such as the lipids which typically comprise a cell membrane, the overall structure of AOT is not very analogous to naturally occurring lipids such as phospholipids, triacylglycerols and even sterols (Figure 1.2). In addition to the similarity of AOT to other lipids, or lack thereof, the presence of

a bulk pool of isooctane surrounding the vesicle can complicate comparison to a biological system. For this reason, the other model membrane that will be focused on for the purposes of this thesis is the liposomal model membrane.

A liposome is a spherical vesicle formed by one or more phospholipid bilayers (unilamellar or multilamellar), and this spherical vesicle is the model membrane of those studied here that has the best resemblance to the structure of a cell membrane.[34] Its structure consists of an amphipathic lipid molecule such as a phospholipid, and the lipids are arranged such that the polar heads are oriented towards the outside of the vesicle on the outer leaflet and pointed inwards towards the contained water droplet in the center of the vesicle on the inner leaflet of the bilayer.[35] Rather than the presence of organic solvent such as isooctane in the reverse micelle, liposomes are contained only in aqueous solution, making them a better approximation of a cellular membrane than a reverse micelle.

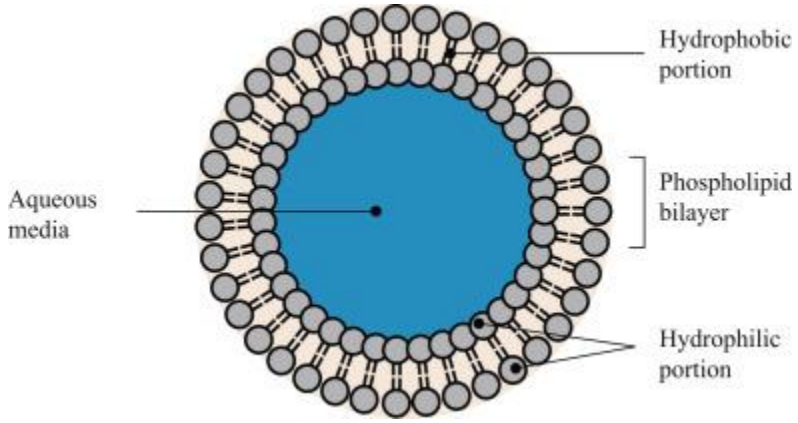

Figure 1.3. Figure of a liposomal model membrane. Phospholipids comprising the bilayer arrange themselves pointing outward toward the outer leaflet of the vesicle and the bulk water pool, and inward toward the contained water droplet, with the hydrophobic tails pointing toward each other. Figure originally published by Deb et al. [36]

Liposomes are useful for a variety of purposes. Current uses of liposomes include targeted drug delivery in which vesicles containing drug are targeted to certain cell types through

the use of cell-surface receptors, and due to their structure and components, liposomes are capable of delivering both hydrophobic and hydrophilic drugs due to the presence of both polar and nonpolar regions of the vesicle (Figure 1.3).[37-38] They also facilitate the study of hydrophobic molecules found in a cell membrane.[39-40] Many molecules such as the lipoquinone electron carrier molecules ubiquinone, menaquinone and plastoquinone and membrane proteins are inherently hydrophobic and as such, difficult to study in an aqueous environment. Liposomes allow the study of such compounds in an environment more analogous to the one in which they would be found while still providing a simplified environment for their study.

1.2. Menaquinones: Electron carriers for *Mycobacterium tuberculosis*

Many of the studies presented here in this thesis are concerning the bacterial lipoquinone, menaquinone. Lipoquinone electron carriers aid the species which use them by shuttling electrons to and from membrane-bound protein complexes in the plasma membrane, which is coupled to the generation of a proton gradient which helps to drive the synthesis of ATP for the organism.[41-42] The most well-known examples of lipoquinones are ubiquinone, which is largely present in eukaryotic cells and consists of a benzoquinone head group covalently bound to an isoprenyl side chain, and menaquinone (MK), which is present in Gram-positive bacteria as well as Gram-negative obligate anaerobes and consists of a naphthoquinone head group covalently bound to an isoprenyl side chain (Figure 1.5).[43-44]

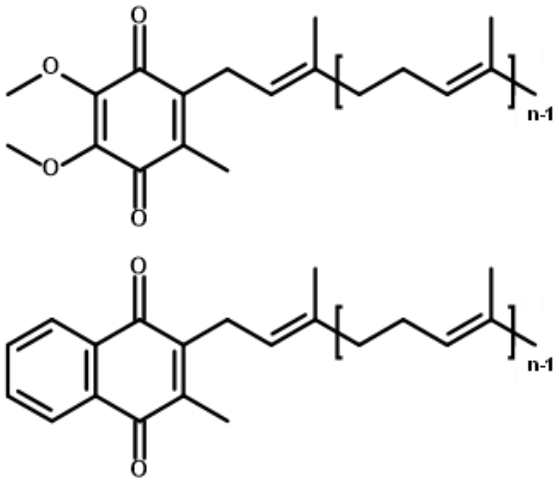

Figure 1.4. Structures of ubiquinone (top) and menaquinone (bottom).

In order to perform its duties as an electron carrier that generates a proton gradient for ATP synthesis, MK is reduced by hydrogenases, dehydrogenases and oxidoreductases in the electron transport system to form menaquinol. It is then re-oxidized by terminal oxidases or terminal reductases, depending upon whether aerobic or anaerobic respiration is taking place. This then generates a proton gradient and proton motive force that helps to drive the synthesis of ATP through the shuttling of electrons to and from membrane-bound protein complexes in the electron transport system.[45]

One of the most notable species which uses MK in their electron transport chain is *Mycobacterium tuberculosis* (Mtb), the pathogen responsible for the disease tuberculosis and for the deaths of 1.4 million people in the year 2019 alone.[46] The cell wall and cell membrane of Mtb is complex. The cell wall consists mainly of a long fatty acid called mycolic acid, , and the inner cell membrane of Mtb, where the electron transport system of Mtb is located and where MK functions to shuttle electrons to and from membrane-bound protein complexes, consists of lipids such as acyl phosphatidylmannosides, phosphatidylinositol, cardiolipin, and

phosphatidylethanolamine.[47] Interestingly, in those species which use MK as their sole electron transporter, different MK analogues are produced by the cell for the purposes of electron transport. For example, Mtb predominantly produces MK-9(II-H_2), or MK with nine isoprene units covalently bound to the naphthoquinone head group, and a saturation at the β-isoprene unit.[45] Other pathogenic bacterial species which use MK in their electron transport system include *Corynebacterium diptheriae*, the causative agent of diptheria, which produces MK-8(II-H_2), and *Listeria monocytogenes,* the causative agent of listeria, which produces MK-7.[48-51] It is unclear what advantages exist for these bacterial species in producing different analogues of MK, but recent studies have shown that its composition and concentration may affect the membrane fluidity of *Listeria monocytogenes* at low temperatures.[51] It is also possible that there are advantages in producing different MK analogues that are related to their ability to undergo oxidation and reduction, and thus aid in ATP synthesis for the cell, and the conformation and location that MKs adopt in the bacterial membrane may also have implications for its ability to undergo oxidation and reduction and participate in the electron transport system. Despite the composition of the Mtb membrane consisting mostly of phosphatidylinositol, phosphatidyl mannosides and cardiolipin as stated earlier, studies done in this thesis will be done with liposomes containing phosphatidylcholine, a common eukaryotic lipid. This is done so that work already performed with ubiquinone, a eukaryotic lipoquinone electron carrier, may be compared to the work obtained here with the menaquinone analogues contained in this thesis.[52-54]

1.3. Methods Used for Probing Molecules of Interest Within Model Membranes

1.3.1. NMR Spectroscopic Techniques for Probing Location and Conformation of Molecules of Interest Within Model Membranes

There are many methods that can be used to study probe molecules within model

membranes, so for the purposes of this thesis only those that were used in subsequent experiments will be discussed.

One of the most powerful tools for probing the location of a molecule of interest within a reverse micelle or a liposome is through nuclear magnetic resonance (NMR). The purpose of an NMR experiment is to place a solution of molecules into a strong magnetic field. Upon exposure to the magnetic field, the nuclei of the atoms will begin to behave like small magnets themselves, and if a broad spectrum of radio frequency waves are applied to the sample then the nuclei will resonate at their own specific frequencies based on the identity of the atom in question as well as the environment (shielded or deshielded) that it is in.[55] The more shielded a molecule is, or the more surrounded by electron density, the more the chemical shift of the nucleus in question will decrease due to the presence of electron density, occluding the signal and shifting it upfield, or towards lower chemical shift values. In contrast, a molecule that is more deshielded will display an increased chemical shift due to the removal of electron density, exposing the nuclei and shifting the peak downfield, or towards higher chemical shift values.[56] This information alone can be useful in determination of the placement of a probe molecule in the context of a reverse micelle or liposomal environment. For example, an NMR spectrum of a compound alone in D_2O compared to a spectrum of the same compound in a reverse micelle or liposome can provide information about how the environment surrounding the compound has changed.[57-58] If the compound peaks have shifted upfield this indicates that they are in a less charged, or more shielded, environment, and if the compound peaks have shifted downfield then it is likely that the compound is in a more charged, or more deshielded environment.[58-59]

In addition to being able to provide information about the environment surrounding a probe molecule, it is also possible to determine how a molecule's pKa changes in the context of a

membrane through pH titrations and confinement within a reverse micelle or liposome through ^{1}H NMR.[57, 60] 2D NMR analysis allows us to take determination of probe molecule environment and location one step further; by examining cross peaks produced by ^{1}H-^{1}H 2D NOESY NMR it is possible to elucidate which compound nuclei are interacting with lipid nuclei, as well as allowing the determination of hydrophobic molecules confined to the bilayer, such as the hydrophobic electron carrier, menaquinone.[42, 61] 2D 1H-1H NOESY NMR (Nuclear Overhauser Effect Spectroscopy) is a 2D NMR spectroscopic method that can be used to identify signals that arise from protons which are close to each other in space, even if they are not bonded, giving through space interactions between protons of interest within the molecule or system of interest. This method can be very useful for determining a molecule's overall 3D conformation since it gives information about which protons are near each other in space. Similar to 2D NOESY, 2D 1H-1H ROESY (Rotating Frame Overhauser Enhancement Spectroscopy) can be used for a similar purpose, giving through space interactions between protons of interest. The two techniques are similar, except that in NOESY the cross-relaxation rate constant goes from positive to negative as the correlation time increases, whereas in ROESY the cross-relaxation rate constant is always positive. Typically when choosing whether NOESY or ROESY experiments should be performed, small molecules (MW<600) should be examined via 2D NOESY, and for medium sized molecules (700<MW<1200) then 2D ROESY spectroscopy is preferred. For large molecules (MW>1200), the choice becomes more complicated, with ROESY offering advantages like less spin diffusion, however, for very large molecules ROESY tends to be less sensitive, so for the purposes of the experiments contained in this thesis (Chapter 3) the focus is on 2D NOESY.[62-64]

1.3.2. Using Cyclic Voltammetry to Determine Electrochemical Properties of Compounds Confined to a Bilayer

Another method of analysis which has proven useful in determining the physical properties of compounds within a liposomal model membrane system is cyclic voltammetry for the determination of the redox properties of the electron transporter, MK-2, as shown in the work presented here. MK is an electron transport molecule found in Gram-positive and Gram-negative obligate anaerobes, and as such the study of its redox ability is of great importance relative to its biological function.[44, 65] However, owing to its limited aqueous solubility, MK can be quite difficult to study in a more aqueous environment, and many studies with both ubiquinone and MK resort to using surfactants or solvents to solubilize the compounds for study, or simply carry out the study through modeling studies.[66-68] In order to investigate the redox properties of a molecule such as MK in an environment analogous to the one in which it is naturally found, they can be confined to a liposome bilayer and subjected to cyclic voltammetry measurements.

In order to collect cyclic voltammograms of MKs loaded into liposomes, a three-electrode system is used (Figure 1.4). This setup consists of a working electrode, a counter electrode, and a reference electrode to apply voltage to the system consisting of supporting electrolyte and liposomal MK and measuring the resulting current.[69]

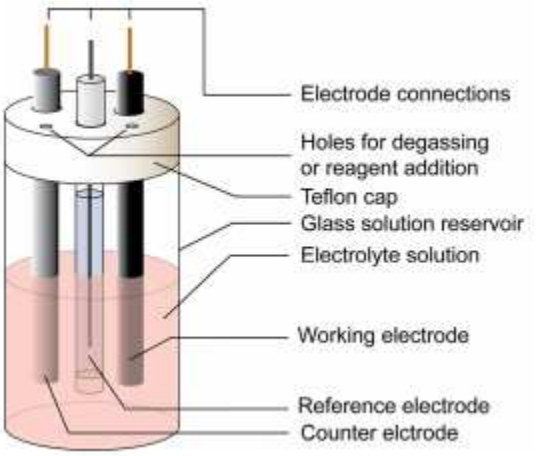

Figure 1.5. Three-electrode system used to collect cyclic voltammograms of MK solutions solubilized in liposomal formulations. Figure was published by Elgrishi et. al.[69]

In this experimental setup, the working electrode makes contact with the analyte and must apply controlled voltage to the system and facilitate the transfer of electrons to and from the analyte, in this case menaquinone. The counter electrode is responsible for passing current needed to balance the current which is observed at the working electrode. The reference electrode, then, is a half cell with known reduction potential, which does not at any point pass current and whose only role is to act as a reference in measuring and controlling the working electrode's potential.[69-70] In this way we are able to study the electrochemical properties of the menaquinone analyte in an aqueous solution analogous to a cell membrane in which it would be found.

1.3.3. Dynamic Light Scattering for Verification of Vesicle Formation and Analysis of Size Differences

Since the model membranes used in the experiments presented in this thesis are spherical vesicles, dynamic light scattering techniques are used both to verify the size of the vesicles to ensure that they were made correctly as well as determine any effects that inclusion of an analyte into the vesicle may have on the overall size. In order to determine the size profile of particles in suspension, such as liposomes or reverse micelles, a monochromatic light source is shot through

a polarizer and into a sample containing the particle suspension of interest.[71] When light hits the particles in solution, the light undergoes Rayleigh scattering and the light is diffracted through a second polarizer where it is collected by a photomultiplier. Because the particles are in a solution, the intensity of the light which is scattered by liposomes or reverse micelles fluctuates, and this fluctuation is dependent on the size of the particle in suspension.[72-73] For example, a smaller particle in solution will display much quicker intensity fluctuations of refracted light, where larger particles will fluctuate in intensity much more slowly. This tells us first and foremost, that our experimental procedure worked and the formation of vesicles was successful. It also gives us information about the interactions that the compound of interest may have with the vesicle: a shrinking of a vesicle (reverse micelle or liposome) treated with a probe molecule relative to a control liposome may indicate that the compound interacts with the head groups of lipids and exerts a condensing effect, potentially through favorable electrostatic interactions. By contrast, increase in the size of a vesicle may indicate that the compound inserts itself into the interface and have a spreading effect on the lipids which make up the vesicle.[74]

1.4. Studies Contained in the Subsequent Chapters

The studies contained in this thesis show the characterization of the membrane interactions (location, conformation) of menaquinone-2 as well as glycine in reverse micelles and liposomes through 1D and 2D ^{1}H NMR. The electrochemical properties of synthesized truncated menaquinone analogues are explored through encapsulation within a liposome and cyclic voltammetry.

The focus of Chapter 2, then, is on the electrochemical properties of truncated menaquinone analogues in soybean phosphatidylcholine liposomes. Previous work in the Crans lab has characterized the half wave potentials of truncated menaquinones in aprotic solvents

pyridine, DMSO and acetonitrile.[42] While these hydrophobic solvents are ideal for working with hydrophobic menaquinones and indeed, the hydrophobicity of the solvent may to some extent mimic the hydrophobicity found in the hydrocarbon tails of a membrane bilayer, these experiments have less biological relevance than studies done with menaquinones in a liposome. The liposomal environment provides both a hydrophobic domain in the hydrocarbon tails of the bilayer as well as dispersal in an aqueous solution, which is much more analogous to the environment in which it would carry out its duties as an electron transporter. While previous experimental work done in the Crans lab found that MK analogues with a reduction at the beta-isoprene unit of the isoprene side chain displayed half wave potentials ($E_{1/2}$) closer to zero (more easily oxidized and reduced), the work contained here comes to a different conclusion. Analysis via cyclic voltammetry found a distinct odd-even effect with respect to the isoprene side chain of the analogue of interest: while there were no statistical differences between $E_{1/2}$ values of the fully unsaturated menaquinone analogues, as the number of saturations increased in the tail the $E_{1/2}$ became more positive (more easily oxidized/reduced) in those analogues with odd-length isoprene chains and became more negative in analogues with even-length isoprene chains. A similar trend was seen with the reversibility data obtained: while there was little statistical significance between fully unsaturated menaquinone analogues, as the number of saturations in the even-length isoprene chains increased, the reversibility increased, and in odd-length isoprene chains, the reversibility decreased with increasing saturations in the isoprene side chain.

Chapter 3 delves into more detail about the interactions of menaquinone-2 (MK-2) with a phosphatidylcholine bilayer in terms of its location and conformation in the membrane, in the hopes of elucidating the underlying cause for the odd-even effect described in Chapter 2. In this chapter, ^{1}H NMR and ^{1}H-^{1}H 2D NOESY spectroscopy are used to examine the chemical shifts of

menaquinone-2 in a bilayer relative to those found in an aqueous environment and determine the placement as well as the conformation of MK-2 in a bilayer. This work finds that with increasing concentrations of MK-2 relative to phosphatidylcholine, the MK-2 is pushed out of the bilayer and resides at the surface of the liposome in contact with the bulk water pool. Both the liposome bound fraction and the fraction that is pushed into the water pool appear to adopt a U-shaped conformation, in which the tail of the molecule is oriented to the side of the naphthoquinone head group moiety.

Finally, Chapter 4 examines glycine and short glycine peptides diglycine, triglycine, and tetraglycine and their location and orientation within the reverse micelle. This work finds that with the exception of monomeric glycine, the short glycine peptides diglycine, triglycine, and tetraglycine prefer to associate themselves with the reverse micelle interface, with the positively charged N-terminus interacting with the negatively charged sulfonate heads of the AOT surfactant molecules. Monomeric glycine, on the other hand, appears to prefer to locate itself within the bulk water pool of the reverse micelle.

The summary, implications and direction that this research should take are presented in Chapter 5. This work presents approaches for studying the membrane interactions and characteristics of hydrophobic molecules in a model membrane setting.

References

1. Cai, M.; Gao, J.; Wang, H., Composition and Function of Cell Membranes. In *Membrane Biophysics*, Springer: 2018; pp 1-20.
2. Goñi, F. M., The basic structure and dynamics of cell membranes: An update of the Singer–Nicolson model. *Biochimica et Biophysica Acta (BBA)-Biomembranes* **2014,** *1838* (6), 1467-1476.
3. Wilkins, M.; Blaurock, A.; Engelman, D., Bilayer structure in membranes. *Nature New Biology* **1971,** *230* (11), 72-76.
4. Stein, W., *The movement of molecules across cell membranes*. Elsevier: 2012; Vol. 6.
5. Gutierrez, M. G.; Gonzalez, A. P.; Anes, E.; Griffiths, G., Role of lipids in killing mycobacteria by macrophages: evidence for NF-κB-dependent and-independent killing induced by different lipids. *Cellular microbiology* **2009,** *11* (3), 406-420.
6. Veerkamp, J.; Mulder, I.; Van Deenen, L., Comparison of the fatty acid composition of lipids from different animal tissues including some tumours. *Biochimica et biophysica acta* **1962,** *57* (1), 299-309.
7. Pichler, H.; Emmerstorfer-Augustin, A., Modification of membrane lipid compositions in single-celled organisms–From basics to applications. *Methods* **2018,** *147*, 50-65.
8. Schneider, N.; Hauser, J.; Oliveira, M.; Cazaubon, E.; Mottaz, S. C.; Neill, B. V.; Steiner, P.; Deoni, S. C., Sphingomyelin in brain and cognitive development: preliminary data. *ENeuro* **2019**.
9. Hussain, G.; Wang, J.; Rasul, A.; Anwar, H.; Imran, A.; Qasim, M.; Zafar, S.; Kamran, S. K. S.; Razzaq, A.; Aziz, N., Role of cholesterol and sphingolipids in brain development and neurological diseases. *Lipids in health and disease* **2019,** *18* (1), 1-12.
10. Giussani, P.; Prinetti, A.; Tringali, C., The role of Sphingolipids in myelination and myelin stability and their involvement in childhood and adult demyelinating disorders. *Journal of Neurochemistry* **2020**.
11. Berry, K. A. Z.; Murphy, R. C.; Kosmider, B.; Mason, R. J., Lipidomic characterization and localization of phospholipids in the human lung. *Journal of lipid research* **2017,** *58* (5), 926-933.
12. Sohlenkamp, C.; Geiger, O., Bacterial membrane lipids: diversity in structures and pathways. *FEMS microbiology reviews* **2016,** *40* (1), 133-159.
13. Strahl, H.; Errington, J., Bacterial membranes: structure, domains, and function. *Annual review of microbiology* **2017,** *71*, 519-538.
14. Krogh, A.; Larsson, B.; Von Heijne, G.; Sonnhammer, E. L., Predicting transmembrane protein topology with a hidden Markov model: application to complete genomes. *Journal of molecular biology* **2001,** *305* (3), 567-580.
15. Martin, J.; Sawyer, A., Elucidating the structure of membrane proteins. Future Science: 2019.
16. Rosenbaum, D. M.; Rasmussen, S. G.; Kobilka, B. K., The structure and function of G-protein-coupled receptors. *Nature* **2009,** *459* (7245), 356-363.
17. Sankaram, M. B.; Marsh, D., Protein-lipid interactions with peripheral membrane proteins. In *New Comprehensive Biochemistry*, Elsevier: 1993; Vol. 25, pp 127-162.

18. Presti, F. T., The role of cholesterol in regulating membrane fluidity. *Membrane fluidity in biology* **1985,** *4*, 97-145.
19. Kaddah, S.; Khreich, N.; Kaddah, F.; Charcosset, C.; Greige-Gerges, H., Cholesterol modulates the liposome membrane fluidity and permeability for a hydrophilic molecule. *Food and Chemical Toxicology* **2018,** *113*, 40-48.
20. Subczynski, W. K.; Pasenkiewicz-Gierula, M.; Widomska, J.; Mainali, L.; Raguz, M., High cholesterol/low cholesterol: effects in biological membranes: a review. *Cell biochemistry and biophysics* **2017,** *75* (3-4), 369-385.
21. Nicolson, G. L., The Fluid—Mosaic Model of Membrane Structure: Still relevant to understanding the structure, function and dynamics of biological membranes after more than 40 years. *Biochimica et Biophysica Acta (BBA)-Biomembranes* **2014,** *1838* (6), 1451-1466.
22. Singer, S. J.; Nicolson, G. L., The fluid mosaic model of the structure of cell membranes. *Science* **1972,** *175* (4023), 720-731.
23. Tiefenauer, L.; Demarche, S., Challenges in the development of functional assays of membrane proteins. *Materials* **2012,** *5* (11), 2205-2242.
24. Gross, D. A.; Silver, D. L., Purification of Integral Membrane Proteins and Lipid-Binding Assays. In *Methods in Cell Biology*, Elsevier: 2013; Vol. 116, pp 191-211.
25. Eeman, M.; Deleu, M., From biological membranes to biomimetic model membranes. *Biotechnologie, Agronomie, Société et Environnement* **2010,** *14* (4), 719-736.
26. Birdi, K., Lipid monolayers at liquid interfaces. In *Lipid and Biopolymer Monolayers at Liquid Interfaces*, Springer: 1989; pp 57-147.
27. Brockman, H., Lipid monolayers: why use half a membrane to characterize protein-membrane interactions? *Current opinion in structural biology* **1999,** *9* (4), 438-443.
28. Schöne, A.-C.; Roch, T.; Schulz, B.; Lendlein, A., Evaluating polymeric biomaterial–environment interfaces by Langmuir monolayer techniques. *Journal of the Royal Society Interface* **2017,** *14* (130), 20161028.
29. Peters, B. J.; Groninger, A. S.; Fontes, F. L.; Crick, D. C.; Crans, D. C., Differences in Interactions of Benzoic Acid and Benzoate with Interfaces. *Langmuir* **2016,** *32* (37), 9451-9459.
30. Peters, B. J.; Van Cleave, C.; Haase, A. A.; Hough, J. P. B.; Giffen-Kent, K. A.; Cardiff, G. M.; Sostarecz, A. G.; Crick, D. C.; Crans, D. C., Structure Dependence of Pyridine and Benzene Derivatives on Interactions with Model Membranes. *Langmuir* **2018,** *34* (30), 8939-8951.
31. Luisi, P. L.; Straub, B., *Reverse micelles: biological and technological relevance of amphiphilic structures in apolar media*. Springer: 1984.
32. Maitra, A., Determination of size parameters of water-Aerosol OT-oil reverse micelles from their nuclear magnetic resonance data. *The Journal of Physical Chemistry* **1984,** *88* (21), 5122-5125.
33. Baruah, B.; Roden, J. M.; Sedgwick, M.; Correa, N. M.; Crans, D. C.; Levinger, N. E., When is water not water? Exploring water confined in large reverse micelles using a highly charged inorganic molecular probe. *Journal of the American Chemical Society* **2006,** *128* (39), 12758-12765.
34. Rideau, E.; Dimova, R.; Schwille, P.; Wurm, F. R.; Landfester, K., Liposomes and polymersomes: a comparative review towards cell mimicking. *Chemical Society Reviews* **2018,** *47* (23), 8572-8610.
35. Eytan, G. D., Use of liposomes for reconstitution of biological functions. *Biochimica et Biophysica Acta (BBA)-Reviews on Biomembranes* **1982,** *694* (2), 185-202.

36. Deb, P. K.; Al-Attraqchi, O.; Chandrasekaran, B.; Paradkar, A.; Tekade, R. K., Protein/peptide drug delivery systems: practical considerations in pharmaceutical product development. In *Basic Fundamentals of Drug Delivery*, Elsevier: 2019; pp 651-684.
37. ud Din, F.; Aman, W.; Ullah, I.; Qureshi, O. S.; Mustapha, O.; Shafique, S.; Zeb, A., Effective use of nanocarriers as drug delivery systems for the treatment of selected tumors. *International journal of nanomedicine* **2017,** *12*, 7291.
38. Lasic, D. D., Novel applications of liposomes. *Trends in biotechnology* **1998,** *16* (7), 307-321.
39. Okumura, N.; Wakamatsu, S.; Uno, B., Electrochemical Analysis in a Liposome Suspension Using Lapachol as a Hydrophobic Electro Active Species. *Chemical and Pharmaceutical Bulletin* **2014,** *62* (1), 88-91.
40. Jesorka, A.; Orwar, O., Liposomes: technologies and analytical applications. *Annu. Rev. Anal. Chem.* **2008,** *1*, 801-832.
41. Cook, G. M.; Hards, K.; Dunn, E.; Heikal, A.; Nakatani, Y.; Greening, C.; Crick, D. C.; Fontes, F. L.; Pethe, K.; Hasenoehrl, E., Oxidative phosphorylation as a target space for tuberculosis: success, caution, and future directions. *Tuberculosis and the Tubercle Bacillus* **2017**, 295-316.
42. Koehn, J. T.; Magallanes, E. S.; Peters, B. J.; Beuning, C. N.; Haase, A. A.; Zhu, M. J.; Rithner, C. D.; Crick, D. C.; Crans, D. C., A synthetic isoprenoid lipoquinone, menaquinone-2, adopts a folded conformation in solution and at a model membrane interface. *The Journal of organic chemistry* **2017,** *83* (1), 275-288.
43. Wang, Y.; Hekimi, S., Understanding ubiquinone. *Trends in cell biology* **2016,** *26* (5), 367-378.
44. Boersch, M.; Rudrawar, S.; Grant, G.; Zunk, M., Menaquinone biosynthesis inhibition: a review of advancements toward a new antibiotic mechanism. *RSC advances* **2018,** *8* (10), 5099-5105.
45. Upadhyay, A.; Fontes, F. L.; Gonzalez-Juarrero, M.; McNeil, M. R.; Crans, D. C.; Jackson, M.; Crick, D. C., Partial saturation of menaquinone in Mycobacterium tuberculosis: function and essentiality of a novel reductase, MenJ. *ACS central science* **2015,** *1* (6), 292-302.
46. Organization, W. H., Tuberculosis. **2020**.
47. Bansal-Mutalik, R.; Nikaido, H., Mycobacterial outer membrane is a lipid bilayer and the inner membrane is unusually rich in diacyl phosphatidylinositol dimannosides. *Proceedings of the National Academy of Sciences* **2014,** *111* (13), 4958-4963.
48. Collins, M.; Jonse, D.; Goodfellow, M.; Minnikin, D., Isoprenoid quinone composition as a guide to the classification of Listeria, Brochothrix, Erysipelothrix and Caryophanon. *Microbiology* **1979,** *111* (2), 453-457.
49. Panthee, S.; Paudel, A.; Hamamoto, H.; Uhlemann, A.-C.; Sekimizu, K., Alteration of menaquinone isoprenoid chain length and antibiotic sensitivity by single amino acid substitution in HepT. *bioRxiv* **2020**.
50. Krogstad, D.; Howland, J., Role of menaquinone in Corynebacterium diphtheriae electron transport. *Biochimica et Biophysica Acta (BBA)-Enzymology and Biological Oxidation* **1966,** *118* (1), 189-191.
51. Seel, W.; Flegler, A.; Zunabovic-Pichler, M.; Lipski, A., Increased isoprenoid quinone concentration modulates membrane fluidity in Listeria monocytogenes at low growth temperatures. *Journal of bacteriology* **2018,** *200* (13).

52. Galassi, V. V.; Arantes, G. M., Partition, orientation and mobility of ubiquinones in a lipid bilayer. *Biochimica et Biophysica Acta (BBA)-Bioenergetics* **2015,** *1847* (12), 1560-1573.
53. Gordillo, G. J.; Schiffrin, D. J., The electrochemistry of ubiquinone-10 in a phospholipid model membrane. *Faraday discussions* **2000,** *116*, 89-107.
54. Hoyo, J.; Guaus, E.; Oncins, G.; Torrent-Burgues, J.; Sanz, F., Incorporation of ubiquinone in supported lipid bilayers on ITO. *The Journal of Physical Chemistry B* **2013,** *117* (25), 7498-7506.
55. Wong, K. C., Review of nmr spectroscopy: Basic principles, concepts and applications in chemistry. ACS Publications: 2014.
56. Steinmann, S. N.; Jana, D. F.; Wu, J. I. C.; Schleyer, P. v. R.; Mo, Y.; Corminboeuf, C., Direct assessment of electron delocalization using NMR chemical shifts. *Angewandte Chemie International Edition* **2009,** *48* (52), 9828-9833.
57. Sripradite, J.; Miller, S. A.; Johnson, M. D.; Tongraar, A.; Crans, D. C., How interfaces affect the acidity of the anilinium ion. *Chemistry–A European Journal* **2016,** *22* (11), 3873-3880.
58. Crans, D. C.; Rithner, C. D.; Baruah, B.; Gourley, B. L.; Levinger, N. E., Molecular probe location in reverse micelles determined by NMR dipolar interactions. *Journal of the American Chemical Society* **2006,** *128* (13), 4437-4445.
59. Chatkon, A.; Chatterjee, P. B.; Sedgwick, M. A.; Haller, K. J.; Crans, D. C., Counterion affects interaction with interfaces: the antidiabetic drugs metformin and decavanadate. *European Journal of Inorganic Chemistry* **2013,** *2013* (10-11), 1859-1868.
60. Crans, D. C.; Levinger, N. E., The conundrum of pH in water nanodroplets: sensing pH in reverse micelle water pools. *Accounts of chemical research* **2012,** *45* (10), 1637-1645.
61. Van Cleave, C.; Murakami, H. A.; Samart, N.; Koehn, J. T.; Maldonado Jr, P.; Kreckel, H. D.; Cope, E. J.; Basile, A.; Crick, D. C.; Crans, D. C., Location of menaquinone and menaquinol headgroups in model membranes. *Canadian Journal of Chemistry* **2020,** *98* (6), 307-317.
62. Kessler, H.; Gehrke, M.; Griesinger, C., Two-Dimensional NMR Spectroscopy: Background and Overview of the Experiments [New Analytical Methods (36)]. *Angewandte Chemie International Edition in English* **1988,** *27* (4), 490-536.
63. Ernst, R. R.; Bodenhausen, G.; Wokaun, A., *Principles of nuclear magnetic resonance in one and two dimensions*. Clarendon press Oxford: 1987; Vol. 14.
64. Crews, P.; Rodríguez, J.; Jaspars, M., *Organic structure analysis*. Oxford university press New York: 2010; Vol. 636.
65. Kurosu, M.; Begari, E., Vitamin K2 in electron transport system: are enzymes involved in vitamin K2 biosynthesis promising drug targets? *Molecules* **2010,** *15* (3), 1531-1553.
66. Prince, R. C.; Leslie Dutton, P.; Malcolm Bruce, J., Electrochemistry of ubiquinones: menaquinones and plastoquinones in aprotic solvents. *FEBS letters* **1983,** *160* (1-2), 273-276.
67. Kishi, S.; Saito, K.; Kato, Y.; Ishikita, H., Redox potentials of ubiquinone, menaquinone, phylloquinone, and plastoquinone in aqueous solution. *Photosynthesis research* **2017,** *134* (2), 193-200.
68. Koehn, J. T.; Beuning, C. N.; Peters, B. J.; Dellinger, S. K.; Van Cleave, C.; Crick, D. C.; Crans, D. C., Investigating Substrate Analogues for Mycobacterial MenJ: Truncated and Partially Saturated Menaquinones. *Biochemistry* **2019,** *58* (12), 1596-1615.
69. Elgrishi, N.; Rountree, K. J.; McCarthy, B. D.; Rountree, E. S.; Eisenhart, T. T.; Dempsey, J. L., A practical beginner's guide to cyclic voltammetry. *Journal of Chemical Education* **2018,** *95* (2), 197-206.

70. Carrish, J. J., Three electrode system in the generation of electrostatic images. Google Patents: 1979.
71. Hallett, F.; Watton, J.; Krygsman, P., Vesicle sizing: number distributions by dynamic light scattering. *Biophysical journal* **1991,** *59* (2), 357-362.
72. Carvalho, P. M.; Felício, M. R.; Santos, N. C.; Gonçalves, S.; Domingues, M. M., Application of light scattering techniques to nanoparticle characterization and development. *Frontiers in chemistry* **2018,** *6*, 237.
73. Palmieri, V.; Lucchetti, D.; Gatto, I.; Maiorana, A.; Marcantoni, M.; Maulucci, G.; Papi, M.; Pola, R.; De Spirito, M.; Sgambato, A., Dynamic light scattering for the characterization and counting of extracellular vesicles: a powerful noninvasive tool. *Journal of nanoparticle research* **2014,** *16* (9), 2583.
74. Lundquist, A.; Wessman, P.; Rennie, A. R.; Edwards, K., Melittin–Lipid interaction: A comparative study using liposomes, micelles and bilayerdisks. *Biochimica et Biophysica Acta (BBA)-Biomembranes* **2008,** *1778* (10), 2210-2216.

Chapter 2: Redox Potentials of Truncated Menaquinone Analogues in Soybean Phosphatidylcholine Liposomes are Sensitive to Odd- or Even-Length of Isoprene Chain

2.1. Menaquinone and its Analogues as Electron Transporters

Lipoquinones play a key role as electron transporters in the electron transport system (ETS) of prokaryotic and eukaryotic species.[1-2] They can be divided into two major structural classes: benzoquinones (ubiquinone, UQ and plastoquinone, PQ) and naphthoquinones (menaquinone, MK). Each of these classes of molecules contains a benzoquinone or naphthoquinone head group, respectively, covalently bound to an isoprenoid side chain of varying length and degree of saturation within the side chain.[3-5] Lipoquinones work to generate proton motive force (PMF) by shuttling electrons to and from membrane-bound e^- donors and acceptors in the electron transport chain.[6-7] The resulting PMF is then used to generate ATP for the cell, making lipoquinones essential for survival.[8-9]

A number of bacteria, particularly Gram-positive and Gram-negative obligate anaerobes, produce MK as their sole electron transporter.[10-11] Examples of Gram-positive bacteria which use MK in their ETS include *Listeria monocytogenes*, *Staphylococcus aureus*, and *Mycobacterium tuberculosis*, which are pathogens that have a significant impact on human disease, as well as a potential impact on bioterrorism, worldwide.[12-13] For some of these bacteria which produce MK, a specific MK derivative has been identified. For example, *Mycobacterium tuberculosis* produces primarily MK9(II-H_2), meaning that there are nine isoprene units covalently attached to the naphthoquinone head group, with a saturation at the II, or β, position.[14] A number of other MK analogues have been identified in other bacteria, such as MK8(II-H_2) in *Corynebacterium diphtheriae,* and differences in the length of isoprene side chain

can have implications for susceptibility of bacterial cells to antibiotics.[15-16] In fact, all bacterial species which have been examined and contain mycolic acid, a long fatty acid, in their cell wall possess partially saturated MK analogues.[17-18] While it is not clear why this regiospecificity in MK composition is conserved within species or what advantages it offers to the species which produce MK, it is possible that this is related to its ability to undergo oxidation and reduction.

Despite the importance of its function as an electron transporter, little is known about how changes in length of the isoprene side chain or degree of saturation affect the redox properties of MK. Previous work in our lab has been done to characterize the electrochemical differences between a number of short truncated MK analogues in aprotic solvents pyridine, DMSO and acetonitrile.[19-20] This work found that the redox potentials of truncated MKs are sensitive to chain length and saturation in aprotic solvent, and that a reduction in the β-isoprene unit results in more positive (more easily reduced) $E_{1/2}$ potentials of quinone to semiquinone. However, there are significant differences between the reduction of MK in aprotic solvents and bacterial membranes. In aprotic solvent, application of electrochemical potential to the quinone results a one-electron reduction to form a semiquinone ($Q^{\bullet -}$), followed by the second one-electron reduction of the formed semiquinone to a dianion (Q^{2-}) (Fig. 2.1).[21-22]

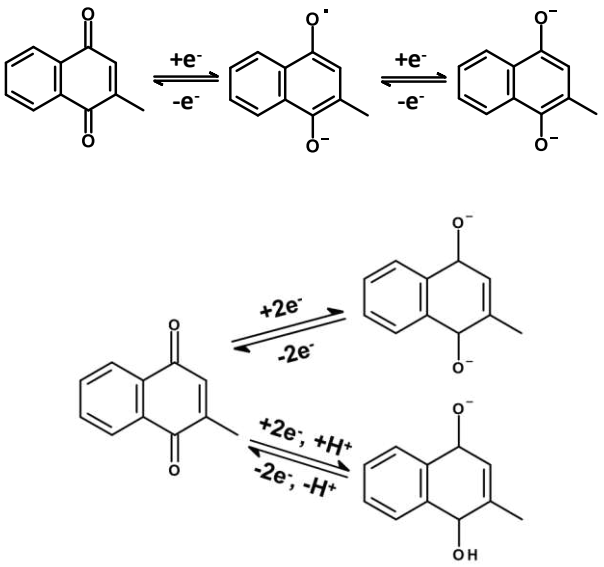

Figure 2.1. Scheme of the reduction of the naphthoquinone head group of MK in aprotic solvent (top) and in aqueous solution (bottom).

In a neutral aqueous environment such as the liposomal model membrane used to study these compounds, however, two electrons are transferred simultaneously with either one proton (forming an anionic hydroquinone) or no protons (forming the dianionic species) (Figure 2.1).[23-24]

In this manuscript, we continue these previous studies in organic solvent by characterizing the electrochemistry of the same truncated MK analogues studied previously and the addition of MK4 and phylloquinone (MK4(II,III,IV-H_6)) in the context of a liposomal bilayer (Figure 2.2).

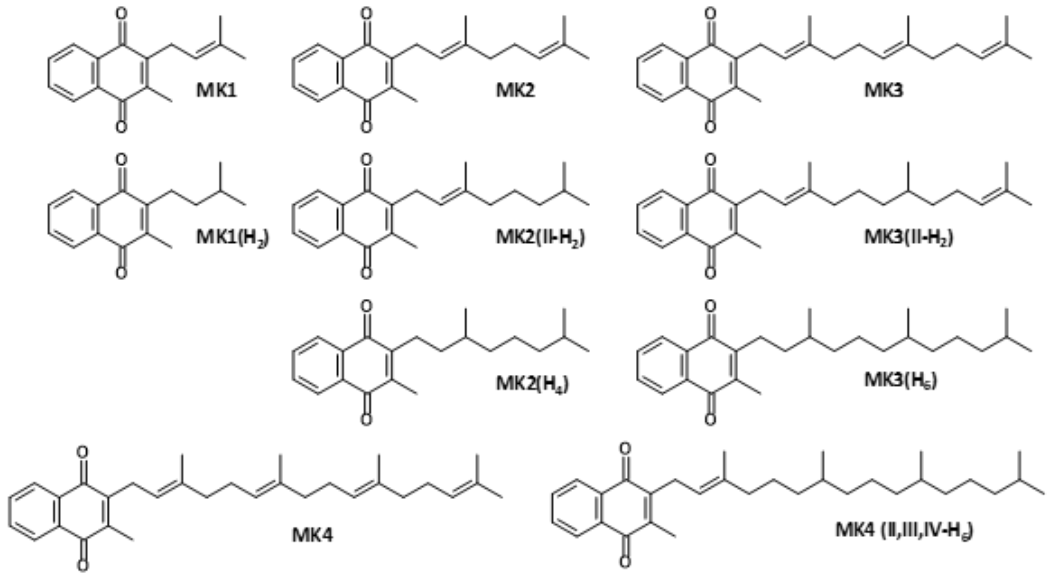

Figure 2.2. The structures of all MK analogues studied in this work: MK1, MK1(H_2), MK2, MK2(II-H_2), MK2(H_4), MK3, MK3(II-H_2), MK3(H_6), MK4, and MK4(II,III,IV-H_6)

Soybean phosphatidylcholine (SPC) is used to create vesicles of uniform size and solubilize MK analogues in an aqueous bilayer environment for studies via cyclic voltammetry. While bacterial membranes containing menaquinone as their major electron carrier are typically more abundant in lipids such as phosphatidylinositol, phosphatidylserine and phosphatidylethanolamine, the work done here is done using phosphatidylcholine derived from soybeans, so that appropriate comparisons may be made to electrochemical data already obtained with ubiquinone, which is typically studied in the context of the eukaryotic lipid phosphatidylcholine.[5, 25-29] We hypothesize that even in the slightly more complex context of a bilayer compared to previous work in organic solvent, the extent of saturation in the isoprene side chain impacts the $E_{1/2}$ redox potentials and electrochemical reversibility of the truncated MK analogues. These studies are important for furthering our understanding of the utility of saturated MK side chains to the pathogenic species, like *M. tuberculosis*, who use them.

2.2. Materials and Methods

2.2.1. Chemicals and Solvents

L-α-phosphatidylcholine from soybean (>30%), chloroform (99.8%), ferrocene (Fc, anhydrous), sodium phosphate monobasic monohydrate (NaH_2PO_4, 98%) were purchased from Sigma-Aldrich, and sodium phosphate dibasic anhydrous (Na_2HPO_4, 99.8%) was purchased from Fisher Scientific. These materials were used without further purification. Distilled deionized water (DDI H_2O) was purified with a Barnstead E-pure system (~18 MΩ cm). Menaquinone-4 and phylloquinone (MK4 and MK4(II,III,IV-H_6) were purchased from Sigma-Aldrich and used without further purification. All MK-*n* analogues were synthesized previously except for MK-3, and the procedures for the synthesis of the MK-*n* analogues are previously reported by us.[19-20, 30]. The synthetic procedure for MK-3 can be found in the following section 2.2.3.

2.2.2. Preparation of MK-*n* Liposomes

Large unilamellar vesicles (LUV) of homogeneous size were prepared with L-α-phosphatidylcholine (PC). Each MK-n sample was made in triplicate with 0.100 g PC in a total of 10 mL solution and the appropriate mass of MK-n for the addition of 0.06 mmol and a final MK-n concentration of 6 mM. PC and MK-n are dissolved in 15 mL of $CHCl_3$ in a round bottom flask, the solvent is then evaporated under vacuum to create a dried film of lipids and MK-n at the bottom of the flask. The film of lipid is then rehydrated by heating at 55◦C and gently agitating in the presence of 10 mL of 0.100 M phosphate buffer at pH 7.4, resulting in large multilamellar MK-*n* vesicles. This solution of multilamellar vesicles of heterogeneous size is then extruded using a Lipex 10 mL Thermobarrel Extruder at 55◦C and passed through a

polycarbonate filter (Whatman Nucleopore Track-Etch Membrane, 110605, 25 mm) with pore size of 0.1 μm to form a solution of LUV of homogeneous size containing MK-*n*.

2.2.3. MK-3 synthesis

2.2.3.1. General Methods

Menadiol was synthesized as previously described.[19, 31-32] Menadione (crystalline), sodium hydrosulfite (85.0%), 1,4-dioxane (anhydrous, 99.9%), BF_3 etherate (≥46.5%), sodium bicarbonate (ACS grade), *trans,trans*-farnesol (96%), and GC grade *n*-pentane were purchased from Sigma-Aldrich and were used as received unless otherwise noted. Ultra-high purity argon gas (99.9%) was acquired from Airgas. SiliCycle®SiliaFlash® F60, 43-60 μm 60 Å silica gel was purchased from SilliCycle. Anhydrous sodium sulfate (Certified ACS, granular) and HPLC grade ethyl acetate (EtOAc) was purchased from Fisher Chemical. Merck TLC Silica gel 60 F_{254} TLC plates were purchased from Merck. Washed sea sand was purchased from Fisher Scientific. Deuterated NMR solvent, CDCl3 (chloroform-d, 99.8% atom % D), was acquired from Sigma-Aldrich. Distilled deionized water (DDI H_2O) was purified with a Barnstead E-pure system (18 MΩ-cm).

All non-aqueous reactions were carried out under an atmosphere of argon in flame-dried glassware and were stirred on a magnetic stir plate using anhydrous solvent unless otherwise noted. All solvents were purchased from commercial sources and either used directly or after drying. Reactions were monitored by thin-layer chromatography (TLC) on Whatman Whatman Partisil® K6F TLC plates (silica gel 60 Å, 0.250 mm thickness) or Merck TLC Silica gel 60 F_{254} plates and visualized using a UV lamp (366 or 254 nm) or Seebach's stain (and heated to visualize). Products were purified by flash chromatography (SiliCycle®SiliaFlash® F60, 43-60 μm 60 Å). Yields refer to dried, chromatographically and spectroscopically (^{1}H NMR)

homogenous materials unless otherwise noted. All chemicals were used without purification unless otherwise noted.

The ^{1}H and ^{13}C spectra were recorded on a Bruker Model Avance Neo400 equipped with BBFO smart probe operating at 400 MHz or 101 MHz, respectively. Chemical shift values (δ) are reported in ppm and referenced against the internal solvent peaks in ^{1}H NMR ($CDCl_3$, δ at 7.26 ppm) and in ^{13}C NMR ($CDCl_3$, δ at 77.16 ppm). All NMR spectra were acquired at 25 °C. Integral values were determined using standard, uncalibrated NMR experiments and should be viewed accordingly. ^{1}H NMR spectra are reported as follows: chemical shift (multiplicity, coupling constant, integration). The following abbreviations are used to indicate multiplicities: s, singlet; d, doublet; t, triplet; q, quartet; m, multiplet; br, broad. NMR spectra were processed using MestReNova version 10.0.1. or 12.0.2. Details of NMR experiments are provided in representative experimental sections and captions of figures. Synthesized compounds were dried under vacuum for ~4 days (~100 Torr) unless otherwise noted to ensure as much residual solvent from purification was removed as possible. Samples for NMR studies were prepared immediately prior to running the samples using deuterated solvents (sealed under an inert atmosphere in glass ampules). High-resolution mass spectrometry (HRMS) experiments were conducted on an Agilent 6224 TOF LC/MS (WTOF) equipped with dual ESI source in positive ion mode.

2.2.3.2. Synthesis of 2-methyl-3-((2E,6E)-3,7,11-trimethyldodeca-2,6,10-trien-1-yl)naphthalene-1,4-dione, (MK-3)

To a dry 100 mL round bottom Schlenk flask were added a dry stir bar, ethyl acetate (16 mL) and 1, 4-dioxane (16 mL), which was then evacuated/purged with argon, repeatedly. Then, crude menadiol (2.2) (2.20 g, 10:1 menadiol:menadione, 11.5 mmol accounting for residual

menadione) and *trans-trans*-farnesol (2.14) (2.78 g, 12.5 mmol, 1.09 equiv.) was added followed by dropwise addition of distilled BF_3 etherate (0.8 mL). The reaction mixture was refluxed at 75-80 °C for 3 h under argon. The red/orange reaction mixture was quenched with iced DDI-H_2O (100 mL) and extracted with diethyl ether (3 x 100 mL). The combined yellow organic extracts were then washed with saturated $NaHCO_3$ (100 mL), DDI H_2O (100 mL), and saturated NaCl (100 mL), dried over anhydrous Na_2SO_4, and then concentrated at reduced pressure at ambient temperature to yield 4.67 g of red crude oil after drying under vacuum overnight. The red crude oil was purified by flash column chromatography (1000 mL of 230-400 mesh SiO_2, 70 mm column, 20:1 *n*-pentane:EtOAc). The red/yellow oil was dried under reduced pressure (~100 Torr) for 4 days to yield 0.930 g (2.47 mmol, 21.5% yield) as an orange-red oil.

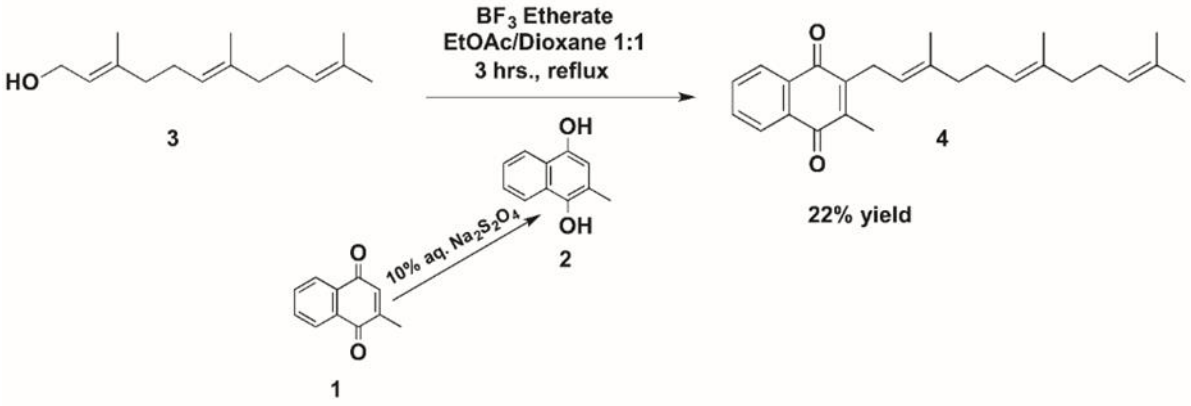

Figure 2.3. Synthetic route to prepare MK-3 (4) from menadiol (2) and *trans,trans*-farnesol (3) using Lewis acid catalyst conditions.[19-20, 32]

The results of the ^1H and ^{13}C NMR and HRMS are summarized below.

^1H NMR (400 MHz, $CDCl_3$) δ: 8.05-8.10 (m, 2H), 7.66-7.71 (m, 2H), 5.00-5.06 (m, 3H), 3.37 (d, J = 7.0 Hz, 2H), 2.19 (s, 3H), 1.88-2.09 (m, 8H), 1.79 (s, 3H), 1.65 (s, 3H), 1.56 (s, 6H).

^{13}C NMR (101 MHz, $CDCl_3$) δ: 185.62, 184.68, 146.31, 143.51, 137.69, 135.34, 133.48, 133.42, 132.34, 132.31, 131.40, 126.46, 126.34, 124.45, 124.00, 119.25, 39.85, 39.82, 26.87, 26.61, 26.17, 25.83, 17.79, 16.57, 16.16, 12.83.

HRMS (ESI, WTOF): calculated for C26H33O2 [(M + H)+], 377.2475; found, 377.2488.

2.2.4. Electrochemical Methods

The electrochemistry was performed using a Pine Research WaveDriver 20 bipotentiostat (Model AFP2) and the AfterMath software program. Cyclic voltammetry (CV) measurements were carried out at ambient room temperature using a classical three-electrode system with a glassy carbon working electrode (BASi, MF2012, area 0.707cm^2, 3mm), a low-profile aqueous Ag/AgCl reference electrode (Pine Research, RRPEAGCL20, 3.5mm), and a platinum wire auxiliary electrode (BASi, MW1032) with 0.1 M phosphate buffer at pH 7.4 as the supporting electrolyte. The scan rate used for all reported redox potentials was 100 mV/s and performed in the direction from -0.850 V to 0.400 V to -0.850 V. Electrodes were cleaned after each set of three measurements. The glassy carbon electrode was polished with water and alumina in a figure-eight motion and then rinsed with DDI H_2O. The Pt wire auxiliary electrode was polished gently with 600 grit sandpaper and rinsed with ethanol, and then was dried with a chem-wipe and compressed air.

Redox potentials are reported as half-wave potentials, $E_{1/2}$, and calculated from Eq 2.1, in which E_{pc} and E_{pa} are cathodic and anodic peak potentials, respectively. The analysis of CV data has been extensively discussed by our group in our previous work on these analogs in aprotic solvents; including the extent of reversibility by the peak current ratio, determination of diffusion coefficients, and determination of the number of electrons participating in the redox process.[20] All half-wave potentials are referenced to the external standard of ferrocene, whose half-wave potential is set to zero (Fc^+/Fc $E_{1/2}$ = 0 V).

$$\text{Eq. 2.1.} \quad E_{1/2} = \frac{1}{2}(E_{pc} + E_{pa})$$

The CVs were graphed using Origin2020 student version, and Microsoft Excel 2016 was used for mathematical analysis and subtraction of external standard Fc^+/Fc $E_{1/2}$ redox potential from experimental MK data to set the potential axis vs. Fc^+/Fc.

2.2.5. Diffusion Coefficient Analysis

Diffusion coefficients were determined for the MK-*n* species using the cathodic peak current. Peak current was measured using the cyclic voltammetry package in Origin2020 student version. Because masses of MK-*n* analogues were weighed in mg quantities, the diffusion coefficients are restricted to two reported significant figures. Diffusion coefficients are calculated based on the exact mass of MK analogue weighed out according to methods previously established in the lab.[19-20] The i_p values for cathodic and anodic current passed were used to determine reversibility, in which most of the anodic peak currents are smaller than the cathodic peak currents, indicating quasireversibility.

2.3. Results

2.3.1. Cyclic Voltammetry and E1/2 Potentials of Truncated Menaquinone Analogues

As noted earlier, mechanism of reduction of MK when an electrochemical potential is applied is different in the context of a bilayered membrane than in aprotic solvent, as is the species formed. In aprotic solvent, the application of electrochemical potential results in a one-electron transfer to the quinone, forming a semiquinone ($Q^{\bullet -}$), and a subsequent one-electron transfer to the semiquinone results in a quinone dianion (Q^{2-}). In the context of a bilayered membrane, however, the semiquinone and dianion species are unstable due to the presence of readily available protons. As a result, at neutral pH in aqueous media either two electrons and one proton or two electrons without the participation of a proton are transferred simultaneously (Figure 2.1).[23-24] So while previous electrochemical work done in aprotic solvent measured the

formation of the semiquinone, work done here on MK analogues in liposomal membranes measures instead the formation of the anionic quinol or hydroquinol species.

Electrochemical analysis of each MK analogue was done with Fc as an external standard in the presence of 0.1 M phosphate buffer and SPC. Each CV shows two distinct peaks corresponding to the reduction (cathodic peak) of menaquinone to menaquinol, and subsequent oxidation back to menaquinone (anodic peak), as shown in Appendix III**.** All half-wave potentials for each redox process for each MK-*n*, referenced to the external standard of Fc+/Fc, are listed in Table 2.1.

Table 2.1. Listed $E_{1/2}$ potentials of each truncated MK-*n* analogue studied in this work with 95% confidence intervals.

MK-*n*	**$E_{1/2}$ vs. Fc/Fc^+, V**
MK1	-0.5131 ± 0.0016
MK1(H_2)	-0.5114 ± 0.0017
MK2	-0.5097 ± 0.0025
MK2(II-H_2)	-0.5240 ± 0.0032
MK2(I,II-H_4)	-0.5348 ± 0.0079
MK3	-0.5239 ± 0.0098
MK3(II-H_2)	-0.5132 ± 0.0016
MK3(I,II,III-H_6)	-0.5115 ± 0.0032
MK4	-0.5116 ± 0.0032
MK4(II,III,IV-H_6)	-0.5466 ± 0.0016

With respect to the $E_{1/2}$ potentials for each truncated MK analogue, values obtained for each truncated analogue are fairly similar with low standard deviation, as the head group which undergoes the redox processes is the same between each compound, only differing in the length and degree of saturation of the isoprene tail. Fully unsaturated analogues, for the most part, are not statistically different from each other (Appendix II). However, there is statistical difference ($p<0.05$) in the $E_{1/2}$ values obtained from these MK analogues with increasing saturations in the

isoprene tails of specifically, the even-length MK analogues MK2 and MK4 (Appendix II) In the case of these MK analogues with an even-length isoprene tail, increasing the number of saturations in the tail leads to more negative $E_{1/2}$ potentials, meaning that more extreme electrochemical potentials are needed to oxidize and reduce the compounds. (Figure 2.3)

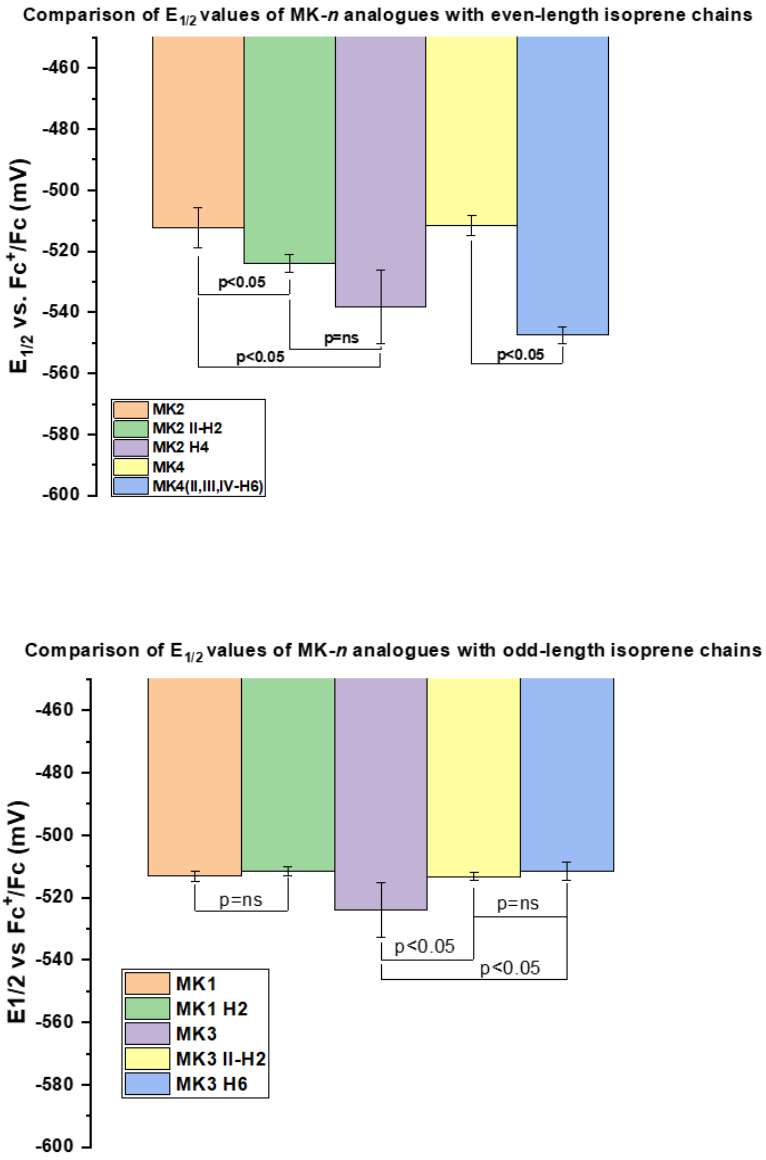

Figure 2.4. Graphical comparison of the change in $E_{1/2}$ potential with increasing saturations in the isoprene side chain of even-length isoprene chains (top) and odd-length chains (bottom).

However, the same is not true for MK analogues with odd-length isoprene chains. In this case, increasing the number of saturations in the isoprene tail of MK3 seems to result in a slight increase in the measured $E_{1/2}$ potentials, however, this increase is only significant between MK3 and the two saturated analogues, not between the saturated MK3 analogues themselves (Fig 2.3, Appendix II).

2.3.2. Reversibility (ip_a/ip_c) Studies

In addition to calculating the $E_{1/2}$ potentials for each of the truncated MK analogues, the cathodic and anodic peaks currents of each CV were used to calculate the electrochemical reversibility of the compounds in a SPC bilayer. Reversibility is calculated by the ratio of the anodic and cathodic peak currents, or ip_a/ip_c, and in a situation in which a compound is perfectly electrochemically reversible, this ratio should be equal to one.

Previous studies in our lab with truncated MK analogues in aprotic solvent found that when the compounds are free to rotate in the aprotic solvents DMSO, pyridine and acetonitrile, each of the analogues was found to be completely electrochemically reversible. However, the reversibility of these analogues when in the confines of a bilayered vesicle as opposed to freely rotating in organic solvent does not indicate complete reversibility, but rather quasireversibility.

Table 2.2. Values calculated for ip_a/ip_c of each of the MK-*n* analogues shown with calculated 95% confidence intervals.

MK-*n*	**Ip_a/ip_c**
MK1	1.611 ± 0.1207
MK1(H2)	1.691 ± 0.1444
MK2	1.952 ± 0.1620
MK2(II-2)	1.568 ± 0.2758
MK2(H4)	1.326 ± 0.3177
MK3	1.024 ± 0.3227
MK3(II-H2)	1.280 ± 0.3237
MK3(H6)	1.714 ± 0.1395
MK4	1.375 ± 0.1896
MK4(II,III,IV-H6)	0.8920 ± 0.1861

Values calculated for ip_a/ip_c are shown in Table 2.2. For the most part, values are greater than one due to the higher peak current observed at the anodic peak as compared to the cathodic peak. Each fully unsaturated MK-*n* analogue is significantly different from the others with the exception of MK3-MK4 and MK1-MK4 (Appendix II), and like the analysis of the $E_{1/2}$ potentials, there appears to be a difference between the behavior of MK-*n* analogues with odd- and even-length isoprene chains. For MK-*n* analogues with even-length chains, increasing the number of saturations in the chain results in an increase in reversibility, or the ip_a/ip_c ratio becomes closer to one, however, this is significant only when comparing fully unsaturated with fully saturated analogues (Appendix II, Figure 2.4). In contrast, MK-*n* analogues with odd-length isoprene chains are inherently more reversible than even-length, with MK-3 showing an ip_a/ip_c of one, however, increasing the number of saturations in the isoprene tail reverses this trend. This trend is also significant only when comparing fully saturated with fully unsaturated

analogues of MK3, and there is no statistical significance at all between the ip_a/ip_c ratios of MK1 and MK1(H_2) (Appendix II, Figure 2.4).

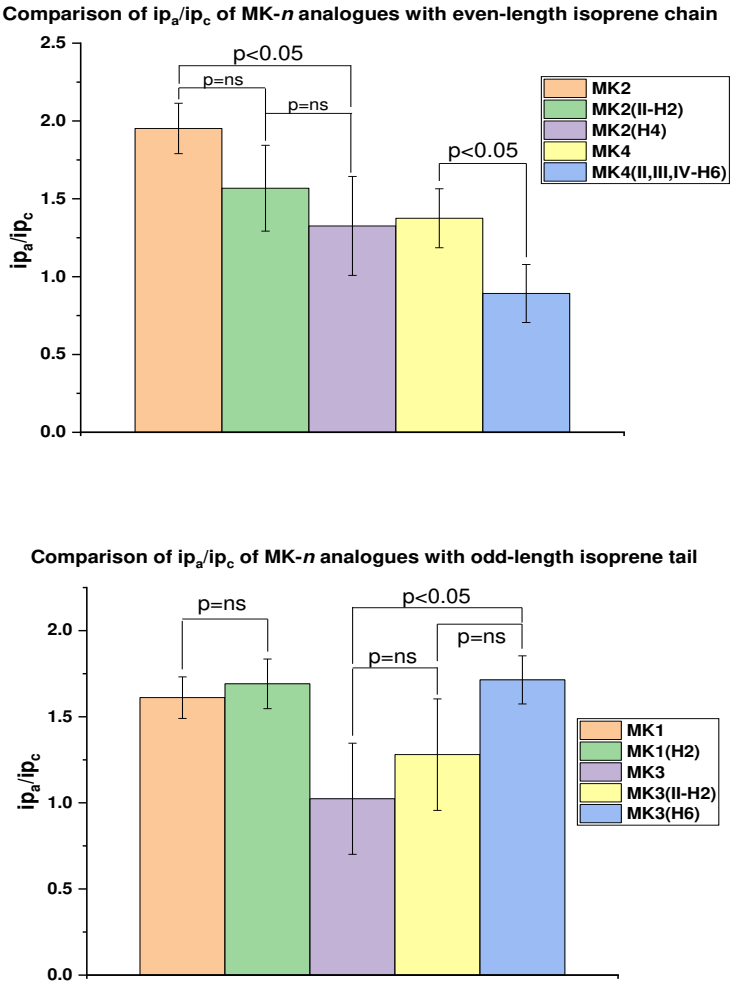

Figure 2.5. Graphical comparison of the change in reversibility as denoted by the ip_a/ip_c ratio with increasing saturations in the isoprene side chain of even-length isoprene chains (top) and odd-length chains (bottom).

2.3.3. Diffusion Coefficient Analysis

Diffusion coefficients for each MK-*n* analogue were calculated from their CVs by using the Randles-Sevcik equation and each MK-*n* redox process was found to be a two-electron

reduction as detailed earlier.[33-34] Diffusion coefficients of each compound are listed in Table 2.3.

Table 2.3. Diffusion coefficients calculated for each MK-*n* analogue with calculated 95% confidence interval.

MK-*n*	**D_O (cm^2/s)**
MK1	$2.25 \cdot 10^{-8} \pm 1.05 \cdot 10^{-8}$
MK1(H_2)	$8.24 \cdot 10^{-9} \pm 5.40 \cdot 10^{-9}$
MK2	$1.40 \cdot 10^{-9} \pm 6.04 \cdot 10^{-10}$
MK2(II-H_2)	$1.09 \cdot 10^{-9} \pm 7.58 \cdot 10^{-10}$
MK2(H_4)	$2.69 \cdot 10^{-10} \pm 1.81 \cdot 10^{-10}$
MK3	$1.73 \cdot 10^{-10} \pm 1.95 \cdot 10^{-10}$
MK3(II-H_2)	$1.62 \cdot 10^{-9} \pm 1.86 \cdot 10^{-9}$
MK3(H_6)	$1.35 \cdot 10^{-9} \pm 2.16 \cdot 10^{-9}$
MK4	$6.88 \cdot 10^{-10} \pm 3.49 \cdot 10^{-10}$
MK4(II,III,IV-H_6)	$2.26 \cdot 10^{-9} \pm 4.01 \cdot 10^{-9}$

Data obtained here shows that with the exception of MK1, and to some extent, MK1(H_2), D_O values are 1-2 orders of magnitude lower than that of a compound freely rotating in aqueous solution (Figure 2.5). This observation is logical in light of the confinement of the MK-*n* compound to a liposomal bilayer; a molecule freely rotating in aqueous solution has only to diffuse to the surface of the electrode, but a molecule confined to a liposomal bilayer must diffuse to the surface of the bilayer as the liposome itself diffuses to the surface of the electrode, lowering the observed D_O value from what would be expected in aqueous solution.

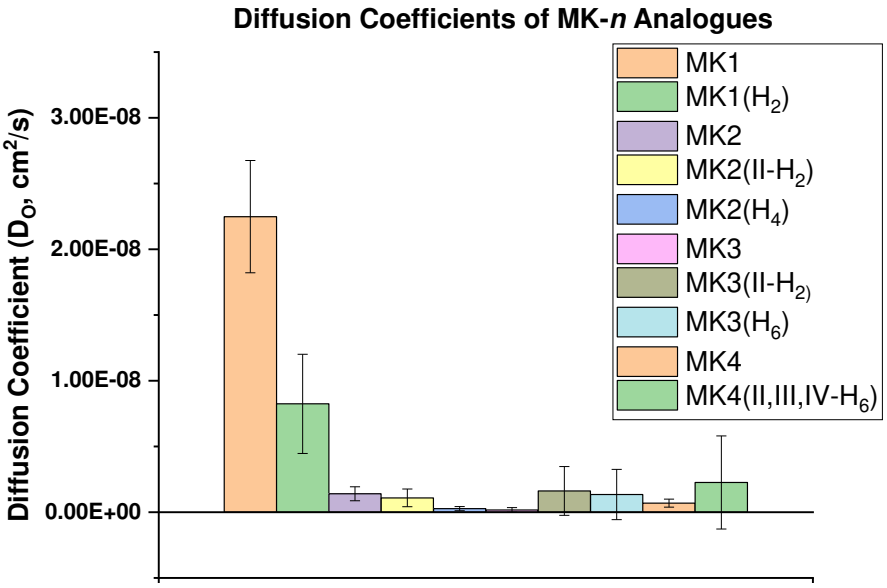

Figure 2.5. Graphical comparison of diffusion coefficient values calculated for MK-*n* analogues.

Only MK1, MK1(H_2), MK2, MK2(II-H_2) and MK2(H_4) are statistically distinct from each other (Appendix II), and as tail length and saturation increases there is a clear decrease in D_O. As the tail length and saturation increase beyond MK3(II-H_2), however, error increases, often beyond the scope of the measurement taken, with MK3(II-H_2) , MK3(H_6), MK4 and MK4(II,III,IV-H_6) giving the highest error. This is likely due to these longer and/or more saturated analogues being more deeply anchored into the membrane and less accessible, resulting in widely differing peak currents used to calculate D_O.

2.4. Discussion

Previous studies with these same MK-*n* analogues in organic solvent showed a clear pattern with regards to the changes in $E_{1/2}$ potentials brought about by structural differences between compounds; that is, it was found that first chain length, then degree of saturation, are the structural components responsible for predictable patterns of change. In organic solvent, it was

found that a reduction in the beta-isoprene unit of the tail results in more positive $E_{1/2}$ potentials, meaning that it is easier to oxidize and reduce. Further saturations in the tail, then, resulted in more negative $E_{1/2}$ potentials. Data in the more biologically relevant context of a liposomal bilayer, however, does not follow as clear of a pattern between the analogues.

As shown in Fig. 2.3, there does appear to be an odd-even effect in the $E_{1/2}$ potentials measured for the analogues. Increasing the tail length of the fully unsaturated MK-*n* analogues has very little difference on the $E_{1/2}$ potentials measured, with no significant differences between any of the unsaturated analogues (Appendix II). However, depending on whether the MK-*n* analogue has an odd- or even-length isoprene chain, addition of saturations in the chain has a much different effect. In the case of MK-*n* analogues that have an even-length isoprene tail, the addition of saturations in the tail results in $E_{1/2}$ potentials that are more negative, meaning that they require more extreme potentials to undergo oxidation and reduction. In contrast, for those MK-*n* analogues which have an odd number of isoprene units in the tail, increasing the number of saturations in the isoprene tail results in increasingly positive $E_{1/2}$ potentials, resulting in a compound that is more easily oxidized and reduced (Fig. 2.3).

While it is unclear why this effect may be occurring, it is not unprecedented for compounds with carbon chains of differing lengths to have different electrochemical properties depending on whether the carbon chain has an odd or even number of carbon atoms. Previous studies with monolayers of $H_2C{=}CH\text{-}(CH_2)_n$-phenyl that were directly bound to Si(111) showed that these compounds with an even number of methylenes were more efficient electrical conductors than those with an odd number of methylenes.[35] This is a result of the orientation of both the ring plane and the long axis of the alkyl spacer being more perpendicular to the substrate plane for these even length methylene molecules. This change in orientation affects the

electron density on the aromatic rings with respect to the shortest tunneling path, which increases the barrier for electron transport through the odd monolayers. Other studies with hydrocarbon chains of odd and even length have also found discrepancies between electrochemical data collected between those compounds with odd and even chains in self-assembled monolayers.[36-38] Despite the widely reported occurrence of an odd-even effect in hydrocarbon chains in self-assembled monolayers (SAMs), this phenomenon is poorly understood, as it is difficult to distinguish the effects that the conformation of the molecule itself has on its electrochemical properties from the effect that the interface may have on its electrochemistry.[36, 39] A similar phenomenon may be occurring here in which a combination of the orientation of the MK-*n* and its confinement in a particular region of the bilayer may affect how much electrochemical potential is required to oxidize and reduce the MK-*n*. It is likely that, with the exception of MK1 and potentially MK1(H_2), the MK-*n* molecules are confined at least to some degree to a particular region of the phosphatidylcholine bilayer due to their hydrophobicity, and a combination of this and the natural conformation that they adopt in solution may lead to the different electrochemical properties observed between MK-*n* analogues with odd- and even-length isoprene chains. Indeed, we see a much sharper contrast between a fully unsaturated MK-*n* analogue and its partially or fully saturated derivatives when the isoprene side chain length increases to two units and beyond (Figure 2.3). This is consistent with previous studies of odd- and even-length hydrocarbons in self-assembled monolayers and may be due to the increased hydrophobicity of the compounds resulting in increased incorporation into the membrane. As a result, the compound is located within the liposome such that it is more tethered to the liposomal bilayer and confined, which, relative to the electrode, may result in a need to pass more electrochemical potential before the compound is able to undergo oxidation and reduction.

Electrochemical reversibility also follows an odd-even trend within the different MK-*n* analogues. Electrochemical reversibility refers to the rate at which electron transfer occurs between the working electrode and the redox-active MK-*n* molecule. Previous work in organic solvent showed that the compounds were perfectly electrochemically reversible, meaning that the electron transfer occurs quickly and without significant thermodynamic barriers. Again, this is not the case when the same MK-n analogues are confined within a phosphatidylcholine bilayer. In the context of a phosphatidylcholine bilayer with the notable exception of MK3 (Figure 2.4) instead the compounds display quasireversibility, indicating that electron transfer from the electrode to the MK-n is impeded. While it is difficult to determine what the cause of this may be due to a lack of prior research on menaquinone or ubiquinone analogues with increasing saturations, this quasireversibility may be due to the surrounding phospholipid environment impeding electron transfer from the electrode to MK-*n*. It is possible, but unlikely, that a different surrounding lipid environment may produce slightly different trends in reversibility between the MK-*n* analogues, since it is speculated that the change in reversibility may be due to the change in orientation of the naphthoquinone head group to the liposomal surface, which could be affected by different lipid head groups. However, similar to the odd-even effect observed with $E_{1/2}$ potentials, this is likely a result of the confinement of the molecule within the liposomal membrane. It is possible that in MK-*n* analogues with even-length isoprene chains, as the saturations in the chain increase they are oriented in such a way that results in a faster, and less impeded electron transfer, and increased saturations in isoprene chains of odd-length MK-*n* analogues causes them to be oriented in such a way that electron transfer is impeded, and more dependent on scan rate (Appendix III).

Interestingly, more negative $E_{1/2}$ potentials seem to be correlated with increased

reversibility. While more extreme potentials are required to reduce, for example, MK-*n* analogues with odd length compared to even length of isoprene chain, the need for these more extreme potentials does not seem to be related to the ease of electron transfer from the electrode to the MK-n analogue. This indicates that while more extreme potentials may be needed for even-length MK-*n* with increasing saturations and less electrochemical potential is required to reduce odd-length MK-*n* with increasing tail saturations, this observation is not related to the ease of electron transfer to and from the electrode as indicated by ip_a/ip_c ratios. It is not likely that this observation has biological implications. The variations in ip_a/ip_c ratios between MK-*n* analogues, while potentially useful for gaining information about electron transfer of MK-*n* compounds within a bilayer or vague information about differing conformations of MK-*n* analogues at a bilayer surface, are not likely to have biological relevance as this is a reflection of electron transfer between MK-*n* and the electrode's surface. In a biological environment such as the electron transport chain, electron transfer is not likely to happen at the liposomal surface, but embedded slightly further in the bilayer by enzymes involved in electron transfer such as hydrogenases, dehydrogenases and oxidoreductases. As a result, while the calculated ip_a/ip_c ratios and $E_{1/2}$ values shown here show a unique chemical relationship that may be due to the conformation of the MK-*n* analogue's naphthoquinone head relative to the electrode or bilayer, it is not likely that this unique and curious relationship has any biological implications. Again, it is likely that this discrepancy is related to the confinement of the compound of interest in the bilayer affecting its orientation relative to the electrode, which may impede the electron transfer process. In the case of ip_a/ip_c ratios between shorter and longer chain MK-*n* analogues, with the most notable example here being the comparison between MK1 with increasing saturations and MK3 with increasing saturations, there is a sharper and more statistically significant difference

between the ip_a/ip_c ratios of compounds with longer isoprene chains. This further supports the hypothesis that the odd-even effect observed here is related to confinement and conformation in the bilayer.

The calculation of diffusion coefficient from the cyclic voltammograms obtained shows that even including the shorter and slightly more hydrophilic MK1, the MK-*n* analogues likely prefer to localize either at the liposomal interface near the polar head groups, or in the case of longer and more hydrophobic analogues like MK3 and MK4, further in the hydrophobic tail region. This is evidenced by diffusion coefficients which are two to four orders of magnitude smaller than values which are typically observed in aqueous solution.[40-41] This decrease in diffusion coefficient as a result of confinement in a liposomal bilayer is due to the need for the liposome to diffuse to the electrodes surface at the same time that the MK-*n* analogue diffuses to the surface of the liposome for electron transfer to and from the MK-*n* and electrode. This observation is supported by the data collected for the diffusion coefficient analysis as well; there is statistical significance observed between MK1, MK1(H2), MK2, and MK2(II-H2) in which the D_O decreases with increasing tail length and saturation. This is likely due to the increased solubility of the MK-*n* analogues with shorter isoprene side chains and fewer degrees of saturation. As the tail length increases, we see a significant decrease in the diffusion coefficient which corresponds to less MK-*n* freely soluble in the aqueous environment surrounding the liposome and increased incorporation of the MK-*n* in the liposomal bilayer. This observation is supported in Chapter 3 as well, in which we will see that with increasing concentrations of MK-2 which are much lower than those used here, a freely soluble species of MK-2 emerges and can be observed via ^{1}H NMR. As tail length and saturation increase, we see this trend continued with the increase in error of the samples collected, and this is likely due to increased incorporation of

the hydrophobic MK-*n* analogues into the bilayer, causing difficulty in detection of the MK-*n* at the electrodes surface and resulting in differing peak current values which are used to calculate D_O.

2.5. Conclusions

There is a distinct odd-even effect with regards to length of isoprene chain of the MK compounds used in this study and experimentally obtained half-wave potentials and electrochemical reversibility when these compounds are confined in phosphatidylcholine liposomes. Interestingly, compounds with higher reversibility (ip_a/ip_c ratio closer to 1) require more extreme potentials to undergo oxidation and reduction, and compounds with lower reversibility (ip_a/ip_c deviates from 1) require less extreme potentials to oxidize and reduce. It is possible that this odd-even effect that is observed is due to the electronic properties of the menaquinone as a result of its conformation and interactions with phosphatidylcholine lipids as it is confined within the liposomal bilayer. The naphthoquinone head group of the MK-*n* analogues may be oriented differently relative to the electrodes surface as a result of having odd- or even-length isoprene chains as well as the interactions of the phosphatidylcholine head groups with the naphthoquinone head, effecting the electrochemical properties which are observed when confined in an artificial bilayer. While the relationship observed between $E_{1/2}$ and ip_a/ip_c is curious and interesting, it is not likely that it carries any biological weight, as the reversibility ip_a/ip_c ratios calculated here are a reflection of electron transfer to and from the MK-*n* analogue and the electrode at the liposomal surface, and electron transfer in a biological system is not likely to happen at a cell surface but rather by membrane-bound enzymes such as hydrogenases, dehydrogenases and oxidoreductases.

Data obtained from diffusion coefficient analysis shows that MK-*n* analogues with shorter and less saturated isoprene side chains are likely to be freely soluble in the bulk water pool as opposed to being confined within the liposomal bilayer. This is shown by a decrease in the value for diffusion coefficient calculated for the longer and more saturated MK-*n* analogues such as MK-3 and MK-4 compared to those calculated for the shorter analogues MK-1 and MK-2 (Figure 2.5). This observation is further supported in the next chapter, Chapter 3, in which increasing concentrations of MK-2 relative to a phosphatidylcholine bilayer result in the emergence of an aqueous MK-2 species which can be observed via ^{1}H NMR.

References

1. Matarlo, J., Menaquinone Biosynthesis: An Antibacterial Target? *The FASEB Journal* **2016,** *30* (1_supplement), 612.2-612.2.
2. Nowicka, B.; Kruk, J., Occurrence, biosynthesis and function of isoprenoid quinones. *Biochimica et Biophysica Acta (BBA)-Bioenergetics* **2010,** *1797* (9), 1587-1605.
3. Seigler, D. S., Benzoquinones, naphthoquinones, and anthraquinones. In *Plant secondary metabolism*, Springer: 1998; pp 76-93.
4. Collins, M. D.; Jones, D., Distribution of isoprenoid quinone structural types in bacteria and their taxonomic implication. *Microbiological reviews* **1981,** *45* (2), 316.
5. Tekin, E.; Erkoc, S., Structural and electronic features of the ubiquinone and ubiquinol molecules: molecular dynamics and quantum chemical treatments. *Molecular Simulation* **2010,** *36* (10), 763-771.
6. Foo, C. S.-Y.; Pethe, K.; Lupien, A., Oxidative Phosphorylation—an Update on a New, Essential Target Space for Drug Discovery in Mycobacterium tuberculosis. *Applied Sciences* **2020,** *10* (7), 2339.
7. Maloney, P. C.; Kashket, E.; Wilson, T. H., A protonmotive force drives ATP synthesis in bacteria. *Proceedings of the National Academy of Sciences* **1974,** *71* (10), 3896-3900.
8. Rao, S. P.; Alonso, S.; Rand, L.; Dick, T.; Pethe, K., The protonmotive force is required for maintaining ATP homeostasis and viability of hypoxic, nonreplicating Mycobacterium tuberculosis. *Proceedings of the National Academy of Sciences* **2008,** *105* (33), 11945-11950.
9. Treberg, J. R.; Quinlan, C. L.; Brand, M. D., Evidence for two sites of superoxide production by mitochondrial NADH-ubiquinone oxidoreductase (complex I). *Journal of Biological Chemistry* **2011,** *286* (31), 27103-27110.
10. Kurosu, M.; Begari, E., Vitamin K2 in electron transport system: are enzymes involved in vitamin K2 biosynthesis promising drug targets? *Molecules* **2010,** *15* (3), 1531-1553.
11. Paudel, A.; Hamamoto, H.; Panthee, S.; Sekimizu, K., Menaquinone as a potential target of antibacterial agents. *Drug discoveries & therapeutics* **2016,** *10* (3), 123-128.
12. Wakeman, C. A.; Hammer, N. D.; Stauff, D. L.; Attia, A. S.; Anzaldi, L. L.; Dikalov, S. I.; Calcutt, M. W.; Skaar, E. P., Menaquinone biosynthesis potentiates haem toxicity in S taphylococcus aureus. *Molecular microbiology* **2012,** *86* (6), 1376-1392.
13. Collins, M.; Jonse, D.; Goodfellow, M.; Minnikin, D., Isoprenoid quinone composition as a guide to the classification of Listeria, Brochothrix, Erysipelothrix and Caryophanon. *Microbiology* **1979,** *111* (2), 453-457.
14. Upadhyay, A.; Fontes, F. L.; Gonzalez-Juarrero, M.; McNeil, M. R.; Crans, D. C.; Jackson, M.; Crick, D. C., Partial saturation of menaquinone in Mycobacterium tuberculosis: function and essentiality of a novel reductase, MenJ. *ACS central science* **2015,** *1* (6), 292-302.
15. Krogstad, D.; Howland, J., Role of menaquinone in Corynebacterium diphtheriae electron transport. *Biochimica et Biophysica Acta (BBA)-Enzymology and Biological Oxidation* **1966,** *118* (1), 189-191.
16. Panthee, S.; Paudel, A.; Hamamoto, H.; Uhlemann, A.-C.; Sekimizu, K., Alteration of menaquinone isoprenoid chain length and antibiotic sensitivity by single amino acid substitution in HepT. *bioRxiv* **2020**.
17. Wang, Y.; Jiang, Y., *Chemotaxonomy of actinobacteria*. InTech: 2016.

18. Collins, M.; Goodfellow, M.; Minnikin, D.; Alderson, G., Menaquinone composition of mycolic acid-containing actinomycetes and some sporoactinomycetes. *Journal of applied bacteriology* **1985,** *58* (1), 77-86.
19. Koehn, J. T.; Magallanes, E. S.; Peters, B. J.; Beuning, C. N.; Haase, A. A.; Zhu, M. J.; Rithner, C. D.; Crick, D. C.; Crans, D. C., A synthetic isoprenoid lipoquinone, menaquinone-2, adopts a folded conformation in solution and at a model membrane interface. *The Journal of organic chemistry* **2017,** *83* (1), 275-288.
20. Koehn, J. T.; Beuning, C. N.; Peters, B. J.; Dellinger, S. K.; Van Cleave, C.; Crick, D. C.; Crans, D. C., Investigating Substrate Analogues for Mycobacterial MenJ: Truncated and Partially Saturated Menaquinones. *Biochemistry* **2019,** *58* (12), 1596-1615.
21. Prince, R. C.; Leslie Dutton, P.; Malcolm Bruce, J., Electrochemistry of ubiquinones: menaquinones and plastoquinones in aprotic solvents. *FEBS letters* **1983,** *160* (1-2), 273-276.
22. Staley, P. A. The Electrochemistry of Quinones in Aprotic Solvents. UC San Diego, 2016.
23. Guin, P. S.; Das, S.; Mandal, P., Electrochemical reduction of quinones in different media: a review. *International Journal of Electrochemistry* **2011,** *2011*.
24. Rich, P. R., Electron transfer reactions between quinols and quinones in aqueous and aprotic media. *Biochimica et Biophysica Acta (BBA)-Bioenergetics* **1981,** *637* (1), 28-33.
25. Sohlenkamp, C.; Geiger, O., Bacterial membrane lipids: diversity in structures and pathways. *FEMS microbiology reviews* **2016,** *40* (1), 133-159.
26. Strahl, H.; Errington, J., Bacterial membranes: structure, domains, and function. *Annual review of microbiology* **2017,** *71*, 519-538.
27. Bansal-Mutalik, R.; Nikaido, H., Mycobacterial outer membrane is a lipid bilayer and the inner membrane is unusually rich in diacyl phosphatidylinositol dimannosides. *Proceedings of the National Academy of Sciences* **2014,** *111* (13), 4958-4963.
28. Hoyo, J.; Guaus, E.; Oncins, G.; Torrent-Burgues, J.; Sanz, F., Incorporation of ubiquinone in supported lipid bilayers on ITO. *The Journal of Physical Chemistry B* **2013,** *117* (25), 7498-7506.
29. Frei, B.; Kim, M. C.; Ames, B. N., Ubiquinol-10 is an effective lipid-soluble antioxidant at physiological concentrations. *Proceedings of the National Academy of Sciences* **1990,** *87* (12), 4879-4883.
30. Koehn, J. T.; Crick, D. C.; Crans, D. C., Synthesis and characterization of partially and fully saturated menaquinone derivatives. *ACS omega* **2018,** *3* (11), 14889-14901.
31. Payne, R. J.; Daines, A. M.; Clark, B. M.; Abell, A. D., Synthesis and protein conjugation studies of vitamin K analogues. *Bioorganic & medicinal chemistry* **2004,** *12* (22), 5785-5791.
32. Suhara, Y.; Wada, A.; Tachibana, Y.; Watanabe, M.; Nakamura, K.; Nakagawa, K.; Okano, T., Structure–activity relationships in the conversion of vitamin K analogues into menaquinone-4. Substrates essential to the synthesis of menaquinone-4 in cultured human cell lines. *Bioorganic & medicinal chemistry* **2010,** *18* (9), 3116-3124.
33. Neghmouche, N.; Lanez, T., Calculation of electrochemical parameters starting from the polarization curves of ferrocene at glassy carbon electrode. *International Letters of Chemistry, Physics and Astronomy* **2013,** *4*, 37-45.
34. Aristov, N.; Habekost, A., Cyclic voltammetry-A versatile electrochemical method investigating electron transfer processes. *World J. Chem. Educ* **2015,** *3* (5), 115-119.

35. Toledano, T.; Sazan, H.; Mukhopadhyay, S.; Alon, H.; Lerman, K.; Bendikov, T.; Major, D. T.; Sukenik, C. N.; Vilan, A.; Cahen, D., Odd–even effect in molecular electronic transport via an aromatic ring. *Langmuir* **2014,** *30* (45), 13596-13605.
36. Chen, J.; Giroux, T. J.; Nguyen, Y.; Kadoma, A. A.; Chang, B. S.; VanVeller, B.; Thuo, M. M., Understanding interface (odd–even) effects in charge tunneling using a polished EGaIn electrode. *Physical Chemistry Chemical Physics* **2018,** *20* (7), 4864-4878.
37. Jiang, L.; Sangeeth, C. S.; Nijhuis, C. A., The origin of the odd–even effect in the tunneling rates across EGaIn junctions with self-assembled monolayers (SAMs) of n-alkanethiolates. *Journal of the American Chemical Society* **2015,** *137* (33), 10659-10667.
38. Newcomb, L. B.; Tevis, I. D.; Atkinson, M. B.; Gathiaka, S. M.; Luna, R. E.; Thuo, M., Odd–even effect in the hydrophobicity of n-alkanethiolate self-assembled monolayers depends upon the roughness of the substrate and the orientation of the terminal moiety. *Langmuir* **2014,** *30* (40), 11985-11992.
39. Feng, Y.; Dionne, E. R.; Toader, V.; Beaudoin, G.; Badia, A., Odd–even effects in electroactive self-assembled monolayers investigated by electrochemical surface plasmon resonance and impedance spectroscopy. *The Journal of Physical Chemistry C* **2017,** *121* (44), 24626-24640.
40. Niesner, R.; Heintz, A., Diffusion coefficients of aromatics in aqueous solution. *Journal of Chemical & Engineering Data* **2000,** *45* (6), 1121-1124.
41. Gharagheizi, F., Determination of diffusion coefficient of organic compounds in water using a simple molecular-based method. *Industrial & engineering chemistry research* **2012,** *51* (6), 2797-2803.

Chapter 3: ^{1}H NMR Analysis of the Conformation and Location of Menaquinone-2 in Phosphatidylcholine Liposomes

3.1. Menaquinone Odd-Even Redox Properties in Chapter Two may be Resultant from Interactions with Phosphatidylcholine Lipids and Conformation Within a Bilayer

Menaquinones, as stated in the previous chapter, are lipoquinone electron transporters which function to shuttle electrons to and from membrane-bound protein complexes in the electron transport systems (ETS) of a number of Gram-positive and Gram-negative obligate anaerobes, including *Mycobacterium tuberculosis, Staphylococcus aureus,* and *Listeria monocytogenes*, pathogens which play a role in human disease worldwide.[1-3] They consist of a naphthoquinone head group covalently bound to an isoprene tail of varying length, and saturation.[4-6] In the species which produce menaquinone as their sole electron transporter, there is often a specific analogue of menaquinone which is produced; for example, *Mycobacterium tuberculosis* produces MK9(II-H_2), or menaquinone with nine isoprene units, selectively saturated at the beta-position.[7-8] While it is clear that there are inherent preferences in which menaquinone species is produced by each organism and the function of menaquinones as an electron transporter are clear, it is not clear why different species may produce different analogues and what advantages may lie therein.[9-10]

Work in the previous chapter, which examined the impact of chain length and saturation in synthesized truncated menaquinone analogues confined to a liposomal bilayer, shows that there may be an odd-even effect at play with respect to the electrochemical properties of the truncated menaquinones and the number of isoprene units in the side chain. A single isoprene unit consists of four carbon units with a methyl group attached (2-methyl-1,3-butadiene), making

the carbon length of the side chain of the MK-*n* analogue an even number for all analogues; however, it is possible that each isoprene unit is held in such a conformation in this environment that may account for the observation of an odd-even effect in the electrochemistry of the MK-*n* analogues. Results from examining half wave potentials ($E_{1/2}$) of truncated menaquinones shown in Figure 2.3 showed that while there may not be a significant difference in $E_{1/2}$ between fully unsaturated analogues, as the number of saturations in the side chain increases the compounds require either more negative potentials (even length) or slightly more positive potentials (odd length). It is hypothesized that, similar to other studies in which the redox active molecule is immobilized on a surface, this may be due to their confinement within the bilayer and the conformation and lipid interactions that they adopt as a result.[11-12] A similar odd-even effect has been documented extensively in electrochemical studies of odd- and even-length hydrocarbon chains in self-assembled monolayers, and though it is well-known it is poorly understood.[13-15] It is possible that the same effect is happening in the MK-*n* analogues studied in the previous chapter. The odd-even effect here could be due to differences in the orientations of the plane of the naphthoquinone head group and isoprene side chain with respect to the outer leaflet of the liposome, which is exposed to the electrodes surface.

To begin to determine what may be causing this observed odd-even effect, 1D and 2D ^{1}H NMR were used to probe the location and conformation of menaquinone-2 (MK-2) within egg phosphatidylcholine (EPC) liposomes rather than the soybean PC used in the last chapter. Phosphatidylcholine lipids are used so that data obtained with MK may be compared with that of ubiquinone, which is frequently studied in the context of lipids found in eukaryotic cells, particularly phosphatidylcholine. In addition to the ability to compare to data gathered with ubiquinone in a liposomal context, EPC used here has higher purity (in addition to being the

most cost-effective option) than soybean PC used for experiments in the previous chapter, making it much more suitable for ^{1}H NMR analysis. In this study, EPC liposomes are used to examine the conformation as well as the behavior and characteristics of MK-2 at increasing concentrations relative to the EPC used to form liposomes to determine what effect MK-2 may have on the bilayer at these elevated concentrations compared to their concentrations in a biological membrane (4.3 ng/10^{8} CFU in *Mycobacterium smegmatis*).[7] Work performed here found that at higher concentrations of MK-2 relative to PC, the compound resides at the outer edge of the bilayer's inner or outer leaflet in an aqueous environment, as evidenced by 1D ^{1}H NMR and 2D ^{1}H -^{1}H NOESY spectroscopic analysis. Dynamic light scattering analysis was performed to verify the formation of liposome vesicles after extrusion and to examine differences in vesicle sizes with increasing concentrations of MK-2 relative to PC. While this study alone is not enough to determine why we observe an odd-even effect with regards to the redox properties of MK in a liposomal bilayer, it lays the foundation for the further study of similar compounds (such as MK-2 with increasing saturations in the isoprenyl side chain. In addition, the work here finds that at the concentrations used to make MK-*n* containing liposomes in the previous chapter, it is likely that some of the MK-2 compound is located just at the outer leaflet of the liposome in an aqueous environment or in the aqueous environment itself in small concentrations, which may account for the higher diffusion coefficient values observed for MK-1 as well as MK-2.

3.2. Materials and Methods

3.2.1. General Methods

Reagents were purchased and used without further purification including L-α-phosphatidylcholine from egg yolk, Type XVI-E (≥99%, Millipore Sigma), chloroform (99.8%,

Sigma-Aldrich), deuterium oxide (D_2O, 99.9%, Cambridge Isotope Laboratories), and tetramethylsilane (TMS, 99.9%, Cambridge Isotope laboratories). Menaquinone-2 was synthesized in the lab as described previously [6]. Distilled deionized water (DDI H_2O) for DLS experiments was purified with a Barnstead E-pure system (~18 MΩ cm). All pH measurements were conducted using a Thermo Orion 2 Star pH meter with a VWR semimicro pH probe. When conducting NMR experiments, deuterium oxide was used as the aqueous solvent, so the pH was adjusted to consider the presence of deuterium (pD = 0.4 +pH).[16-17] The pD was adjusted using 0.1 M solutions of DCl and NaOD, and since pD is customarily referred to as pH, for the remainder of the manuscript we refer to the pD as pH.

3.2.2. Preparation of MK-2 and Control Liposomes for 1D and 2D ^{1}H NMR

Large unilamellar vesicles (LUV) of homogeneous size were prepared with L-α-phosphatidylcholine from egg yolk (EPC) in pure D_2O in 1 mL batches. Each MK-2 liposome sample was made with the appropriate mass of MK-2 for 4, 6, 8, and mg/mL MK-2 with a total sample concentration of MK and PC of 100 mg/mL (corresponding to molar ratios of MK-2:PC of 1:10, 1:6, 1:5, and 1:3 respectively). Briefly, EPC and MK-2 are dissolved in 15 mL of $CHCl_3$ in a round bottom flask. The $CHCl_3$ is evaporated under vacuum to create a dried film of only lipids (control) or lipids and MK-2 at the bottom of the flask, which is then rehydrated by gently agitating in the presence of D_2O at pH 7.39 in a water bath heated to 45˚C, resulting in large multilamellar vesicles. The solution of multilamellar vesicles of heterogeneous size is then extruded using an Avanti Mini-Extruder incubated at 45˚C and passed through a polycarbonate filter (Whatman Nucleopore Track-Etch Membrane, 110606, 25 mm) with pore size of 0.1 μm to form a solution of LUV of homogeneous size.

3.2.3. 1D ^{1}H NMR Spectroscopy of MK-2 liposomes

Data was collected using a Varian model MR400 operating at 400 MHz using routine parameters (1.0 s relaxation time, 25°C temperature control and 45° pulse angle). Liposomal spectra are referenced to the HOD peak, which is determined by using tetramethylsilane (TMS) as an internal reference in D_2O alone prior to collecting each spectrum. The NMR instrument was locked onto the deuterium signal from D_2O and each spectrum was collected using 64 scans per sample. The data were processed using MestReNova NMR processing software version 10.0.1. The spectra were manually phased and the baseline was corrected using a Bernstein polynomial fit (polynomial order 3).

3.2.4. ^{1}H-^{1}H 2D NOESY spectroscopy of MK-2 liposomes

2D NMR spectroscopic studies in liposomal solutions were carried out on a Varian model MR400 magnet operating at 400 MHz at 25°C. A standard NOESY pulse sequence consisting of 256 transients with 16 scans in the f1 direction using a 200 ms mixing time, 45° pulse angle, and relaxation delay of 2.0 s. The instrument was locked onto the deuterium signal from D_2O and the spectrum was referenced to the HOD peak as previously described. The resulting spectrum was processed using MestReNova NMR software version 10.0.1 as previously described.
To obtain visual aids of MK-2 conformations Merck molecular force field 94 (MMFF94) molecular mechanics simulations were conducted using ChemBio3D Ultra 12.0 at 25˚C. Starting conformations were obtained from ChemDraw structures or by rotating desired bonds and then either had simulations run or simply an anergy minimization to achieve the desired conformation.

3.2.5. Preparation of MK-2 and Control Liposomes for DLS

LUVs of homogeneous size were prepared from PC in diH_2O in 1mL batches, similar to

the preparation of LUVs for NMR analysis. MK-2 and PC were dissolved in $CHCl_3$ to make stock solutions of 1 mg/100 µL and 1 mg/10 µL, respectively (6.4 mg MK-2 in 640 µL $CHCl_3$ and 94 mg EPC in 940 µL $CHCl_3$). Samples were made by adding appropriate volumes of each stock solution to a round bottom flask to contain 4, 6, 8, and 12% MK-2 relative to PC (w/w%) with a total combined mass of PC and MK-2 of 20 mg in 1 mL samples and the same molar ratios of MK-2:PC as were used for ^1H NMR analysis. A control sample consisting of pure PC was also implemented. $CHCl_3$ was evaporated to create a dried film of lipids, and DDI H_2O at pH 7.0 was added to the lipid film for a total final sample concentration of 20 mg/mL. LUVs of homogeneous size are prepared using the same method as those made for NMR analysis by using an Avanti Mini-Extruder and polycarbonate filter with pore size of 0.1 µm.

3.2.6. DLS Measurements of MK-2 Liposomes

DLS measurements were carried out using a Zetasizer nano-ZS at 25°C. Each measurement consisted of a 600 s equilibration time followed by 10 acquisitions consisting of 15 scans for each acquisition. The data was analyzed using Zetasizer software and the values reported in Table 3.1 are the average of triplicate sample measurements. For statistical analysis of DLS data, a standard t-test and one-way ANOVA were performed using Graphpad Prism 84.3 software. A p-value lower than 0.05 was used as an indicator of statistical significance.

3.3. Results and Discussion

3.3.1. DLS analysis of Liposomes with increasing MK-2 concentration

In order to confirm that liposomes of the appropriate size were formed (100nm) as well as determine any effects that the increasing concentration of MK-2 may have on the size of the vesicle, dynamic light scattering (DLS) was used according to the methods laid out in the experimental section.

Table 3.1. Dynamic light scattering measurements of EPC liposomes containing increasing concentrations of MK-2.

Sample	Size (d.nm)	Standard Deviation (d.nm)	Polydispersity Index
Empty liposome	162	51.0	0.082
4 mg/mL MK-2	153	47.7	0.091
6 mg/mL MK-2	164	55.6	0.137
8 mg/mL MK-2	174	67.4	0.145
12 mg/mL MK-2	184	78.7	0.165

DLS measurements presented here are an average of triplicate measurements and show that there seems to be some minor effect on the liposomes by MK-2, in which increasing concentrations cause increased vesicle size after an initial drop in vesicle diameter compared to control upon addition of 4 mg/mL MK-2. However, these results are not statistically significant as determined by a one-way ANOVA as detailed in the experimental section. While the standard deviation within samples is high, the PDI is defined as the standard deviation of the particle diameter distribution, divided by the mean particle diameter. It is thus a tool in DLS used to estimate the average uniformity of a particle solution, with larger values corresponding to larger size distribution in the sample. An acceptable PDI for distribution of particle size is typically defined as PDI<0.2, as seen in the samples above.[18-19]

3.3.2. ^{1}H NMR Analysis of MK-2 Liposomes with Increasing Concentrations of MK-2

Samples containing a total of 100 mg of EPC and MK-2 were prepared to make vesicles containing varying concentrations of MK-2 (0, 4, 6, 8, and 12 mg/mL, or molar ratios of MK-2 to PC of 1:10, 1:6, 1:5, and 1:3 respectively) in 1mL total of D_2O as described in the experimental methods. ^{1}H NMR spectra of each liposome formulation were recorded at 300K, well above the gel-to-liquid phase transition of the EPC, which is reported to be between 243 and 253, with the proton labeling scheme shown in Figure 3.1.

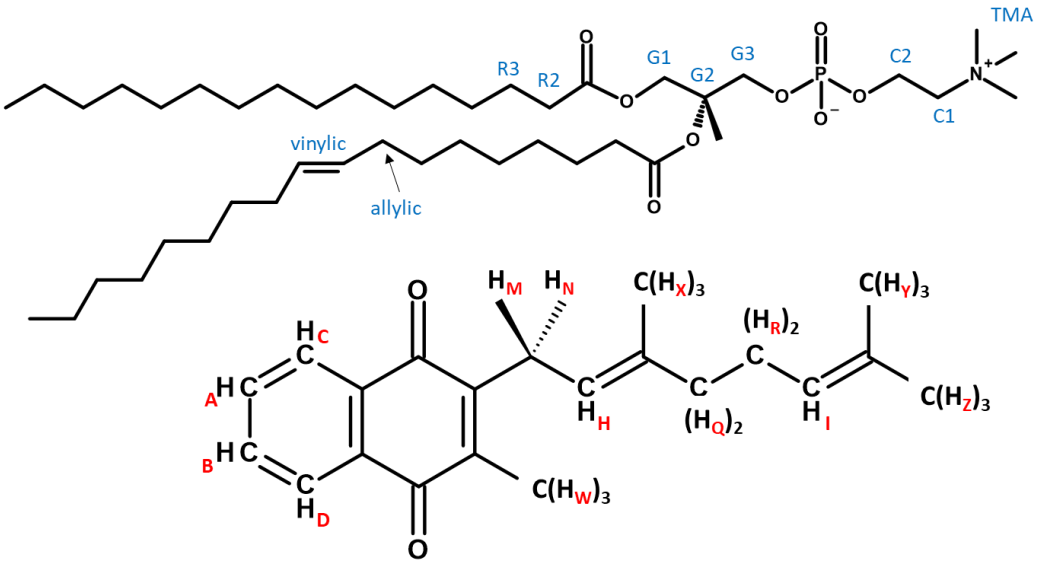

Figure 3.1. Proton labeling scheme of MK-2 (shown bottom, red proton labels) and EPC (shown top, blue proton labels) used in the following NMR spectra.

Results obtained with MK-2 and EPC controls in D_2O are in good agreement with what has previously been published in our lab as well as literature. [20-21] MK-2 peaks are readily observed in all spectra containing both PC liposomes and MK-2 alone in D_2O (Figure 3.2).

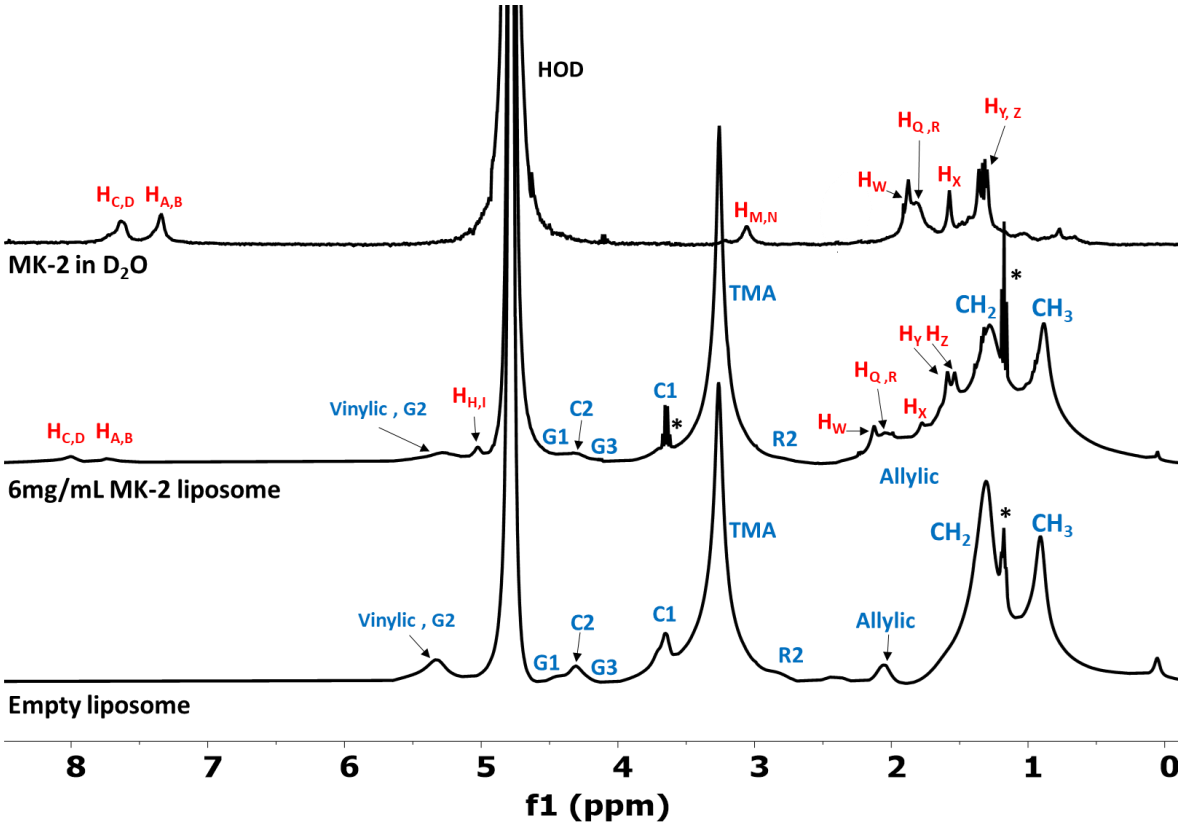

Figure 3.2. Stacked ^{1}H NMR spectra of MK-2 in D_2O alone (top), 6mg/mL MK-2 liposome (middle), and empty EPC vesicles (bottom). Spectra are labeled according to Figure 3.1. Black asterisks (*) denote an impurity as a result of residual ethanol.

As can be seen in Figure 3.2, the chemical shifts of MK-2 in the context of the EPC bilayer are shifted slightly downfield compared to their chemical shift in D_2O alone. Due to this slight downfield shift of liposomal MK-2 relative to its chemical shifts in D_2O, MK-2 peaks H_M and H_N within the bilayer are occluded by the trimethylamine (TMA) peak of the EPC, and the liposome-bound $H_{H,I}$ peak is visible just downfield of the HOD peak rather than appearing as a barely discernable shoulder to the left of the HOD peak. All other MK-2 peaks are easily observed within the context of the bilayer. The slight downfield shift of liposomal MK-2 relative to aqueous MK-2 indicates that the compound is likely in a more charged environment than it is in D_2O alone. This would be consistent with MK-2 being located near the lipid-water interface, in the region of the charged phosphate group and acyl groups of the EPC (Figure 3.1).

In order to determine if the downfield shift of MK-2 in the context of the EPC bilayer remains consistent or changes as the concentration of MK-2 increases, samples containing 4, 6, 8, and 12 mg/mL MK-2 were analyzed via ^{1}H NMR and compared to MK-2 in D_2O and empty liposome controls (Figure 3.3).

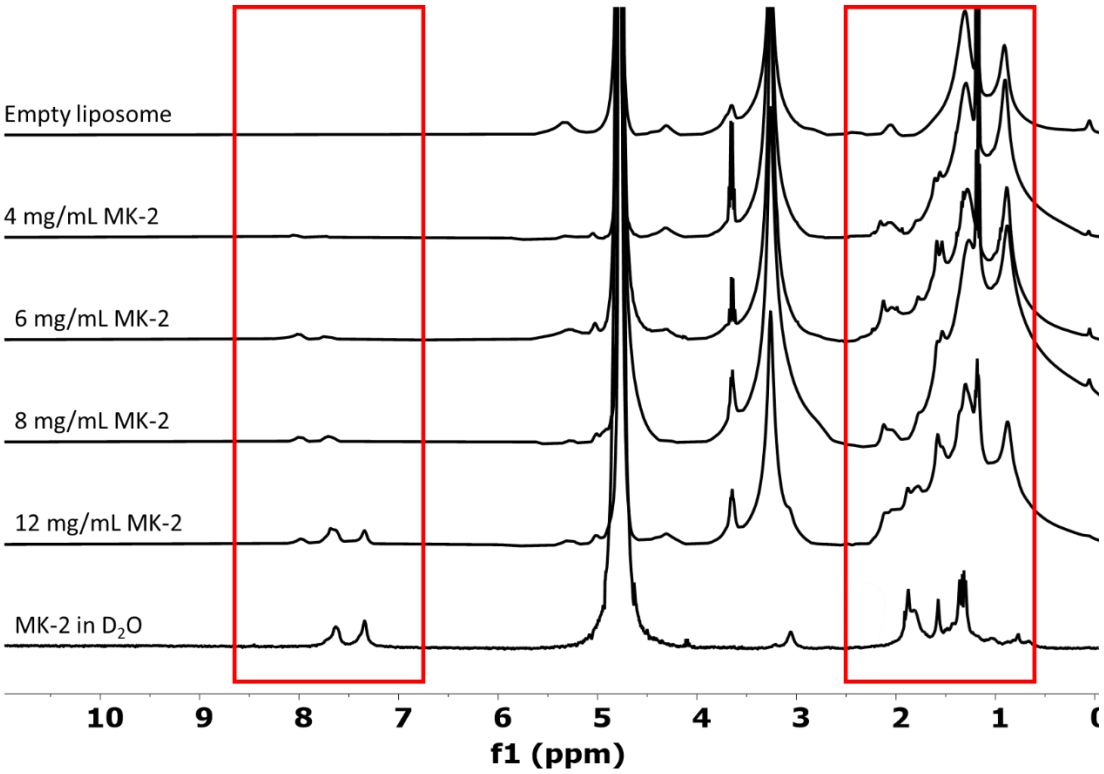

Figure 3.3. Stacked ^{1}H NMR spectra of EPC liposomes containing increasing concentrations of MK-2. Red boxes highlight major areas of change in the appearance of MK-2 peaks with increasing MK-2 concentration. Boxes highlighted in red are shown zoomed in and annotated below in Figures 3.4 (MK-2 head group protons, left) and 3.5 (MK-2 isoprenyl side chain protons, right).

Differences between the spectra as the concentration of MK-2 increases appear subtle at first, with the most prominent difference being visible in the head group peaks of MK-2 ($H_{A,B}$ and $H_{C,D}$) between 7 and 8 ppm (Figure 3.3). As the concentration of MK-2 increases from 6 to 8 mg/mL, the appearance of an additional peak, barely discernable, at 7.35 ppm occurs, at at 12 mg/mL this extra peak becomes more prominent (Figure 3.3, 3.4). Integration of the three peaks at 8.00, 7.68, and 7.35 ppm in the 12 mg/mL sample reveals a 1:2:1 ratio, and the 7.35 ppm peak

that appears at higher concentrations of MK-2 coincides with the $H_{A,B}$ peak of MK-2 in D_2O alone, indicating the possibility that at higher concentrations (~8 mg/mL or 8% MK-2 relative to EPC) the MK-2 is localized further out of the liposomal interface near the phosphate groups and acyl chains, and further into the water pool.

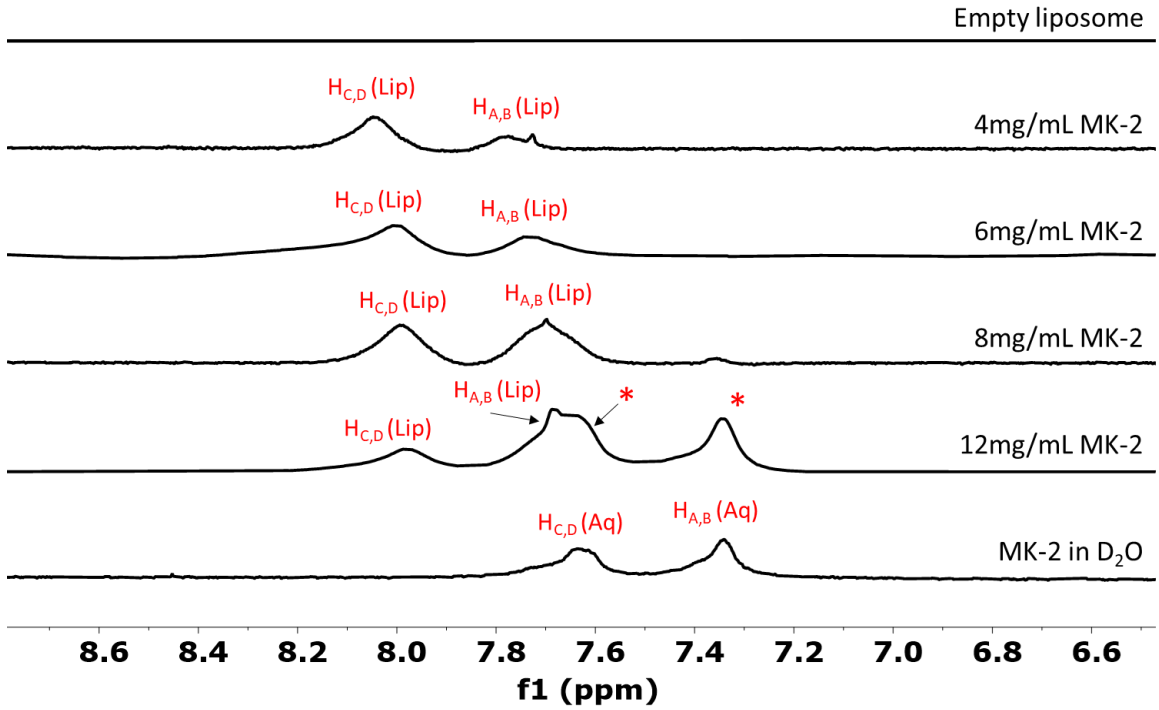

Figure 3.4. Comparison of head group ^1H NMR chemical shifts of MK-2 in EPC liposomes with its shifts in D_2O alone. Red asterisks (*) denote the appearance of peaks in the 12 mg/mL MK-2 spectrum that correlate to MK-2 peaks in D_2O alone. Small impurity at 7.73 ppm in 4 mg/mL and 8 mg/mL samples correspond to a slight impurity from residual $CHCl_3$.

Further comparison of the 12 mg/mL sample of MK-2 to its counterparts with decreased MK-2 concentration show the appearance of a peak at 3.06 ppm that coincides with the $H_{M,N}$ peak in the aqueous MK-2 spectrum, as well as the appearance of several small peaks in the region from 1.0-2.0 ppm where the aqueous peaks corresponding to the isoprene tail of MK-2 reside (H_W, H_X, $H_{Q,R}$, $H_{Y,Z}$) (Figure 3.5).

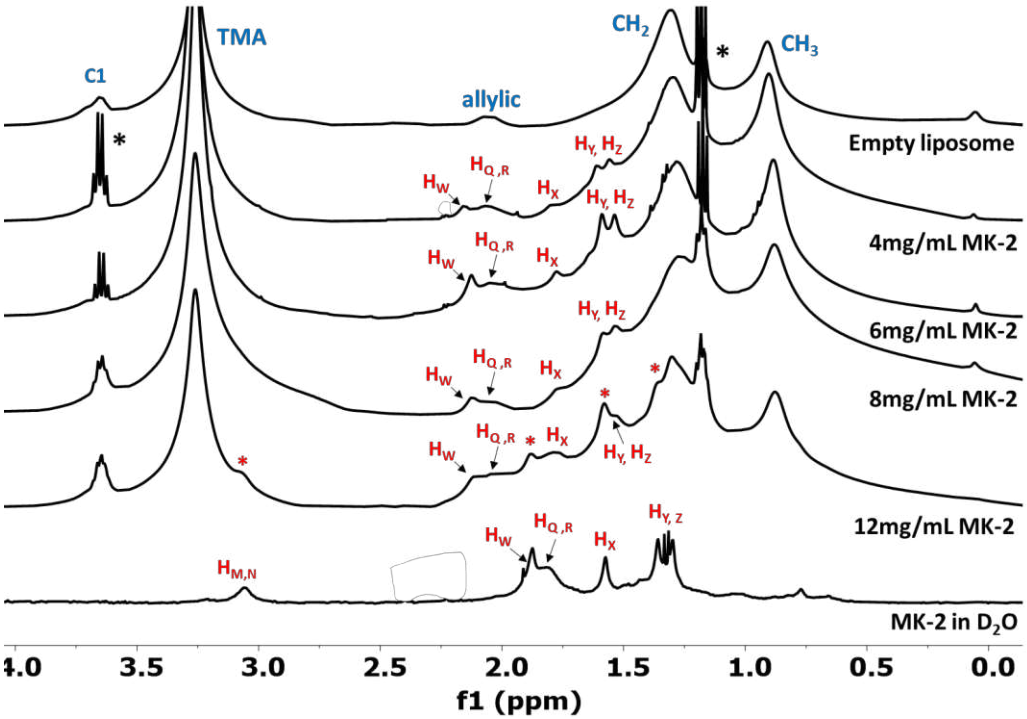

Figure 3.5. Comparison of ^{1}H NMR chemical shifts of MK-2 isoprene protons in EPC liposomes. Red asterisks (*) on the 12 mg/mL spectrum denote the appearance of peaks in the liposomes which coincide with MK-2 peaks in the aqueous spectrum. Black asterisks (*) indicate a slight impurity as a result of residual ethanol.

The appearance of peaks belonging to protons in the MK-2 isoprenyl chain which correspond to their peaks in D_2O alone further suggests that MK-2 is in two environments at higher concentrations: a liposome-bound environment and an aqueous one. It is possible that at higher concentrations of MK-2 relative to PC, the MK-2 is pushed out of the bilayer and into the surrounding aqueous environment, which contribute to the appearance of these additional upfield chemical shifts at higher concentrations. Notably, the additional shifts in the 12 mg/mL spectrum of MK-2 in PC liposomes coincide perfectly with the chemical shifts corresponding to protons Hw, $H_{Q,R}$, H_X, and $H_{Y,Z}$ in D_2O alone.

3.3.3. ^{1}H-^{1}H 2D NOESY NMR Analysis of 6 mg/mL MK-2 Liposomes

In order to determine whether or not the appearance of additional peaks in the 12 mg/mL MK-2 NMR spectrum correspond to an aqueous, non-liposome bound species of MK-2, as well

as what conformation the MK-2 may adopt in each environment, the 2D NMR method ^{1}H-^{1}H 2D NOESY was used. First, the sample containing 6 mg/mL MK-2 was studied via 2D NOESY NMR, as this is the most concentrated sample of MK-2 that does not display the appearance of additional MK-2 peaks, and will be best suited to give information about the conformation and location of MK-2 when it is confined in a liposomal bilayer. Additional experiments were performed with ^{1}H-^{1}H 2D ROESY NMR, however, these spectra did not contain adequate information for analysis (Appendix IV).

The ^{1}H-^{1}H 2D NOESY spectrum of 6 mg/mL MK-2 in PC vesicles (Figure 3.6) shows NOE cross peaks between protons $H_{A,B}$ and protons $H_{Q,R}$ (very weak NOE cross peak), a stronger cross peak with protons $H_{Y,Z}$, with protons $H_{C,D}$ displaying cross peaks with the same protons. Head group protons $H_{C,D}$ also show NOE interactions with protons $H_{H,I}$, but this is not observed between $H_{H,I}$ and $H_{A,B}$. Protons $H_{H,I}$ display a strong NOE cross peak with $H_{Y,Z}$, and a medium NOE cross peak with H_X. Additionally, it appears that there may be an NOE cross peak between $H_{H,I}$ and either the allylic peak of PC or $H_{Q,R}$ peak of MK-2, however, owing to the overlap of the allylic PC peaks and the $H_{Q,R}$ peak of MK-2 bound by a liposomal environment it is difficult to distinguish whether the cross-talk peak corresponds to the allylic peak or $H_{Q,R}$**.** It is likely that a peak here corresponds to an interaction between $H_{Q,R}$ and $H_{H,I}$ due to their proximity within the molecule itself. Additionally, owing to the overlap of peaks $H_{M,N}$ with the HOD peak, it is difficult to distinguish NOE cross peaks between $H_{M,N}$ and any other MK-2 or lipid protons at the 6 mg/mL concentration. Proton H_W displays NOE cross peaks with $H_{Y,Z}$. This information together strongly suggests that MK-2 adopts a folded conformation in a liposomal environment.

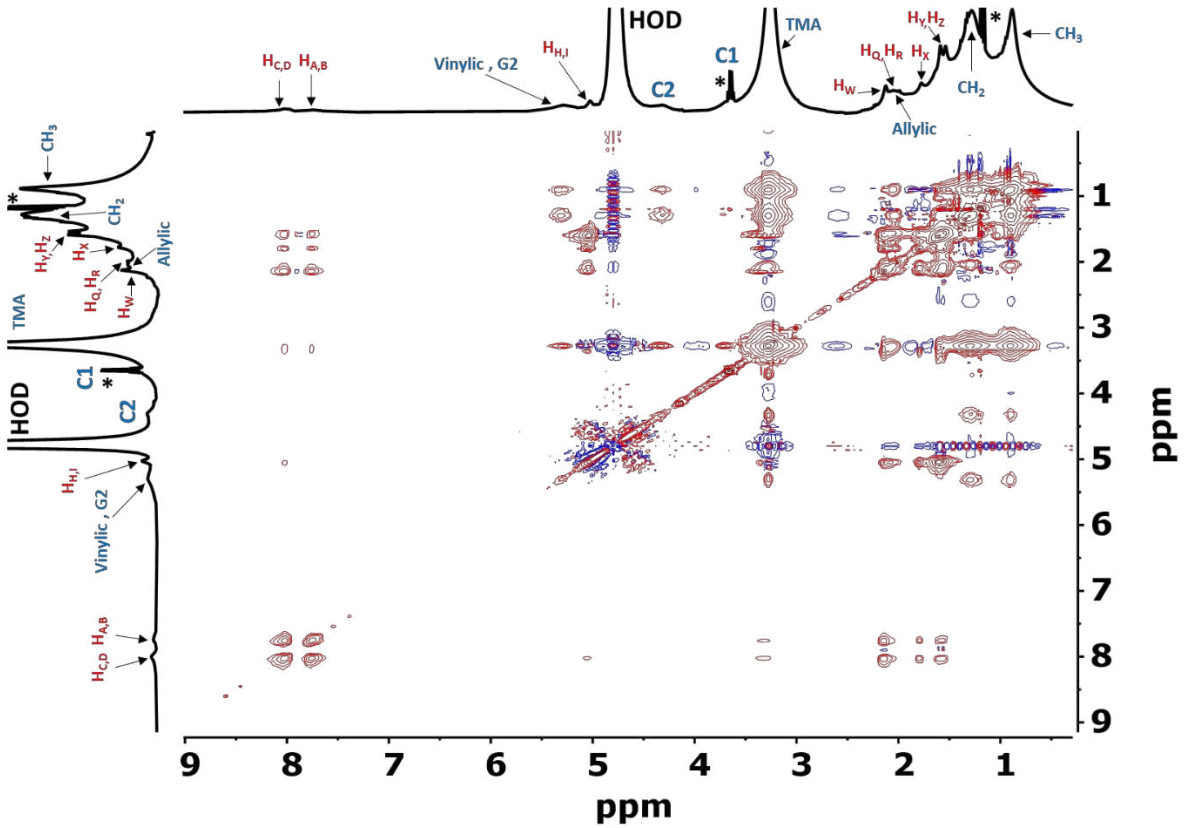

Figure 3.6. ^{1}H-^{1}H 2D NOESY spectrum of 6 mg/mL MK-2 in soybean PC liposomes. Red labels denote MK-2 peaks and blue labels denote PC peaks, as outlined in Figure 3.1. Black asterisks (*) denote a slight impurity as a result of residual ethanol.

From the spectrum in Figure 3.6, NOE cross peaks between the head group protons $H_{A,B}$ and $H_{C,D}$ with protons in the isoprene tail of MK-2 (weak interactions with H_W due to proximity of the protons on the molecule, a weak interaction with protons $H_{Q,R}$, and stronger interactions with $H_{Y,Z}$) are visible, as well as NOE cross talk between $H_{H,I}$ and $H_{C,D}$, indicating that H_I is likely located near the $H_{C,D}$ protons in space. Given the pattern of cross-talk that is displayed between protons on MK-2 as well as the similarity of these NOE cross peaks with previous work in the lab with MK-2 it is reasonable to conclude that MK-2, when confined in a bilayer, is in a folded conformation with the isoprene tail folded over in a way that causes it to have through-space interactions with the naphthoquinone head protons.[21]

Most MK-2 cross peaks and PC cross peaks display NOE interactions only within their

respective compounds (MK-2 peaks display cross talk with MK-2 peaks and PC peaks display cross talk with PC peaks), and there are very few EPC-MK-2 NOE interaction that are seen in the 6 mg/mL MK-2 NOESY spectrum that help to determine the placement of MK-2 bound in a liposome with regards to the bilayer. In this regard, it appears that protons $H_{A,B}$, $H_{C,D}$, and $H_{Y,Z}$ of the isoprene tail display NOE cross peaks with the trimethylamine (TMA) group of PC (Figure 3.6, 3.1). The slight downfield shift of the MK-2 protons in liposomes relative to their chemical shifts in water and the spatial proximity indicated by NOE cross peaks between TMA and $H_{Y,Z}$ and naphthoquinone head group protons $H_{A,B}$ and $H_{C,D}$ indicates that when confined in a liposomal bilayer, MK-2 resides mainly at the interface of the liposome, with the molecule folded such that the end of the isoprene tail interacts with the TMA group of the lipids. It is likely that the liposome-bound MK-2 resides just at the lipid water interface in the region of the phosphate and acyl groups of the lipid. This is further supported by the observation that there is no other lipid-MK-2 cross talk observed, as all the proton signals in that area are very faint or not present at all in the ^{1}H-^{1}H NOESY of 6 mg/mL MK-2. This conformation and location are also in good agreement with data that has previously been published in our lab on the placement and confirmation of MK-2 within AOT reverse micelles rather than liposomes.

3.3.4. 2D ^{1}H-^{1}H NOESY NMR of 12 mg/mL MK-2 liposomes.

In order to compare the chemical shifts and NOE cross peaks of liposome bound MK-2 with the appearance of additional peaks at 12 mg/mL MK-2 in liposomal spectra, ^{1}H-^{1}H 2D NOESY spectroscopy was used to examine the 12 mg/mL MK-2 liposomal sample. Like with the 6 mg/mL MK-2 sample, experiments were performed to collect the 2D ^{1}H-^{1}H ROESY spectrum of the 12 mg/mL sample, however, these spectra did not contain adequate information for analysis (Appendix IV).

The ^{1}H-^{1}H 2D NOESY spectrum of 12 mg/mL MK-2 in PC vesicles (Figure 3.7) is a much more complex spectrum, with the appearance of several new NOE cross peaks with the increase in MK-2 concentration relative to PC. Interestingly, looking first at the NOE peaks corresponding to the new head groups of MK-2, it becomes apparent that these new peaks only display NOE cross peaks with other peaks that emerged as a result of the increase in MK-2 concentration. There are no interactions of emergent peaks with MK-2 peaks associated with the MK-2 fraction that is presumed to be bound within the bilayer. It is also worth noting that peaks corresponding to liposome-bound MK-2 are very faint, indicating that the new species is likely much greater in concentration than the liposome-bound MK-2.

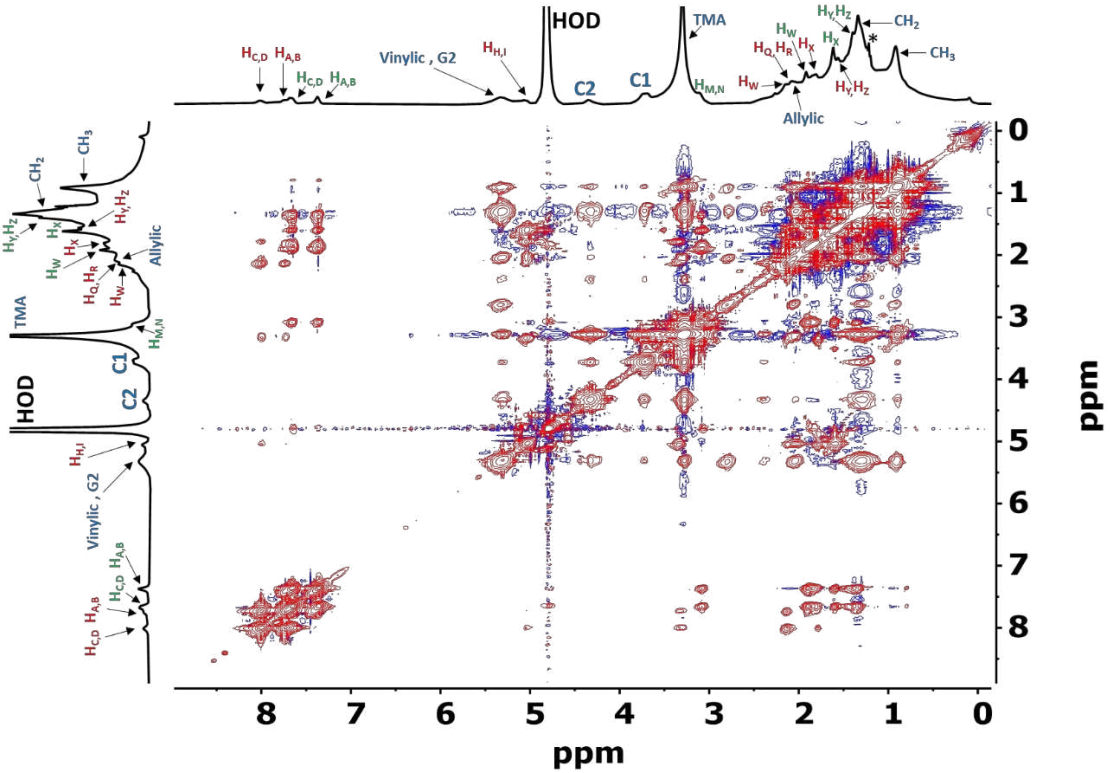

Figure 3.7. ^{1}H-^{1}H 2D NOESY NMR of 12 mg/mL MK-2 in EPC liposomes. Peaks marked in green denote peaks that likely correspond to aqueous MK-2 peaks at higher concentrations of MK-2 relative to PC. Black asterisk (*) denotes a slight impurity as a result of residual ethanol.

Similar to what was observed with the 6 mg/mL ^{1}H-^{1}H 2D NOESY of MK-2 in PC liposomes, the emergent peaks that likely correspond to a the head groups of MK-2 in a different environment (aqueous $H_{A,B}$, $H_{C,D}$ at 7.68 and 7.35 ppm respectively) show NOE cross peaks with peaks that correspond to MK-2 peaks in an aqueous environment in that there is clearly a strong NOE cross peak with $H_{A,B}$ and $H_{C,D}$ with $H_{Y,Z}$ (Figure 3.7). Unlike in the 6 mg/mL liposomal MK-2 spectrum, protons corresponding to aqueous MK-2 peaks $H_{C,D}$ at 7.68 ppm do not show NOE cross peaks between protons $H_{H,I}$, and the NOE cross peaks between $H_{A,B}$ or $H_{C,D}$ and protons $H_{Q,R}$ are very weak, indicating in this emergent set of peaks, that protons $H_{C,D}$ are not likely spatially near proton H_I or $H_{Q,R}$. Also, unlike in the 6 mg/mL spectrum, it is not possible to tell whether H_W is interacting with $H_{Y,Z}$ to further support a similar U-shaped conformation to what is seen in the liposome-bound MK-2 due to the increased number of peaks corresponding to MK-2 causing the diagonal near the MK-2 isoprene tail to become less distinguishable. This information suggests that even in an aqueous environment, MK-2 is still folded over on itself in a U-shaped conformation similar to what has been observed in the 6 mg/mL MK-2 NOESY spectrum and similar to what has previously been observed in other solvents, most notably DMSO.[6]

Similar to the 6 mg/mL MK-2 ^{1}H-^{1}H 2D NOESY spectrum, there are few EPC-MK-2 NOE cross peaks. Also similar to what is seen in the 6 mg/mL MK-2 NOESY spectrum, there are no peaks between MK-2 and HOD despite the compound likely being located at the edge of the liposomal interface near to the bulk water. This is likely due to the labile nature of the EPC head groups, MK-2 and water in solution: their transient interactions with each other make it unlikely to see any consistent NOE cross peaks. It initially appears that protons $H_{C,D}$ show an NOE cross peak with HOD; however, this is most likely protons $H_{C,D}$ displaying an NOE cross

peak with proton H_I, much like what is seen in the 6 mg/mL MK-2 sample, indicating that MK-2 is still tightly folded over itself. Given the observations of the NOE cross peaks of MK-2 protons with each other as well as the upfield shift of MK-2 protons at this higher concentration, it seems likely that as the concentration of MK-2 relative to PC increases, the MK-2 resides further at the edge of the bilayer, at the interface near bulk water. Its conformation appears to be U-shaped, similar to its liposome-bound form as well as its conformation in a variety of other solvents, with the head group and isoprene tail of the MK-2 pointing outward towards the outer edge of the liposomal bilayer.

3.3.5. Illustration of MK-2 Conformation in a Bilayer using Molecular Mechanics

Despite the short isoprenyl side chain of MK-2, there are enough carbons in the side chain that there are numerous degrees of rotational freedom, and thus even this short, truncated version of MK-2 is able to adopt several conformations based on what is most energetically favorable. In order to illustrate potential MK-2 conformations which correspond to the ^{1}H-^{1}H 2D NOESY spectral data collected and energy minima, and to provide a visual aid, molecular mechanics were performed. This work was done as it has been previously in our lab.[21] to determine possible conformations for MK-2 within a bilayer based on the ^{1}H-^{1}H 2D NOESY spectra of the 6 mg/mL and 12 mg/mL liposomal MK-2 spectra.

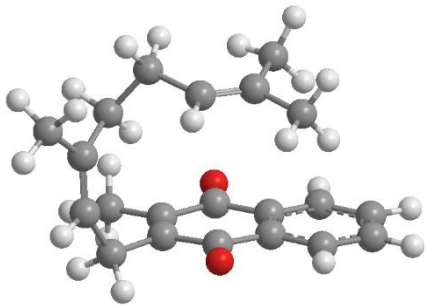

Figure 3.8. Possible conformation of liposome-bound as well as aqueous species of MK-2 using MMFF94 calculations to illustrate the conformations elucidated by 2D NMR studies. Possible structure determined by ^{1}H-^{1}H 2D NOESY NMR and MMFF94 calculations of liposomal-bound MK-2 (65.4 kcal/mol, internuclear distance $H_{H,I}$ - $H_{C,D}$ of 4.3 Å.

Based on the NOE cross peaks observed in 6 mg/mL and 12 mg/mL MK-2 liposomal samples, there is little to no difference between the conformations of MK-2 which is bound by the liposome and MK-2 which is located at the outer leaflet of the liposome in the region of the bulk surrounding water. Of particular note is that in the 6 mg/mL MK-2 ^{1}H-^{1}H 2D NOESY spectrum, there was a small NOE cross peak observed between $H_{C,D}$ and $H_{H,I}$, indicating that $H_{C,D}$ is within 5 Å of peak $H_{H,I}$, likely corresponding to proton H_I, and this NOE cross peak is also present in the 12 mg/mL spectrum of MK-2 in ^{1}H NMR peaks which correspond to the aqueous species of MK-2. All other cross talk peaks within the MK-2 compound either in aqueous or liposome-bound form remain the same. This information together indicates that the liposome-bound MK-2 as well as MK-2 which is at the edge of the liposomal interface and more associated with the bulk water environment adopt the same conformation, as evidenced by similarities in intramolecular distance indicated by NOE peaks between $H_{C,D}$ and $H_{H,I}$ in both samples. (Figure 3.8, 3.9).

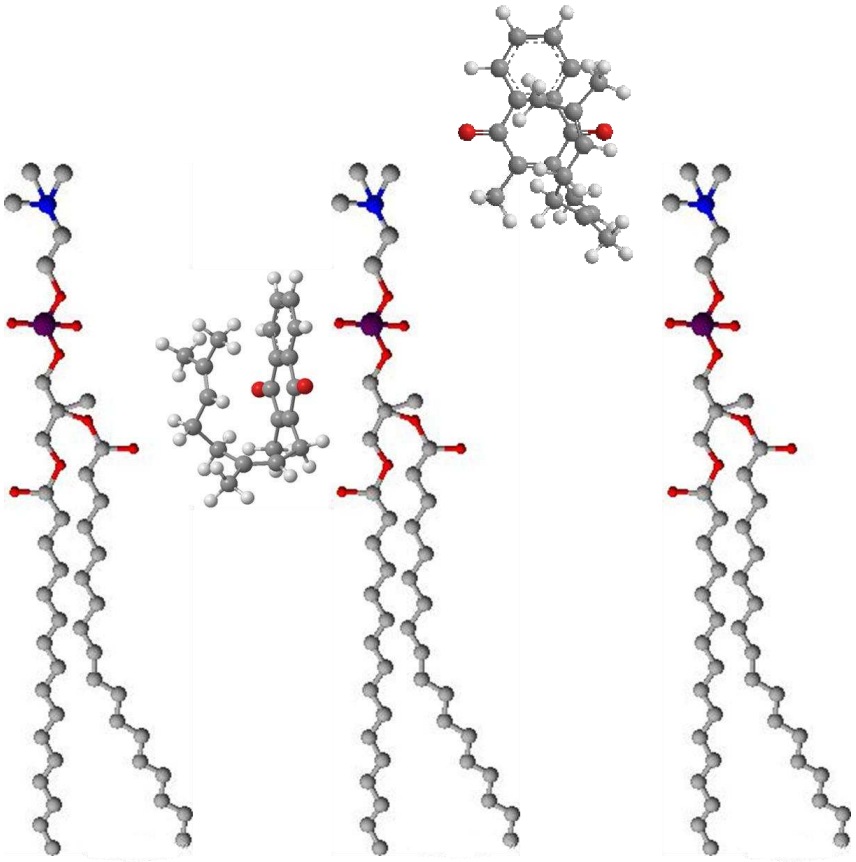

Figure 3.9. Likely location of MK-2 in a PC liposome in the liposome bound environment (left) and at higher concentrations when it is located at the edge of the bilayer (right).

After determination of the NOE cross peaks that MK-2 has with itself in both a liposome-bound and aqueous environment as well as the cross peaks that MK-2 shares with both lipid and solvent peaks as detailed in sections 3.3.2 and 3.3.3, the placement of liposome-bound MK-2 is likely just within the liposomal interface in the region of the phosphate groups and acyl chains, with head group and isoprene tail pointing towards the outer liposomal leaflet. At increasing concentrations of MK-2 relative to PC when MK-2 is located at the edge of the bilayer and loosely associated with the interface in the bulk water environment, it likely still resides at the surface of the liposome with the naphthoquinone head group protons and the isoprene tail interacting with water.

3.4. Conclusions

Previous research in our lab has examined the conformation of MK-2 in a number of aprotic solvents (pyridine, acetonitrile and DMSO) as well as AOT reverse micelles, and the work presented here takes this one step further by examining the overall conformation and placement of MK-2 in the context of a liposomal bilayer. Typically, menaquinones that are used as electron transporters in bacterial species are much longer and thus are likely to have a different conformation and potentially different location in a membrane bilayer than MK with only two isoprene units in the side chain. However, this work lays the foundation for the study of menaquinones in an environment that is more analogous to the one that would be found in; that is, a membrane bilayer in an aqueous context.

The work presented here is in good agreement with this work that has been published previously. This study, similar to previous work, finds that MK-2 adopts a U-shaped conformation, both when it is bound by an EPC liposome as well as when it resides at the edge of the liposomal interface in contact with the water pool. This is a logical conclusion; owing to the size of the isoprene side chain of MK-2 it is not likely to be confined in the hydrophobic tails of the bilayer. Additionally, previous work with ubiquinone analogues of varying length of isoprene chain show that while the location of the isoprenoid tail changes within the bilayer with increasing length, the ubiquinone head group remains in the region of the glycerol groups of EPC.[22 29, 23-24] Despite the lack of presence of phosphatidylcholine in bacterial cells compared to other lipids such as phosphatidylserine, phosphatidylinositol and phosphatidylethanolamine, it is likely that the conformation and location of MK-2, or indeed, longer MK-*n* analogues, would not change much with the change in lipid head group, since the hydrophobic nature of the compounds causes them to localize in the region of the acyl and glycerol groups. Also owing to

its size and location in the bilayer, it is not likely to deviate much from the U-shaped conformation previously determined in aprotic solvents as well as reverse micelles except for minor rotational or conformational changes to minimize unfavorable solvent or lipid head group interactions, which are difficult to determine in the complex context of the liposomal ^{1}H-^{1}H 2D NOESY spectra.

It appears that at low concentrations, MK-2 is located just within the head groups of the lipids in the region of the acyl chain and phosphate groups, with minimal to no contact with the bulk water solution. At higher concentrations, though, MK-2 appears to have two distinct sets of chemical shift peaks, one corresponding to MK-2 which is bound by the liposome, as evidenced by the downfield shift of peaks indicating that MK-2 is in a more charged environment. The other set of peaks corresponds directly to the aqueous spectrum of MK-2 and is also evidenced by the increased number of NOE cross peaks between HOD and MK-2. There are no NOE cross peaks between chemical shifts corresponding to liposome-bound MK-2 and aqueous MK-2, but MK-2 in liposome-bound and aqueous environments have the same NOE cross peaks within the molecule. It is reasonable to conclude from this that at higher concentrations of MK-2, the compound resides further out of the liposomal interface, still associated with the liposome but largely in the bulk water pool. This conclusion is further supported by the minimal solubility (logP=5.2) of MK-2 in water and additionally, with increasing MK-2 DLS measurements show a slight increase in vesicle size, though this increase is not statistically significant. While these conclusions are not enough to explain why we observe the odd-even effect in the electrochemistry of MK-*n* analogues from the previous chapter, these results may account for the increased diffusion coefficients observed for MK-1 and MK-2 analogues. It is likely that at the concentrations used to study the electrochemistry of the MK-*n* analogues in the previous chapter

(6 mM, or 18 mg/mL MK-2 in 100 mg/mL SPC and 14 mg/mL MK-1 in 100 mg/mL SPC) that some of the MK-1 and MK-2 may not have been bound by the liposome at all, but loosely associated with the outer leaflet in the bulk water or freely solubilized in the aqueous surroundings.

This work builds off previous work examining the conformation and placement of MK-2 in AOT reverse micelles and examines it in the more biologically relevant context of a liposomal bilayer. It lays the foundation for the study of menaquinones with longer side chains as well as the study of other hydrophobic molecules that may be found in a membrane bilayer via 1D and 2D ^{1}H NMR, and may also provide information that, with future studies, will help to elucidate the electrochemical odd-even effect observed in the previous chapter. The results found here are in good agreement with literature previously published both on the conformation of MK-2 and ubiquinone in different environments as well as recent literature showing the ^{1}H NMR spectra of PC liposomes.[20-23]

References

1. Boersch, M.; Rudrawar, S.; Grant, G.; Zunk, M., Menaquinone biosynthesis inhibition: a review of advancements toward a new antibiotic mechanism. *RSC advances* **2018,** *8* (10), 5099-5105.
2. Kurosu, M.; Begari, E., Vitamin K2 in electron transport system: are enzymes involved in vitamin K2 biosynthesis promising drug targets? *Molecules* **2010,** *15* (3), 1531-1553.
3. Collins, M.; Pirouz, T.; Goodfellow, M.; Minnikin, D., Distribution of menaquinones in actinomycetes and corynebacteria. *Microbiology* **1977,** *100* (2), 221-230.
4. Collins, M. D.; Faulkner, M.; Keddie, R. M., Menaquinone composition of some sporeforming actinomycetes. *Systematic and applied microbiology* **1984,** *5* (1), 20-29.
5. Halder, M.; Petsophonsakul, P.; Akbulut, A. C.; Pavlic, A.; Bohan, F.; Anderson, E.; Maresz, K.; Kramann, R.; Schurgers, L., Vitamin K: double bonds beyond coagulation insights into differences between vitamin K1 and K2 in health and disease. *International journal of molecular sciences* **2019,** *20* (4), 896.
6. Koehn, J. T.; Crick, D. C.; Crans, D. C., Synthesis and characterization of partially and fully saturated menaquinone derivatives. *ACS omega* **2018,** *3* (11), 14889-14901.
7. Upadhyay, A.; Fontes, F. L.; Gonzalez-Juarrero, M.; McNeil, M. R.; Crans, D. C.; Jackson, M.; Crick, D. C., Partial saturation of menaquinone in Mycobacterium tuberculosis: function and essentiality of a novel reductase, MenJ. *ACS central science* **2015,** *1* (6), 292-302.
8. Upadhyay, A.; Kumar, S.; Rooker, S. A.; Koehn, J. T.; Crans, D. C.; McNeil, M. R.; Lott, J. S.; Crick, D. C., Mycobacterial MenJ: an oxidoreductase involved in menaquinone biosynthesis. *ACS chemical biology* **2018,** *13* (9), 2498-2507.
9. Amadi, E.; Alderson, G., Menaquinone composition of some micrococci determined by high performance liquid chromatography. *Journal of applied bacteriology* **1991,** *70* (6), 517-521.
10. Da Costa, M. S.; Albuquerque, L.; Nobre, M. F.; Wait, R., The extraction and identification of respiratory lipoquinones of prokaryotes and their use in taxonomy. In *Methods in microbiology*, Elsevier: 2011; Vol. 38, pp 197-206.
11. Toledano, T.; Sazan, H.; Mukhopadhyay, S.; Alon, H.; Lerman, K.; Bendikov, T.; Major, D. T.; Sukenik, C. N.; Vilan, A.; Cahen, D., Odd–even effect in molecular electronic transport via an aromatic ring. *Langmuir* **2014,** *30* (45), 13596-13605.
12. Feng, Y.; Dionne, E. R.; Toader, V.; Beaudoin, G.; Badia, A., Odd–even effects in electroactive self-assembled monolayers investigated by electrochemical surface plasmon resonance and impedance spectroscopy. *The Journal of Physical Chemistry C* **2017,** *121* (44), 24626-24640.
13. Long, Y.-T.; Rong, H.-T.; Buck, M.; Grunze, M., Odd–even effects in the cyclic voltammetry of self-assembled monolayers of biphenyl based thiols. *Journal of Electroanalytical Chemistry* **2002,** *524*, 62-67.
14. Thuo, M. M.; Reus, W. F.; Nijhuis, C. A.; Barber, J. R.; Kim, C.; Schulz, M. D.; Whitesides, G. M., Odd− even effects in charge transport across self-assembled monolayers. *Journal of the American Chemical Society* **2011,** *133* (9), 2962-2975.
15. Jiang, L.; Sangeeth, C. S.; Nijhuis, C. A., The origin of the odd–even effect in the tunneling rates across EGaIn junctions with self-assembled monolayers (SAMs) of n-alkanethiolates. *Journal of the American Chemical Society* **2015,** *137* (33), 10659-10667.

16. Rubinson, K. A., Practical corrections for p (H, D) measurements in mixed H 2 O/D 2 O biological buffers. *Analytical Methods* **2017,** *9* (18), 2744-2750.
17. Kosicki, G. W.; Lipovac, S. N., The pH and pD dependence of the spontaneous and magnesium-ion-catalyzed decarboxylation of oxalacetic acid. *Canadian Journal of Chemistry* **1964,** *42* (2), 403-415.
18. Danaei, M.; Dehghankhold, M.; Ataei, S.; Hasanzadeh Davarani, F.; Javanmard, R.; Dokhani, A.; Khorasani, S.; Mozafari, M., Impact of particle size and polydispersity index on the clinical applications of lipidic nanocarrier systems. *Pharmaceutics* **2018,** *10* (2), 57.
19. Schmitz, K. S., *Introduction to dynamic light scattering by macromolecules*. Elsevier: 2012.
20. Cardia, M. C.; Caddeo, C.; Lai, F.; Fadda, A. M.; Sinico, C.; Luhmer, M., 1 H NMR study of the interaction of trans-resveratrol with soybean phosphatidylcholine liposomes. *Scientific reports* **2019,** *9* (1), 1-11.
21. Koehn, J. T.; Magallanes, E. S.; Peters, B. J.; Beuning, C. N.; Haase, A. A.; Zhu, M. J.; Rithner, C. D.; Crick, D. C.; Crans, D. C., A synthetic isoprenoid lipoquinone, menaquinone-2, adopts a folded conformation in solution and at a model membrane interface. *The Journal of organic chemistry* **2017,** *83* (1), 275-288.
22. Galassi, V. V.; Arantes, G. M., Partition, orientation and mobility of ubiquinones in a lipid bilayer. *Biochimica et Biophysica Acta (BBA)-Bioenergetics* **2015,** *1847* (12), 1560-1573.
23. Kaurola, P.; Sharma, V.; Vonk, A.; Vattulainen, I.; Róg, T., Distribution and dynamics of quinones in the lipid bilayer mimicking the inner membrane of mitochondria. *Biochimica et Biophysica Acta (BBA)-Biomembranes* **2016,** *1858* (9), 2116-2122.
24. Söderhäll, J. A.; Laaksonen, A., Molecular dynamics simulations of ubiquinone inside a lipid bilayer. *The Journal of Physical Chemistry B* **2001,** *105* (38), 9308-9315.

Chapter 4: The Interfacial Interactions of Glycine and Short Glycine Peptides in Confined Spaces

4.1. Glycine as the Simplest Amino Acid

Small peptides play an essential role in a variety of biological functions, acting as chemical messengers, intra- and intercellular mediators, hormones and neurotransmitters [1-3]. Peptides also play an important role as antibiotics, such as bacitracin and colistin, as well as antimicrobial peptides (AMPs, also referred to as host defense peptides), also referred to as host defense peptides [4-6]. AMPs are peptides produced by multicellular organisms as part of the innate immune response found in all classes of life, and function as a defense against pathogenic microbes. They exert this function in a number of ways, such as the suppression of biofilm formation, induction of the dissolution of existing biofilms, and attracting phagocytes via chemotaxis to induce non-opsonic phagocytosis [5, 7-8]. In addition to their antimicrobial function, recently it has been found that AMPs may also have anticancer activity; they are able to trigger cytotoxicity of a number of cancer cells through the interaction of the amphipathic or cationic peptide with the plasma membrane of the cell, which selectively exposes negatively charged phosphatidylserine lipids [9-10]. The combination of the function of AMPs as antimicrobial agents as well as anticancer agents makes them a promising starting point for antimicrobial and anticancer drug design [11-14].

In order to exert their antimicrobial or anticancer properties, AMPs must interact with the plasma membrane of the bacterial or cancer cell [5, 15]. This interaction with the membrane is associated with their mechanism of action which can include disruption of the membrane, disruption of membrane-associated physiological processes such as cell wall synthesis, or even translocation across the membrane for interaction with a cytoplasmic target [5, 16-18]. The

interactions of these small peptides are dependent on a variety of variables, such as size, amino acid composition, secondary structure and amphiphilic behavior, and their mechanism of action is generally unknown with the exceptions of a few representative examples [8-9, 19-20]. Additionally, AMP interactions with the membrane depend on the composition of the membrane itself, as they tend to be attracted more to negatively charged membranes such as bacterial membranes or plasma membranes of cancer cells, which selectively expose negatively charged phosphatidylserine lipids [10, 21]. Because of this, AMPs prefer membranes with high concentration of anionic lipids, those that maintain a high electrical potential gradient, and membranes that tend to lack cholesterol [5, 22-23]. It is thus important to study the interactions of peptides at a membrane interface using a small representative amino acid and a membrane mimetic interface to determine the molecular placement of the molecules at the membrane as well as the manner by which they interact.

Of the twenty amino acids that are found in peptides, glycine (G, Fig. 4.1) is both the smallest and most versatile.[24] Having only a hydrogen atom as its substituent, it is the only amino acid that is achiral, and as such it is compatible with either hydrophobic or hydrophilic environments. In addition, it has many biological functions, one of the most notable of which as a simple inhibitory and excitatory neurotransmitter and as such, it is a logical representative amino acid for investigation simple peptide and amino acid interactions with a membrane.[25] Because we are interested in obtaining molecular information on how simple peptides interact with membrane interfaces, we will use monomeric, dimeric, trimeric and tetrameric G-containing peptides, hereafter referred to as G, GG, GGG and GGGG (Fig. 4.1). To study how these small peptides behave near cellular membranes, we use a reverse micellar (RM) system (Fig. 4.1), which consists of a self-assembled ternary system containing surfactant, organic solvent and

water.[26-29] The surfactant, aerosol-OT (AOT), also known as sodium 2-diethylhexylsulfosuccinate, arranges itself such that the water pool is contained by the negatively charged head groups of the AOT, and surfactant tails extend outward into the organic solvent, isooctane (2,2,4-trimethylpentane).[30-31] Commonly, water droplets contained in this system range from a size of 1-10 nm.[32-33] The RM system provides both a hydrophilic and hydrophobic environment at a negatively charged interface, making it a good model system to investigate the interactions of molecules with membrane interfaces.

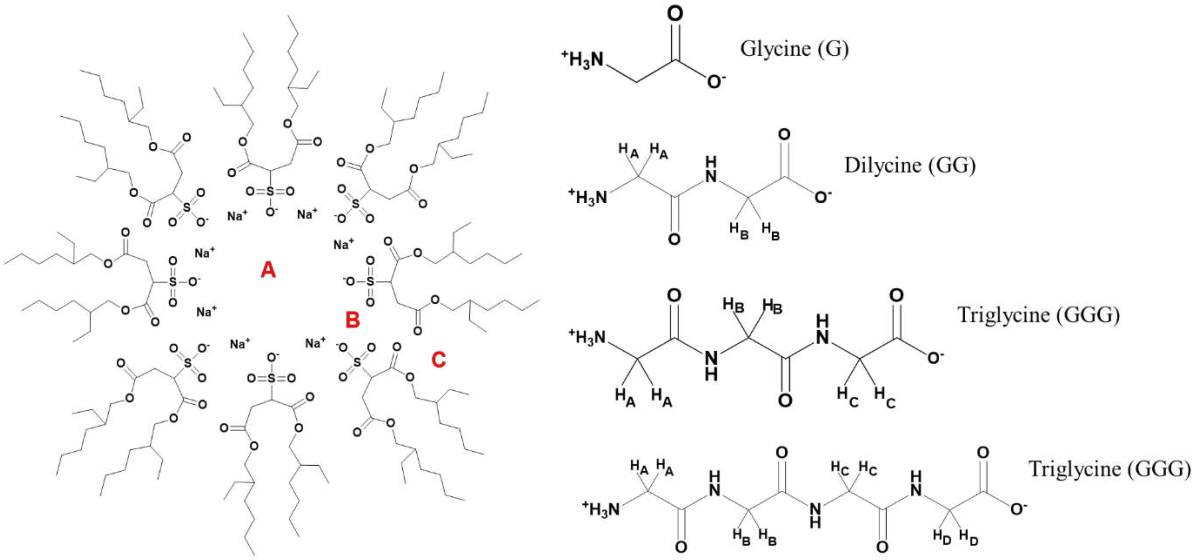

Figure 4.1. The structure of glycine (G) analogues (right) and the AOT reverse model system (left). Protons on G, GG, GGG and GGGG are labeled according to subsequent ^{1}H NMR proton assignments. Areas labeled in red in the AOT RM figure refer to possible locations of the G analogues within the RM: A) within the bulk water pool, B) at the RM interface or C) deeper into the interface, near the acyl chains of the AOT and nearer to the hydrophobic tails.

To investigate the interactions of G and G-containing peptides with model membranes, it is of interest to determine its location within the RM. That is, whether it is located near the charged AOT heads, bulk water pool or in the ordered, interstitial water between the charged interface and the water pool, referred to as the stern layer.[34] Furthermore, the location of the molecule of interest may be closely related to the pH of the RM interior.

In this study, we use AOT RMs and Langmuir monolayers to gain insight into how G and

G-based peptides interact with simple membrane model systems. Specifically, we investigate here the interaction of G, GG, GGG and GGGG with an AOT RM interface and with dipalmitoyl phosphatidylcholine (DPPC) and dipalmitoyl ethanolamine (DPPE) monolayers to determine the interactions and placement of G compounds at a model membrane interface.

4.2. Experimental

4.2.1. General Materials and Methods

The following materials were purchased and used without purification: glycine HCl (G, Mallinckrodt, 99.0%), diglycine (GG, Sigma-Aldrich, 99.0%), triglycine acid (GGG, Sigma-Aldrich, 99.0%), tetraglycine (GGGG, Aurum Pharmatech, >96%), activated charcoal (carbon 6-12 mesh), 2,2,4-trimethylpentane (isooctane) (Sigma-Aldrich, 99.0%), deuterium oxide (Sigma-Aldrich, 99.0% deuterium), 4,4,-dimethyl-4-silapentane-1-sulfonic acid sodium salt (DSS, Wilmad). The chemicals methanol (>99%), citric acid anhydrous (>99.5%), sodium citrate dihydrate (>99%), sodium hydroxide (>99%) and hydrochloric acid were purchased from Fisher Scientific. The lipids 1,2-dipalmitoyl-*sn*-glycero-3-phosphocholine (DPPC, >99%) and 1,2-dipalmitoyl-*sn*-glycero-3-phosphoethanolamine (DPPE, >99%) were purchased from Avanti Polar Lipids. Sodium aerosol-OT (AOT) (bis(2-ethylhexyl)sulfosuccinate sodium salt, Sigma Aldrich, ≥99.0%) was purified as described previously to remove an acidic impurity.[35] Briefly, 50.0g of AOT was dissolved into 150 mL of methanol to which 15g of activated charcoal was added. This suspension was stirred for 2 weeks. After mixing ,the suspension was filtered to remove the activated charcoal. The filtrate was then dried under rotary evaporation at 50°C until the water content was below 0.2 molecules of water per AOT as determined by ^{1}H NMR spectroscopy.[36] The pH of aqueous solutions measured at 25°C on an Orion 2STAR pH meter prior to formation of the AOT RM in isooctane. The pH was adjusted throughout the experiment

using varying concentrations of NaOH or HCl dissolved in diH_2O or D_2O, depending on experimental need. NaOH or HCl dissolved in D_2O is referred to as NaOD or DCl, respectively.[36]

4.2.2. Preparation of Samples for Analysis

4.2.2.1. Preparation of stock solutions of G, GG, GGG and GGGG for 1H NMR and Dynamic Light Scattering

Each of the 200 mM stock solutions used in the ^1H NMR experiments were prepared with 2.00×10^{-3} mol of each G, GG, GGG and GGGG dissolved in 10 mL D_2O in a volumetric flask and pH adjusted to the appropriate value as needed for the overall concentration of 200 mM. Each of the 50 mM stock solutions used for dynamic light scattering experiments were prepared with 5.0×10^{-3} mol of each G, GG, GGG and GGGG and dissolved in 10 mL diH_2O.

All stock solutions were sonicated until clear if not already, and all stock solutions were pH adjusted with DCl or HCl and NaOD or NaOH, depending on experimental need. The pH of the stock solutions was measured at 25°C with an Orion 2STAR pH meter. The pH values are measured directly in D_2O, and are not a reflection of the solution pD (pD = pH + 0.4) before addition to the RM suspension. [37-39]

4.2.2.2. Preparation of AOT-isooctane stock solution and RMs containing G, GG, GGG, and GGGG for ^1H NMR

The 750 mM AOT-isooctane stock solution was prepared by dissolving 7.5×10^{-3} mol AOT in 10 mL isooctane. This mixture was sonicated and vortexed until clear, approximately 15 minutes. Once dissolved, the solution was equilibrated to ambient room temperature. RMs of w_0 values of 6, 10, 14, 16, and 20, where w_0 = [H_2O]/[AOT], were prepared by combining appropriate volumes of the appropriate prepared stock AOT stock solution, depending on

experimental need, and appropriate volumes of 200 mM stock solutions of G, GG, GGG or GGGG, to create the desired size of RM.

4.2.2.3. Preparation of AOT-isooctane stock solution and RMs containing G, GG, GGG and GGGG for Dynamic Light Scattering

The 200 mM AOT-isooctane solution was prepared by dissolving 2.00×10^{-3} mol AOT in 10 mL isooctane. This mixture was sonicated and vortexed until clear, approximately 15 minutes. Once dissolved, the mixture was equilibrated to ambient room temperature. To prepare the RM solutions, specific volumes of AOT stock solution and aqueous 50 mM G stock solution were combined for a total of 5 mL to form RM sizes of w_0 10 and 20. This mixture was vortexed until clear, consistent with the formation of RMs.

4.2.2.4. Preparation of Lipid Stock Solutions and Aqueous Subphase

Sodium phosphate buffer (20 mM) was prepared in distilled deionized water and adjusted to pH 6.00, 7.00, 8.00, 9.00 (±0.02) with either 1.0 M HCl or 1.0 M NaOH. Sodium phosphate citrate buffer (20 mM) was prepared in distilled deionized water and adjusted to pH 4.00 ± 0.02 in the same manner as the sodium phosphate buffers. Glycine subphase (1 mM) was prepared by dissolving 75.0 ± 0.1 mg glycine into one liter of the previously prepared buffers. The pH was readjusted to the previously mentioned values with 1.0 M HCl or 1.0 M NaOH. Stock solutions of DPPC and DPPE were prepared by dissolving 0.025 mmol of powdered phospholipid into 5.0 ± 0.1 mL of freshly prepared 9:1 chloroform methanol (v:v).

4.2.3. ^{1}H NMR spectroscopy and analysis of D_2O and RM samples

The ^{1}H NMR experiments were performed using a 400 MHz Varian ^{1}H NMR spectrometer using standard parameters (1s relaxation time, 25°C temperature control and 45° pulse angle). The aqueous samples were referenced to an internal DSS sample. RM samples

were referenced to the isooctane methyl peak at δ=0.90 ppm as has been previously reported and were originally referenced to tetramethylsilane.[40] The resulting spectra were referenced, baseline corrected, normalized and analyzed using MestReNova version 10.0.1.

The pKa values were determined by plotting chemical shifts of the samples at their varying pH values in D_2O and w_0 10 RMs and calculating the first derivative of the best fit curve using OriginPro version 9.1.[41]

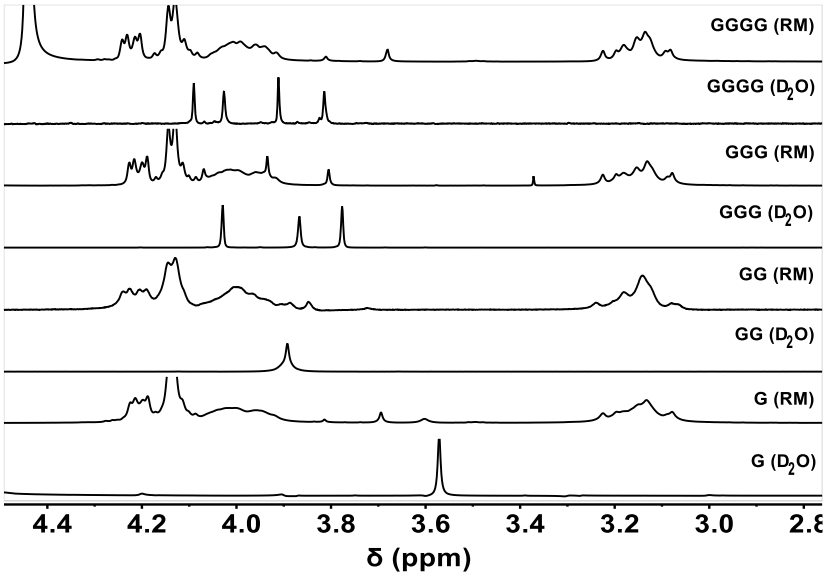

Figure 4.2. A comparison of each of the studied compounds and their chemical shifts as determined by ^1H NMR in *w0 10* reverse micelles (RMs) and D_2O. A) Spectra beginning from the bottom correspond to G, GG, GGG, and GGGG in D_2O and RM alternately at pH 7. Asterisk in GGG RM spectrum denotes acetone impurity.

In the case of peaks corresponding to GGG and GGGG in RMs as shown in Figure 4.2, these shifts were often masked by the AOT peaks, as shown in Figure 2. To elucidate these peaks, the spectra were analyzed by MestReNova version 10.0.1 and baseline corrected, referenced and normalized. The Arithmetic function was then used so that control spectra could be subtracted from spectra containing probe molecule.

4.2.4. Langmuir Trough instrument preparation

Compression isotherms were obtained with a Kibron μTrough XS (stainless steel)

equipped with a hydrophobic Teflon ribbon barrier. The trough was cleaned thoroughly with three isopropanol washes, three ethanol washes, and a water rinse before each experiment. Excess water was evaporated with compressed air. The wire probe used as a Wilhemy plate was flamed with a Bunsen burner to remove lipids before each experiment.

After cleaning, approximately 50 mL of 20 mM buffer or 1 mM glycine in 20 mM buffer was added to the trough. The subphase surface was then cleaned with vacuum aspiration to remove dust contamination. The surface was considered clean when the surface pressure remained at 0.0 ± 0.5 mN/m throughout a full compression.

4.2.5. Formation and compression of Langmuir monolayers

Either DPPC or DPPE (20 μL, 20 nmol) was added to the surface in a drop-wise manner with a glass Hamilton syringe (50 μL) followed by a 15-minute equilibration period. Monolayers were compressed at a speed of 10 mm/min (5 mm/min on each side). The temperature of the subphase was maintained at 25˚C by an external water bath. All experiments were run in triplicate, and the data presented was obtained by averaging the triplicate measurements. Error bars are the standard deviation of the area taken every 5 mN/m of surface pressure.

4.2.6. Percent difference calculations

The percent difference between control monolayers and monolayers with glycine present in the subphase was calculated with Equation 1, where A_{gly} is the area of monolayers with glycine present and A_{con} is the area of control monolayers. Calculations were performed at every 5 mN/m of surface pressure.

Equation 1. $\%diff = (\frac{A_{gly} - A_{con}}{A_{con}}) \times 100$

4.2.7. Dynamic Light Scattering (DLS)

Dynamic light scattering (DLS) experiments were performed using a Malvern Instrument (Malvern Instruments Limited, UK) MAN0486.[33, 40] DLS and the autocorrelation method of analyzing scattering were used to measure hydrodynamic radius of AOT RMs, temperature controlled at 25.0˚C. Each sample was equilibrated for 600 s at 25◦C and then run for 10 scans per acquisition for a minimum of ten measurements for every solution with and without G-compounds at neutral pH (7.4) for each w_0 value. A 1mL aliquot of sample was required for measurement. The viscosity (0.4670cP) and refractive index (1.391) are needed for RM size determination in the isooctane solvent used in this work.[35] The photons scattered by the RMs were collected at a 173˚ angle. Data processing was carried out using the Zetasizer version 7.11 software.

4.3. Results

The chemical shifts of G, GG, GGG and GGGG were examined by ^{1}H NMR spectroscopy to compare their chemical shifts in aqueous solution with those peaks obtained in the environment of the RM model membrane (sections 4.3.1-4.3.4). Solutions containing each of the G compounds were made at varying pH values to determine the pKa values of each in both aqueous environment and in the environment of the RM (summarized in Discussion section), and representative NMR spectra for each compound in RM and D_2O as well as exact chemical shift values are given in the Supplemental Materials. Each of these compounds showed a slight difference in chemical shift values between RMs and the compound alone in D_2O, indicating a difference in environment for the probe molecule. This data gives some structural information about the location of the probe within the reverse micelle. The systems were also investigated

using dynamic light scattering (DLS) to verify formation of the RMs and to examine the impact of the G compounds on the RM system (section 4.3.5).

In section 4.6 we further support the observations made in this paper in sections 4.3.1-4.3.5 by using Langmuir trough. These studies used a natural lipid as well as a different method, and this was done to investigate whether the conclusion obtained by using the microemulsions system could be confirmed and extended to studies physiological lipids and human cells.

4.3.1 ^{1}H NMR spectroscopy of L-Glycine (G) in RM

A series of samples with RMs of size w_0 10 (where w_0 = [AOT]/[H_2O]) were made containing G at varying pH values by adding 200 mM G solution in D_2O at the pH specified to the appropriate volume of 750 mM AOT solution dissolved in isooctane. The chemical shifts of these were recorded using ^{1}H NMR spectroscopy and chemical shifts are compared with representative spectra shown (Fig. 4.3). The pKa values were calculated from the spectra both in D_2O and in microemulsions are listed in Table 2 in the Discussion. Values obtained from G in aqueous and RM environments show that the pK_a of the C-terminus differs very little between aqueous and RM environments, but the N-terminus differs significantly, with a pK_a of 10.7 in D_2O and 8.51 in the RM model membrane. This difference or lack thereof in pK_a values between the two environments gives some information about the environments surrounding the carboxy- and amine-terminal ends of G within the RM [42]. Because there is little change between the carboxyl pK_a in RM and D_2O, this suggests that this portion of the compound is in an environment that is the same. In the context of the RM model system, this observation is consistent with the C-terminus is in the Stern layer/aqueous environment directed toward the bulk water pool (Fig. 4.1). The significant decrease in pK_a between aqueous and RM

environment for the amine-terminal end of G indicates a significant change in environment, such that the amine-terminal end is located near or in the charged region of the RM interface.

It is likely that the experimental N-terminal pK_a of G in RM is lower than what is reported in the literature due to the higher ionic strength near the charged interface. In pure aqueous solution, the amine is free to hydrogen bond to the carboxyl moiety of the amino acid, forming an energetically favorable 5-membered ring and stabilizing the amine. However, in high ionic strength solutions, this H-bonding may be disrupted by the presence of the counterions, which are known to accumulate near the interface of the AOT (Fig. 4.1) [43-44], lowering the pK_a of the N-terminus. Additionally, this H-bonding phenomenon could be disrupted by the interaction of the amine with the sulfonate groups on the AOT head groups. This disruption of H-bonding is consistent with the lowering of the pK_a values in the reverse micelle, which contains more Na^+ ions, the presence of charged sulfonate groups and therefore a higher ionic strength.

To further support this conclusion, experiments were performed in which the size of RM containing the G solutions was varied so that the chemical shifts could be analyzed as a function of increasing vesicle size to give further information about their placement within the RM system. The pH of the G solutions used to prepare the RMs was varied at representative pH values: alkaline pH (pH 9), neutral/physiological pH (pH 7.4) and acidic pH (pH 2). By this experiment, it was found that as the size of the water pool in the RM increased, the chemical shift of the G peak in the neutral and alkaline pH RM environments decreased and approached its shift value in D_2O alone, which is 3.55 at pH 2 and 7.4 (Fig. 4.3). This suggests that the neutral and negatively charged forms of G, predictably, are not attracted to the interfacial region of the RM due to their charges not interacting with the negatively charged AOT heads [45]. As the

vesicle size increases, the interstitial water region becomes less ordered and more analogous to bulk water, and as a result, the compounds that are not highly attracted to the polar interface begin to transition to water that behaves more as bulk water. However, in the case of G at pH 2, the carboxylate moiety is fully protonated, leading to an overall +1 charge of the molecule. As a result, the positive charge of the molecule interacts with the negatively charged polar heads of the AOT consistently, leading to the plateau in chemical shift as the size of the RM increases.

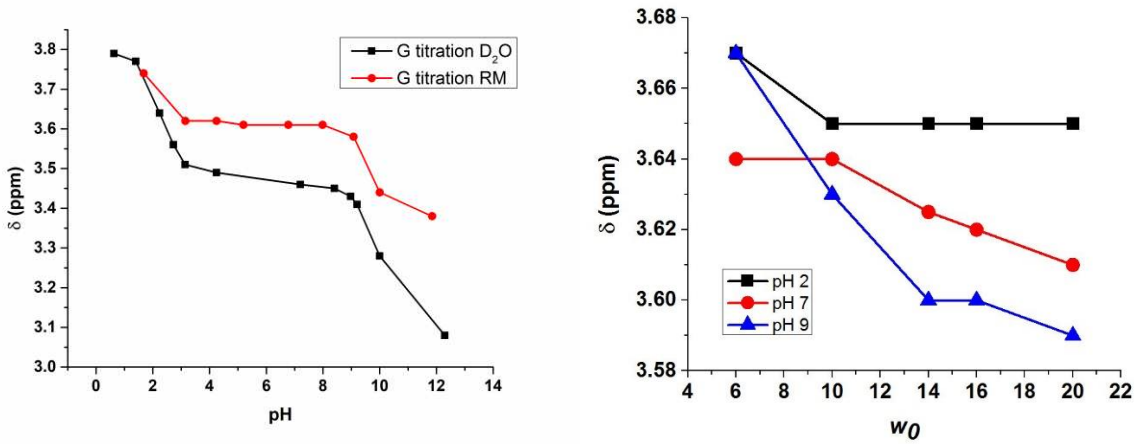

Figure 4.3. G plotted as a function of pH in RM and aqueous (D_2O) environments. (Right) Comparison of ^1H NMR chemical shifts of G in aqueous and RM environments. (Left) The ^1H NMR chemical shift of G is plotted with increasing w_0 at pH 2 (squares), pH 7 (circles) and pH 9 (triangles).

To test the hypothesis that as the vesicle size increases at neutral and alkaline pH, the chemical shift of G approaches that of its shift in pure aqueous environment, experiments were performed in which the pK_a of G was calculated in a w_0 30 RM (12.4nm diameter) instead of the w_0 10 (6.8 nm diameter) that was previously used [32]. These experiments found that the carboxy-terminal pK_a in this larger vesicle stayed the same at 2.5, but the amine-terminal pK_a decreased significantly to 9.6 from 8.51, a value much closer to the pK_a when G is in an aqueous environment under ionic strength (Fig. 4.3). This is consistent with our hypothesis; that the G is likely positioned such that the N-terminus is in the interstitial water region of the RM facing the

negatively charged interface, while the C-terminus is located closer to the bulk water pool of the RM [45]. As the size of the RM increases, the interstitial water region becomes less ordered and behaves more as bulk water, and the N-terminus is in a more aqueous-like environment, and the pK_a reflects this as it increases with larger vesicle size.

4.3.2. ^{1}H NMR Spectroscopy of Diglycine (GG) in RM

In a similar fashion to G, ^{1}H NMR spectroscopy of solutions containing GG in the RM model membrane system and aqueous solution was recorded and analyzed to identify any differences in chemical shift that may occur as a result of confinement by w_0 10 RM. Chemical shift values are plotted and compared between environments, with representative spectra for each given in Appendix V (Fig. 4.4).

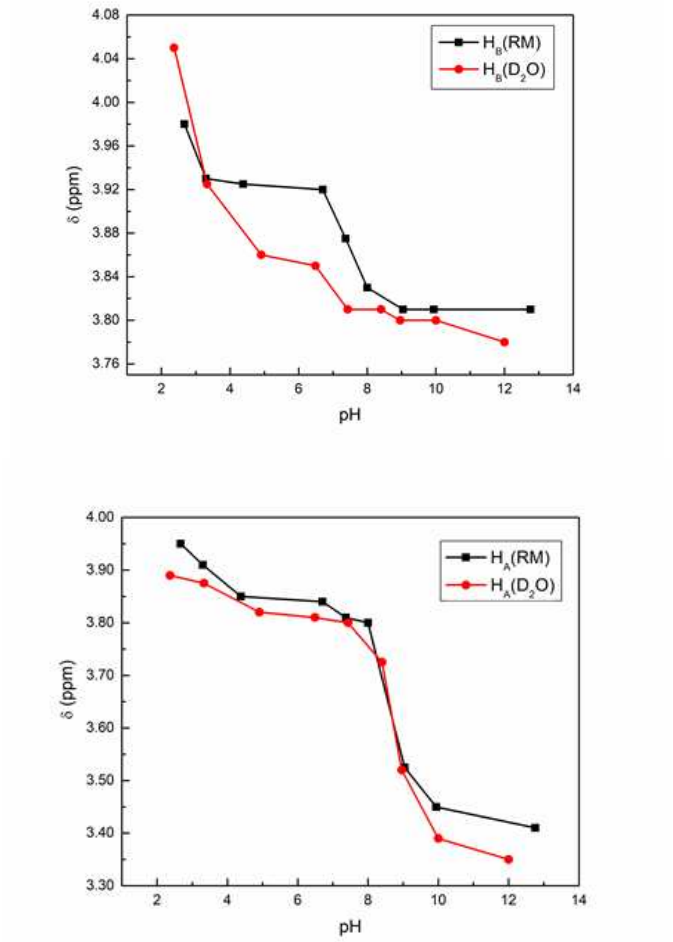

Figure 4.4. Chemical shifts of GG as a function of pH in D_2O and RM samples based on ^1H NMR spectroscopic titration studies. Top) ^1H NMR chemical shift values of protons B (CH_2 near N-terminus) of GG measured at different pH values in D_2O, with the proton labeling scheme shown in Figure 4.1. Bottom) ^1H NMR chemical shift values of protons A (CH_2 near C-terminus) of GG measured at different pH values in RMs, with the proton labeling scheme shown in Figure 4.1.

The solution pH values and resulting pK_a that was calculated show that GG displays a small increase in chemical shift from aqueous environment to the RM, indicating that the compound is in a slightly more charged environment consistent with the interfacial water layer containing the Na^+ counterions (Fig. 4.1). However, this change within pK_a values from aqueous to RM is small, with a pK_a of 2.85 in D_2O and 2.99 in RM for the C-terminal CH_2, and 8.60 in D_2O and 8.48 for the N-terminal CH_2.

4.3.3. ^{1}H NMR Spectroscopy of Triglycine (GGG) in RM

Solutions containing GGG were also studied in comparison in D_2O and RMs of w_0 10 using ^{1}H NMR to investigate its potential interactions within the confines of the RM. Results obtained from solutions of GGG are similar to those obtained from GG in that there is little change in the chemical shifts of the solutions in aqueous environment and in the AOT RM (Fig. 4.5). There was little change in the pK_a of the N- and C-terminal ends of the peptide, with the C-terminal pK_a in D_2O at 3.18 and in RM 3.27, and the N-terminal pK_a in D_2O at 8.29 and in RM 8.11.

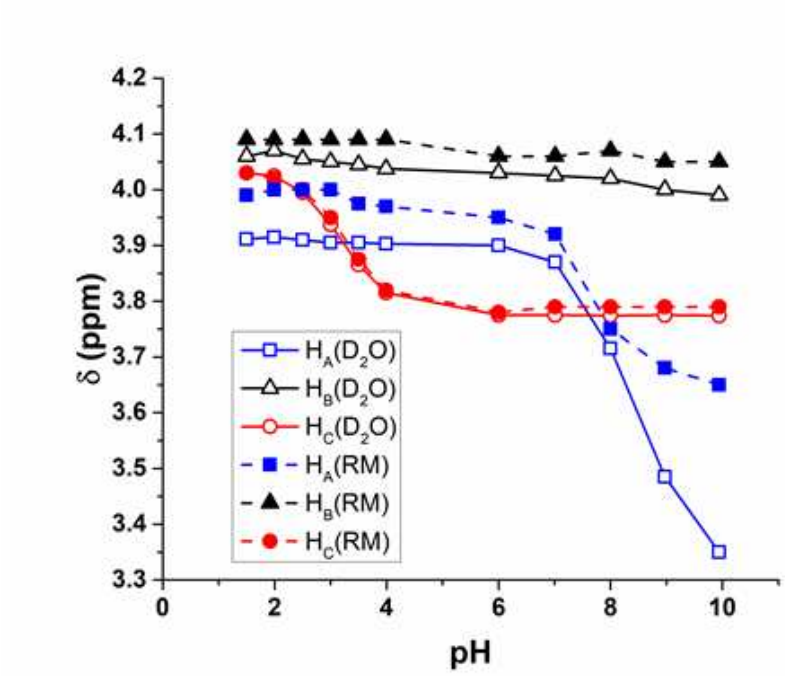

Figure 4.5. GGGG proton shifts compared at varying pH values in aqueous (D_2O) and RM environments, as determined by ^{1}H NMR spectroscopy.

Further exploring this observation, that the chemical shift of the C-terminal CH_2 remains relatively unchanged between aqueous and RM environments, consistent with the interpretation that the C-terminal end of the peptide resides within the bulk water pool of the RM or the molecule has folded over on itself. The chemical shifts of the middle CH_2 at all pH values tested

is slightly elevated in the RM as compared to D_2O, consistent with being located in a more charged environment, and the N-terminal CH_2 protons show the most change in chemical shift with values in the RM being higher than that of D_2O, consistent with being located in a more charged environment, or possibly if it is in a folded conformation (Fig. 4, Fig. S13-16). However, similarly to those calculated for GG, there is little change in the calculated pK_a values with differences of only 0.1 pH unit.

4.3.4. ^1H NMR Spectroscopy of Tetraglycine (GGGG) in RM

Aqueous solutions of GGGG at varying pH values and corresponding AOT RMs were analyzed via ^1H NMR spectroscopy similarly to the other G compounds above. The results obtained from GGGG in terms of pK_a differences are small, as what was found for the GGG and GG peptides. The pK_a value found for the C-terminal end of the peptide in D_2O was determined to be 3.05 and that in RM was determined to be 2.82. The pK_a value found for the N-terminal end of GGGG was found to be 7.75 in D_2O and 7.94 within the RM. These small differences may be attributed to the slight changes in the environment of the RM as compared to aqueous solution, and suggest that the peptide itself resides between the interface of the RM and the Stern layer. The increased pK_a of the N-terminal protons as well as the slightly decreased pK_a of the C-terminal protons indicate that the zwitterionic form of GGGG is equally or more stable in the RM, which is also consistent with the compound being between the bulk water and interface of the RM (Fig. 4.6).

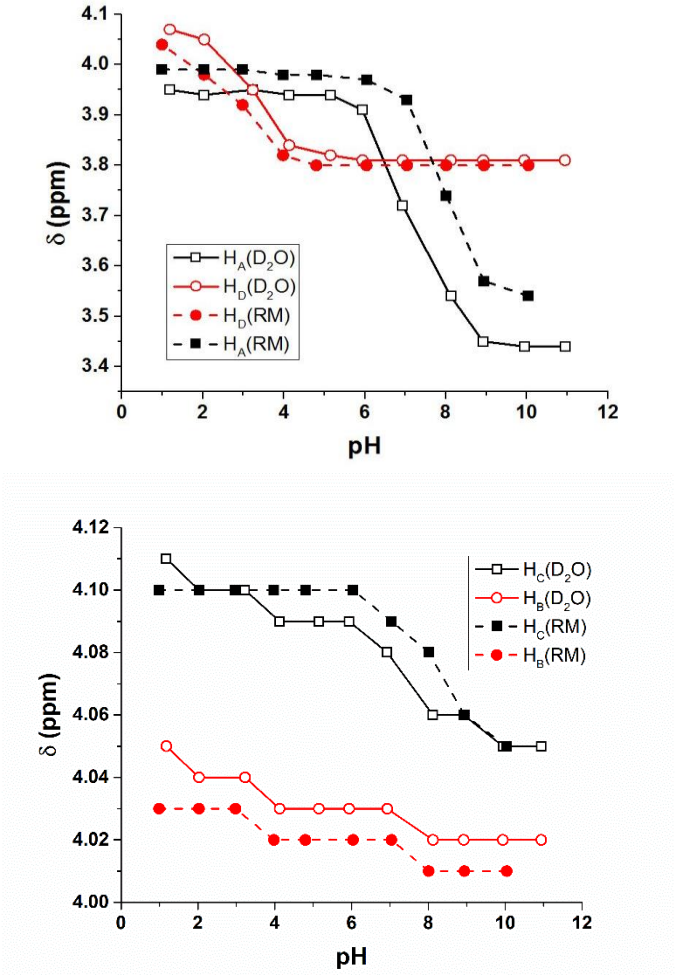

Figure 4.6. Chemical shift values as determined by ^{1}H NMR of GGGG at varying pH values in RM and D_2O with peaks corresponding to labels in Figure 1D. Top) N- and C- terminal CH_2 protons of GGGG in D_2O and RM, or protons A and D as labeled in Fig. 1D. Bottom) Interior CH_2 protons on N- or C-terminal side of GGGG in D_2O and RM, or protons B and C as labeled in Figure 4.1.

It is also noteworthy when looking at the chemical shifts of the middle protons (H_B and H_C) of the compound, the difference in shift is ≤0.1ppm, indicating that the environment is essentially the same between the two systems (Fig. 5B).

4.3.5. Dynamic Light Scattering of RM Samples

To verify that RMs formed in the RM samples for experimental analysis the solutions were subjected to DLS analysis. Sizes of w_0 20 RMs were made as representative for these investigations to better visualize any changes, and the results are summarized in Table 2.

Measurements were done for each solution of RMs containing G compounds and corresponding RM sample with no probe molecule. As seen in Table 4.1, the size of the RMs did not significantly change by the addition of G, GG, GGG, or GGGG and the values observed are in agreement with the literature value of 8.9 nm for a $w_0$20 RM [32].

Table 4.1. DLS size measurements of RM containing each of the G peptides. Each of these measurements was taken at pH 7.

Sample[a]	$W_0$20 diameter (nm)	$W_0$20 Std. Dev. (nm)
Control (no probe)	9.5	0.44
G	9.5	0.43
GG	9.2	0.47
GGG	9.2	0.36
GGGG	9.3	0.39

4.3.6. Compression Isotherms of Langmuir Monolayers Containing Glycine

Compression isotherm data is plotted as the percent difference in the area per molecule from the control versus the surface pressure, as shown in Fig. 7. At pH 4, 6, 7, and 8, DPPC monolayers containing glycine all exhibit a similar trend in which monolayers with glycine present have an expanded area at low surface pressure, but the amount of expansion decreases as surface pressure increases. However, for pH 6 and 7, monolayers exposed to glycine always

remain at least slightly expanded from the control. At pH 4, monolayers with glycine transition from expanded to contracted around 30-35 mN/m, which is what is commonly regarded as physiological surface pressure.[46-47] The pH 8 monolayer with glycine transitioned from expanded to condensed around 25 mN/m. The pH 9 monolayer with glycine in the subphase remained relatively near the control monolayer at all pressures, though slightly condensed. Importantly, at physiological-like conditions at pH7 with glycine in the subphase and DPPC as the lipid, the monolayer was 4-5% expanded relative to the control, implying that some glycine was positioned at the interface, as opposed to the subphase or the acyl chains of the DPPC. Overall, DPPC monolayers with glycine in the subphase have a trend of expanding the monolayer at lower surface pressures and then transition to only a slight expansion, or to condensing the monolayer as surface pressure increases. At pH 7, which is the most physiologically relevant pH used in this study, the monolayer remains expanded relative to the control, which suggests that glycine interacts weakly with the interface.

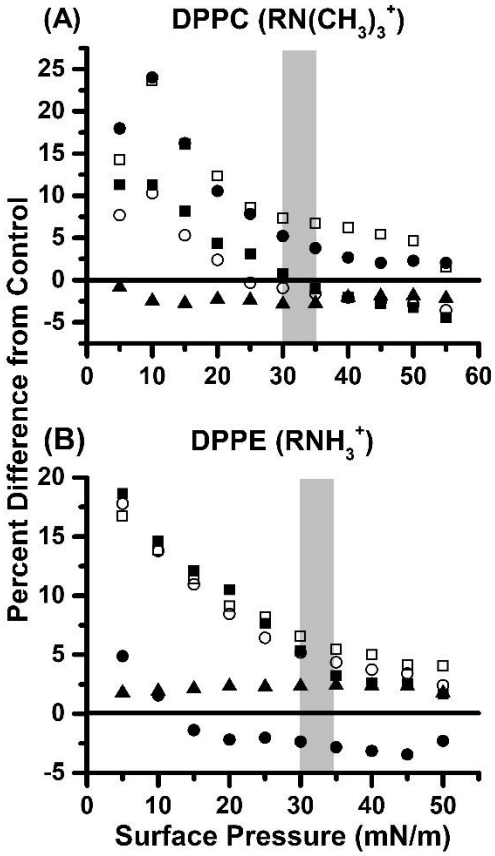

Figure 4.7. Calculated percent difference between the area per molecule of control Langmuir monolayers and monolayers with glycine in the subphase for (A) DPPC and (B) DPPE. R represents the phosphate group, glycerol, and saturated C_{16} tails. Symbols each represent a different pH, where solid squares are pH 4, hollow squares are pH 6, solid circles are pH7, hollow circles are pH8 and solid triangles are pH 9. The region shaded grey represents physiological surface pressure.

DPPE monolayers, then, followed nearly the same trend at pH 4,6, and 8; all are 15-20% expanded relative to the control at a surface pressure of 5 mN/m and decreased as surface pressure increased. All three monolayers reached an equilibrium of remaining approximately 5% expanded relative to the control at 35 mN/m. Much like with the DPPC monolayers, the pH 9 monolayer remained relatively constant, remining between 1.8 and 2.4% expanded relative to the control throughout compression. While glycine slightly condensed DPPC at pH9, it slightly expanded DPPE at the same pH. Interestingly, pH 7 differs greatly between DPPC and DPPE. For DPPE, the pH 7 monolayer is 5% expanded relative to the control at 5 mN/m and then

becomes condensed between 10 and 15 mN/m. The monolayer remains slightly condensed, and at physiological surface pressure the monolayer exposed to glycine is approximately 2-3% condensed relative to the control. However, the calculated error is such that the glycine exposed monolayer is not significantly different from the control. Overall, DPPE monolayers with glycine in the subphase at all pH values but 7 follow similar patterns to each other in which the monolayer is expanded 15-20% at lower surface pressures and decreases to 5% expansion as the surface pressure increases. Interestingly, at pH 7 the monolayer exposed to glycine becomes slightly condensed and does not follow patterns typical of the other pH values, and the experimental error is such that there is no statistical difference between glycine-exposed and control monolayers. This suggests that glycine may interact with the membrane interface, but it does not do so strongly.

4.4. Discussion

The studies described above determine pKa measurements of G-containing peptides, and in doing so compare the data of small G-peptides in aqeuous solution and associated with the AOT interface. The longer G peptides, in the case of GGG and GGGG have chemical shifts in the same region as the AOT and overlap in chemical shifts, as can be seen in Fig. S15 and S19. G and GG are found to appear in a region where AOT and isooctane peaks are not observed, however, GGG and GGGG show signals in the same region as the AOT, therefore limiting observation of the signals of these short G-containing peptides. As a result, a subtraction method was utilized in which the AOT RM spectra containing no compound were subtracted from AOT RM spectra containing the G compound of interest. Analyzing the spectra using the subtraction method described in the experimental section allows us to calculate the chemical shifts for all G compounds and is also used to obtain the pK_a results summarized in Table 4.2. The pK_a values

were calculated for both the R-group protons near the C-terminus and the N-terminus of the G peptides in both aqueous environment and in the environment of the RM. The resulting pKa values calculated in this work are summarized in Table 4.2 for all the systems investigated in this work and detailed in the descriptions below.

Table 4.2. Comparison of experimental pK_a values obtained for G compounds in aqueous (D_2O) and w_0 10 RM systems, shown with 95% confidence interval, with literature aqueous pK_a values.

Compound	System	pK_a(1) Carboxylic acid	pK_a(1) lit.	pK_a(2) Protonated amine	pK_a(2) lit.	lit. citation
G	D_2O	2.51	2.46 I=0.2 ($NaClO_4$)	10.7	9.60 I=0.2 ($NaClO_4$)	[48]
	RM	2.49		8.51		This work
GG	D_2O	2.85	3.15 I=0.1 (KCl)	8.60	8.10 I=0.1 (KCl)	[48]
	RM	2.99		8.48		This work
GGG	D_2O	3.18	3.18 I=0.1 ($NaClO_4$)	8.29	7.87 I=0.1 ($NaClO_4$)	[48]
	RM	3.27		8.11		This work
GGGG	D_2O	3.05	3.25	7.75	7.98	[48]
	RM	2.82		7.94		This work

Our hypothesis; that the G is likely positioned such that the N-terminus is near or in the interstitial water region of the RM either facing the negatively charged interface or actually associated with the interface is in line with previous observations and predictions with other charged molecules [40, 49]. This pattern was observed for all the G peptides, to different degrees and with the largest change for G. The larger difference for G can be explained because this is a smaller amphiphilic molecule, and penetration of the interface by the N-terminus will impact the amphiphilic molecule more than with peptides. Although penetration will bring the C-terminus

closer to the interface, little change is observed in the pKa of the C-terminal, suggesting that the N-terminal is loosely associated with the interface, and not deeply penetrated in the the interface (Figure 4.8). This difference in the pK_a of the protonated amine of G may also be due to the presence of ions at the RM interface: in pure water G forms an energetically favorable 5-membered ring between the protons of the positively charged amine and the negatively charged oxygen on the carboxyl group, which is disrupted by the presence of ions at the RM interface where the N-terminus is likely located. This will result in a lower pK_a as shown in Table 2. The changes in the pKa value of the amino-terminus in the three G-peptides, by contrast, are much smaller. Differences in pK_a between different sizes of RMs containing G suggest that there may be some subtle differences in the specific location of the amino-terminus of these G-peptides as anticipated because the charge distributions are somewhat different depending on the specific conformation of the molecule. Importantly, modest change is observed in the pKa value of the C-terminus consistent with its environment changing much less compared to the aqueous and microemulsion preparations of the G compounds, consistent with their location closer to or in the bulk water pool of the RM as expected if the environment changed little [45].

The presented data for all the G-peptides investigated indicate that they all interact with the interface, albeit in a different way. The smallest G which is a zwitterion at neutral pH is likely to interact more strongly with the interface based on the large changes in the pKa of the free amine part of the peptide. As we demonstrated with aniline, the observed differences are likely to be caused by changes in location and not to an inherent different in pKa values in the new environment [49]. This may also be due to the disruption of the favorable 5-membered ring that is formed by the positively charged protons on the amine and the negatively charged oxygen on the carboxylate group in water by the presence of Na^+ at the RM interface as mentioned

previously. In the case of the GG, GGG and GGGG peptides, the observed difference is much less and there are also variations in the direction of the change; for G, GG and GGG the pKa value decreased (acidity increased) in the presence of the interface, whereas in the case of GGGG the pKa value increased (acidity decreased). In order to get more information on this system we examined the interactions of glycine with a lipid interfaces in the Langmuir monolayer system. Since the major responses were observed with glycine, we limited these studies with glycine but examined its response in a pH-dependent manner (section 2.6). These result showed that glycine is likely to associate with the lipid interface at pH near neutral hence confirming the observations made with the microemulsion system.

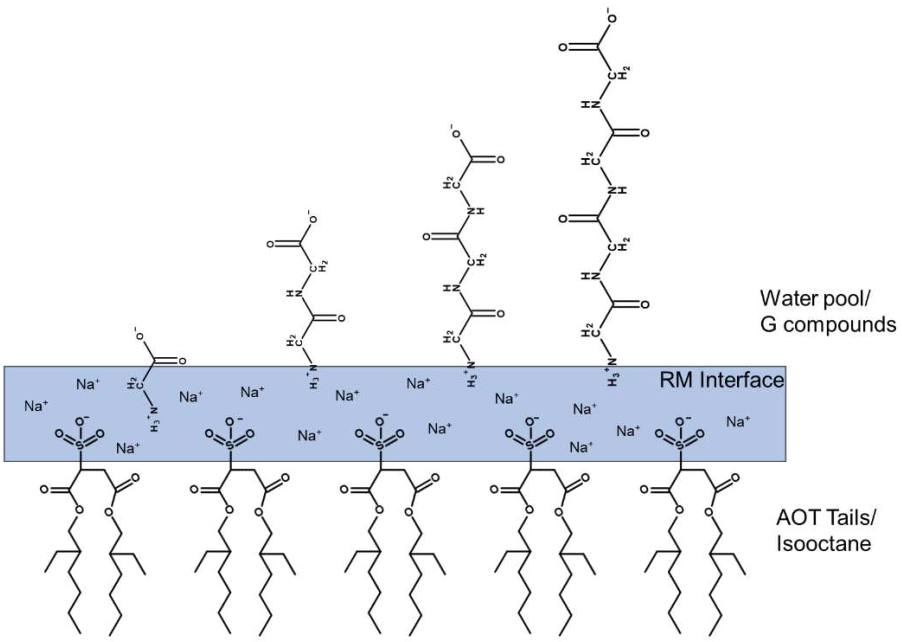

Figure 4.8. Schematic figure depicting the likely positioning of the G compounds used in this study relative to the RM interface. G compounds depicted here are shown in a linear conformation; however, it is likely that longer G compounds, such as GGG and GGGG, rotate around C-C bonds in solution such that the conformation of the molecule may be bent as discussed previously, but the C-terminal end is still located at the bulk water pool.

Comparison of the pKa values in aqueous solution and near RM-interfaces are most valuable when considering the inherent differences between the two systems and recognizing that the aqueous solution can change significantly depending on the other ions in solution and overall ionic strength. Previous work done with GGG in aqueous solution found that GGG adopts a U-shaped conformation in the presence of Na^+ and SO_3^- [50], with no similar studies being found for GG or GGGG. In this study, it was found that there is a strong interaction between the sodium ions and the sulfite, which then interacts with the protonated amine of GGG, and favoring a bending that adopts a U-shape. A similar phenomenon may be occurring in the RM systems, in which the Na^+ ions interact with the sulfate groups on the AOT surfactant molecules, which then interact more strongly with the protonated amine. This would be consistent with the increase in chemical shift of the protonated amine for GGGG in RM as compared to its shift in D_2O (Table 4.2). Additionally, the increased pK_a of the N-terminal protons as well as the slightly decreased pK_a of C-terminal protons indicates that the zwitterionic form is equally or more stable in the RM, consistent with being at the edge of the bulk water pool of the RM between bulk water and interface (Fig 4.6, Fig. 4.8).

These results implicate that it is unlikely that peptides containing numerous glycine residues will have a strong effect as a membrane-penetrating peptide for the use of development of novel antibacterial or anticancer therapeutics unless there are other amino acids present which are more likely to interact with a membrane interface, such as lysine. Even in the context of the reverse micelle, which has a strongly negatively charged interface to mimic the exposure of phosphatidylserine residues by cancerous cells, there is little to no interaction of the G peptides with the RM interface, indicating that even when the interface has a negative charge characteristic to bacterial or cancerous cells, there is still no penetration of the interface by a

peptide, despite numerous reports of glycine-rich AMPs [51-53]. This result stands in contrast with the studies with G alone which is found to interact with the interface. Together these results suggest that for AMP peptides to be effective in penetrating membranes resides other than G are necessary for the action of these peptides. This is consistent with the fact that many AMP peptides contain significantly higher concentrations of lysine residues and/or aromatic residues such as phenylalanine and tyrosine in addition to higher concentrations of glycine than the average presence of these amino acids in other proteins due to the two physical features required for antimicrobial peptide activity: charge and hydrophobicity [54-56]

4.5. Conclusions

Studies exploring the interaction of G, GG, GGG and GGGG compounds with model membrane interfaces measured in microemulsions (AOT RMs) using ^{1}H NMR spectroscopy and DLS indicate that G-peptides prefer to locate themselves at the edge of the charged reverse micellar interface, between the water pool and interface at the Stern layer. This location is different for the single amino acid G which is penetrated further into the interface. These findings are supported by the calculated pK_a values of the G compounds in both aqueous and RM systems. Minor differences are observed for the pK_a values and the chemical shift between the aqueous and micellar environments indicating similarity between environments that the G peptides are inhabiting. Larger changes are observed for the amine-group on the G amino acid suggesting that the N-terminus is further anchored into the interface. This finding is also consistent with studies done with Langmuir monolayers containing DPPE and DPPC exposed to glycine; in the case of DPPC, at physiological pH the interface remains only slightly expanded relative to the control indicating weak interaction with the interface. At physiological pH, there was no significant difference between DPPE monolayers exposed to glycine and the control. In

the case of the short G peptides GG, GGG and GGGG, it is likely that they associate with the RM interface by orienting themselves such that the N-termini interact weakly with the RM interface and the C-termini oriented towards the bulk water pool of the RM (Figure 4.8).

The case of G is very different from that of its longer peptides. In an aqueous environment the protons on the positively charged amine hydrogen bond with the negatively charged carboxyl end and form an energetically favorable five-membered ring. This may explain the large difference between the pK_a measured in the aqueous environment compared to the reverse micellar environment. In the RM, this hydrogen bonding is disrupted, likely by the presence of the Na^+ counter-ions. Additionally, the observed gradually decreasing chemical shift of G at pH 7 and 9 indicates that the amino acid likely is placed in the interstitial water layer between the interface and the bulk water pool. As the RM grows larger and the water becomes more similar to bulk water, the chemical shift approaches a shift more analogous to that in D_2O consistent with the G moving from the interface into the interior water pool. This conclusion is very important because of the role of G as a neurotransmitter; that is, for G to function and propagate a signal to be received after it has been confined within synaptic vesicles and excreted through the synapse. These results suggest that in the large synaptic vesicle (40 nm), it is not likely that G will have any significant interactions with the membrane interface and is readily released for uptake [57].

Considering that AMPs (host defense peptides) generally contain a high level of G as well as other key amino acids (Lys, Phe/Tyr) it was of interest to determine the effects of G and G peptides to obtain a better understanding how specific amino acid residues and their corresponding peptides interact with membranes. The data suggests that the amino acid G does associate with the membrane whereas the G peptides interact less strongly with a membrane, and

likely function to increase the hydrophobicity of reported AMPs which are glycine-rich. These studies support the interpretation that the properties of the AMP peptides are more related to other amino acids such as Lys and aromatic amino acids with regard to translocation of these peptides across a membrane for anticancer or antimicrobial activities.

References

1. Malandrino, N.; Smith, R. J., Synthesis, secretion, and transport of peptide hormones. *Principles of Endocrinology and Hormone Action; Belfiroe, A., LeRoith, D., Eds* **2018**, 29-42.
2. Snyder, S. H., Brain peptides as neurotransmitters. *Science* **1980,** *209* (4460), 976-983.
3. Peters, G. H.; Werge, M.; Elf-Lind, M. N.; Madsen, J. J.; Velardez, G. F.; Westh, P., Interaction of neurotransmitters with a phospholipid bilayer: a molecular dynamics study. *Chemistry and Physics of Lipids* **2014,** *184*, 7-17.
4. Gallo, R. L.; Murakami, M.; Ohtake, T.; Zaiou, M., Biology and clinical relevance of naturally occurring antimicrobial peptides. *Journal of Allergy and Clinical Immunology* **2002,** *110* (6), 823-831.
5. Fjell, C. D.; Hiss, J. A.; Hancock, R. E.; Schneider, G., Designing antimicrobial peptides: form follows function. *Nature Reviews Drug Discovery* **2012,** *11* (1), 37-51.
6. Ambroggio, E. E.; Separovic, F.; Bowie, J. H.; Fidelio, G. D.; Bagatolli, L. A., Direct visualization of membrane leakage induced by the antibiotic peptides: maculatin, citropin, and aurein. *Biophysical Journal* **2005,** *89* (3), 1874-1881.
7. Zasloff, M., Antimicrobial peptides of multicellular organisms. *Nature* **2002,** *415* (6870), 389-395.
8. Brogden, K. A., Antimicrobial peptides: pore formers or metabolic inhibitors in bacteria? *Nature Reviews Microbiology* **2005,** *3* (3), 238-250.
9. Roudi, R.; Syn, N. L.; Roudbary, M., Antimicrobial peptides as biologic and immunotherapeutic agents against cancer: a comprehensive overview. *Frontiers in Immunology* **2017,** *8*, 1320.
10. Tornesello, A. L.; Borrelli, A.; Buonaguro, L.; Buonaguro, F. M.; Tornesello, M. L., Antimicrobial peptides as anticancer agents: Functional properties and biological activities. *Molecules* **2020,** *25* (12), 2850.
11. Hancock, R. E.; Sahl, H.-G., Antimicrobial and host-defense peptides as new anti-infective therapeutic strategies. *Nature Biotechnology* **2006,** *24* (12), 1551-1557.
12. Peschel, A.; Sahl, H.-G., The co-evolution of host cationic antimicrobial peptides and microbial resistance. *Nature Reviews Microbiology* **2006,** *4* (7), 529-536.
13. Zandsalimi, F.; Talaei, S.; Noormohammad Ahari, M.; Aghamiri, S.; Raee, P.; Roshanzamiri, S.; Yarian, F.; Bandehpour, M.; Zohrab Zadeh, Z., Antimicrobial peptides: a promising strategy for lung cancer drug discovery? *Expert Opinion on Drug Discovery* **2020,** *15* (11), 1343-1354.
14. Maravilla, E.; Le, D. P.; Tran, J. J.; Chiu, M. H.; Prenner, E. J.; Weers, P. M., Apolipophorin III interaction with phosphatidylglycerol and lipopolysaccharide: a potential mechanism for antimicrobial activity. *Chemistry and Physics of Lipids* **2020**, 104909.
15. Felício, M. R.; Silva, O. N.; Gonçalves, S.; Santos, N. C.; Franco, O. L., Peptides with dual antimicrobial and anticancer activities. *Frontiers in Chemistry* **2017,** *5*, 5.
16. Chen, Y.; Guarnieri, M. T.; Vasil, A. I.; Vasil, M. L.; Mant, C. T.; Hodges, R. S., Role of peptide hydrophobicity in the mechanism of action of α-helical antimicrobial peptides. *Antimicrobial Agents and Chemotherapy* **2007,** *51* (4), 1398-1406.
17. Yeaman, M. R.; Yount, N. Y., Mechanisms of antimicrobial peptide action and resistance. *Pharmacological Reviews* **2003,** *55* (1), 27-55.

18. Chiangjong, W.; Chutipongtanate, S.; Hongeng, S., Anticancer peptide: Physicochemical property, functional aspect and trend in clinical application. *International Journal of Oncology* **2020,** *57* (3), 678-696.
19. Shai, Y., Mode of action of membrane active antimicrobial peptides. *Peptide Science: Original Research on Biomolecules* **2002,** *66* (4), 236-248.
20. Hale, J. D.; Hancock, R. E., Alternative mechanisms of action of cationic antimicrobial peptides on bacteria. *Expert Review of Anti-Infective Therapy* **2007,** *5* (6), 951-959.
21. Melo, M. N.; Ferre, R.; Castanho, M. A., Antimicrobial peptides: linking partition, activity and high membrane-bound concentrations. *Nature Reviews Microbiology* **2009,** *7* (3), 245-250.
22. Teixeira, V.; Feio, M. J.; Bastos, M., Role of lipids in the interaction of antimicrobial peptides with membranes. *Progress in Lipid Research* **2012,** *51* (2), 149-177.
23. Dathe, M.; Wieprecht, T., Structural features of helical antimicrobial peptides: their potential to modulate activity on model membranes and biological cells. *Biochimica et Biophysica Acta (BBA)-Biomembranes* **1999,** *1462* (1-2), 71-87.
24. Wang, W.; Wu, Z.; Dai, Z.; Yang, Y.; Wang, J.; Wu, G., Glycine metabolism in animals and humans: implications for nutrition and health. *Amino Acids* **2013,** *45* (3), 463-477.
25. Eulenburg, V.; Armsen, W.; Betz, H.; Gomeza, J., Glycine transporters: essential regulators of neurotransmission. *Trends in Biochemical Sciences* **2005,** *30* (6), 325-333.
26. Sager, W., Systematic study on the influence of impurities on the phase behavior of sodium bis (2-ethylhexyl) sulfosuccinate microemulsions. *Langmuir* **1998,** *14* (22), 6385-6395.
27. Ahmad, S. I.; Shinoda, K.; Friberg, S., Microemulsions and phase equilibria. Mechanism of the formation of so-called microemulsions studied in connection with phase diagram. *Journal of Colloid and Interface Science* **1974,** *47* (1), 32-37.
28. Shinoda, K.; Friberg, S., Microemulsions: colloidal aspects. *Advances in Colloid and Interface Science* **1975,** *4* (4), 281-300.
29. Giorgio, G.; Colafemmina, G.; Mavelli, F.; Murgia, S.; Palazzo, G., The impact of alkanes on the structure of Triton X100 micelles. *RSC Advances* **2016,** *6* (1), 825-836.
30. Pileni, M., Reverse micelles as microreactors. *Journal of Physical Chemistry A* **1993,** *97* (27), 6961-6973.
31. Quintana, S. S.; Dario Falcone, R.; Silber, J. J.; Mariano Correa, N., Comparison between Two Anionic Reverse Micelle Interfaces: The Role of Water-Surfactant Interactions in Interfacial Properties. *ChemPhysChem* **2012,** *13* (1), 115-123.
32. Maitra, A., Determination of size parameters of water-Aerosol OT-oil reverse micelles from their nuclear magnetic resonance data. *Journal of Physical Chemistry A* **1984,** *88* (21), 5122-5125.
33. Baruah, B.; Roden, J. M.; Sedgwick, M.; Correa, N. M.; Crans, D. C.; Levinger, N. E., When is water not water? Exploring water confined in large reverse micelles using a highly charged inorganic molecular probe. *Journal of the American Chemical Society* **2006,** *128* (39), 12758-12765.
34. Tan, H.-S.; Piletic, I. R.; Fayer, M., Orientational dynamics of water confined on a nanometer length scale in reverse micelles. *The Journal of Chemical Physics* **2005,** *122* (17), 174501.
35. Peters, B. J.; Groninger, A. S.; Fontes, F. L.; Crick, D. C.; Crans, D. C., Differences in Interactions of Benzoic Acid and Benzoate with Interfaces. *Langmuir* **2016,** *32* (37), 9451-9459.

36. Stahla, M. L.; Baruah, B.; James, D. M.; Johnson, M. D.; Levinger, N. E.; Crans, D. C., H-1 NMR studies of aerosol-OT reverse micelles with alkali and magnesium counterions: Preparation and analysis of MAOTs. *Langmuir* **2008,** *24* (12), 6027-6035.
37. Crans, D. C.; Schoeberl, S.; Gaidamauskas, E.; Baruah, B.; Roess, D. A., Antidiabetic vanadium compound and membrane interfaces: interface-facilitated metal complex hydrolysis. *Journal of Biological Inorganic Chemistry* **2011,** *16* (6), 961-972.
38. Koehn, J. T.; Magallanes, E. S.; Peters, B. J.; Beuning, C. N.; Haase, A. A.; Zhu, M. J.; Rithner, C. D.; Crick, D. C.; Crans, D. C., A synthetic isoprenoid lipoquinone, menaquinone-2, adopts a folded conformation in solution and at a model membrane interface. *The Journal of Organic Chemistry* **2017,** *83* (1), 275-288.
39. Samart, N.; Beuning, C. N.; Haller, K. J.; Rithner, C. D.; Crans, D. C., Interaction of a biguanide compound with membrane model interface systems: probing the properties of antimalaria and antidiabetic compounds. *Langmuir* **2014,** *30* (29), 8697-8706.
40. Crans, D. C.; Trujillo, A. M.; Bonetti, S.; Rithner, C. D.; Baruah, B.; Levinger, N. E., Penetration of Negatively Charged Lipid Interfaces by the Doubly Deprotonated Dipicolinate. *Journal of Organic Chemistry* **2008,** *73* (24), 9633-9640.
41. Peters, B. J.; Van Cleave, C.; Haase, A. A.; Hough, J. P. B.; Giffen-Kent, K. A.; Cardiff, G. M.; Sostarecz, A. G.; Crick, D. C.; Crans, D. C. J. L., Structure Dependence of Pyridine and Benzene Derivatives on Interactions with Model Membranes. *Langmuir* **2018,** *34* (30), 8939-8951.
42. Crans, D. C.; Rithner, C. D.; Baruah, B.; Gourley, B. L.; Levinger, N. E., Molecular probe location in reverse micelles determined by NMR dipolar interactions. *Journal of the American Chemical Society* **2006,** *128* (13), 4437-4445.
43. Harpham, M. R.; Ladanyi, B. M.; Levinger, N. E.; Herwig, K. W., Water motion in reverse micelles studied by quasielastic neutron scattering and molecular dynamics simulations. *The Journal of Chemical Physics* **2004,** *121* (16), 7855-7868.
44. Harpham, M. R.; Ladanyi, B. M.; Levinger, N. E., The effect of the counterion on water mobility in reverse micelles studied by molecular dynamics simulations. *The Journal of Physical Chemistry B* **2005,** *109* (35), 16891-16900.
45. Riter, R. E.; Willard, D. M.; Levinger, N. E., Water immobilization at surfactant interfaces in reverse micelles. *Journal of Physical Chemistry B* **1998,** *102* (15), 2705-2714.
46. Brown, R. E.; Brockman, H. L., Using monomolecular films to characterize lipid lateral interactions. In *Lipid Rafts*, Springer: 2007; pp 41-58.
47. Miyoshi, T.; Kato, S., Detailed analysis of the surface area and elasticity in the saturated 1, 2-diacylphosphatidylcholine/cholesterol binary monolayer system. *Langmuir* **2015,** *31* (33), 9086-9096.
48. Serjeant, E. P.; Dempsey, B., *Ionisation constants of organic acids in aqueous solution*. Pergamon: 1979; Vol. 23.
49. Sripradite, J.; Miller, S. A.; Johnson, M. D.; Tongraar, A.; Crans, D. C., How interfaces affect the acidity of the anilinium ion. *Chemistry–A European Journal* **2016,** *22* (11), 3873-3880.
50. Schwartz, C. P.; Uejio, J. S.; Duffin, A. M.; England, A. H.; Kelly, D. N.; Prendergast, D.; Saykally, R. J., Investigation of protein conformation and interactions with salts via X-ray absorption spectroscopy. *Proceedings of the National Academy of Sciences* **2010,** *107* (32), 14008-14013.
51. Lu, J.; Chen, Z.-w., Isolation, characterization and anti-cancer activity of SK84, a novel glycine-rich antimicrobial peptide from Drosophila virilis. *Peptides* **2010,** *31* (1), 44-50.

52. Xie, Y.; Wan, H.; Zeng, X.; Zhang, Z.; Wang, Y., Characterization and antimicrobial evaluation of a new Spgly-AMP, glycine-rich antimicrobial peptide from the mud crab Scylla paramamosain. *Fish & Shellfish Immunology* **2020,** *106*, 384-392.
53. Rahman, M. S.; Choi, Y. H.; Choi, Y. S.; Yoo, J. C., Glycin-rich antimicrobial peptide YD1 from B. amyloliquefaciens, induced morphological alteration in and showed affinity for plasmid DNA of E. coli. *AMB Express* **2017,** *7* (1), 8.
54. Zasloff, M., Magainins, a class of antimicrobial peptides from Xenopus skin: isolation, characterization of two active forms, and partial cDNA sequence of a precursor. *Proceedings of the National Academy of Sciences* **1987,** *84* (15), 5449-5453.
55. Nguyen, L. T.; Haney, E. F.; Vogel, H. J., The expanding scope of antimicrobial peptide structures and their modes of action. *Trends in Biotechnology* **2011,** *29* (9), 464-472.
56. Wang, Z.; Wang, G., APD: the antimicrobial peptide database. *Nucleic Acids Research* **2004,** *32* (suppl_1), D590-D592.
57. Zhang, B.; Koh, Y. H.; Beckstead, R. B.; Budnik, V.; Ganetzky, B.; Bellen, H. J., Synaptic vesicle size and number are regulated by a clathrin adaptor protein required for endocytosis. *Neuron* **1998,** *21* (6), 1465-1475.

Chapter 5: Model Membranes as a Tool for Probing Membrane Interactions

5.1. The Utility of Model Membranes for Studying Electrochemical Properties of Menaquinones

Chapters two and three of this thesis explore the redox properties, conformation and placement of hydrophobic molecules such as menaquinones in a bilayer. These studies would not have been possible, or would have been extremely difficult, without the use of liposomes as a model membrane.

In Chapter 2, the electrochemistry of a variety of truncated menaquinones was examined in the context of a simple soybean phosphatidylcholine liposomal bilayer. Previous work in our lab has studied these compounds electrochemical properties in the aprotic solvents pyridine, dimethyl sulfoxide (DMSO), and acetonitrile. This was good preliminary work for a number of reasons. First, it is much easier to study menaquinones of varying chain length in solvents such as these due to their increased solubility compared to water. Additionally, it provides a much more simplified environment for the study of such molecules. Such a simplified environment allows the experimental set-up to examine the electrochemical properties of menaquinones: they have increased solubility in these solutions and there is minimal interference from other compounds or structures in the sample. The molecule is able to freely rotate in solution to come into contact with the electrode rather than needing to diffuse to the surface of a liposome, which must then diffuse to the surface of the electrode as it must in a liposomal formulation. Additionally, work done in aprotic solvent allowed the observation of two one-electron transfers to the menaquinone, which is not observable in protic solvent or in the liposomal environment. However, while these preliminary studies laid the groundwork for observing the properties of menaquinones in solution, they do not provide as much biologically relevant information as

studies done in a liposome can.

Studies done here examining the half-wave potentials of truncated menaquinone analogues in liposomes provide more biologically relevant information, however, their confinement in the bilayer does not provide information that is as straightforward or as easily interpretable as that obtained in aprotic solvent. Unpublished studies in our lab show that in the same truncated analogues studied in Chapter 2 of this thesis, half-wave potentials of analogues saturated at the β-isoprene unit required less extreme potentials to oxidize and reduce than fully unsaturated or fully saturated analogues. Examination of half-wave potentials of truncated menaquinone analogues in a liposomal context showed a much more complex, and less easily interpretable result. While there was no significant difference in half-wave potential between fully unsaturated analogues, as the number of saturations in the isoprene chain increased a distinct odd-even effect manifested, in which an increase in saturations of the isoprene chain results in a menaquinone analogue that requires either more or less extreme potentials to be oxidized and reduced depending on chain length, or in the case of MK1, there was no effect at all. While initially puzzling, this odd-even effect has been documented extensively in the literature when studying self-assembled monolayers, or SAMs. Self-assembled monolayers are layers of material, typically one molecule thick, that are bonded to a surface in an ordered way (Figure 5.1).[1-2]

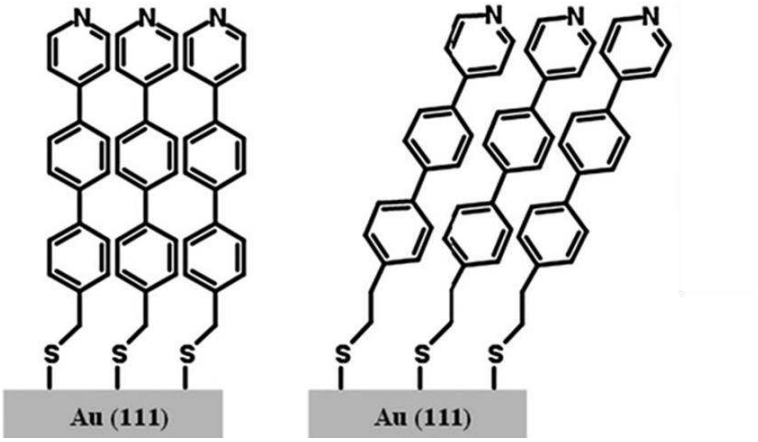

Figure 5.1. Example of self-assembled monolayer in which pyridine-terminated thiolates are assembled on gold. Figure published by Liu et. al.[1]

It has previously been found in a number of instances that differences between odd-length and even-length hydrocarbon chains of molecules bound to a surface to create SAMS have different electrochemical properties, despite potentially only differing by one carbon atom.[3-5] This is due to the length of the carbon chain affecting the placement of the aromatic head group, in the case of menaquinone, naphthoquinone, relative to the plane of the electrode's surface as well as to the molecules surrounding it (Figure 5.1).[6] As a result, it is often difficult to determine what is causing the odd-even effect observed, since it is difficult to separate the intramolecular effects of the packing of the molecules from the effects that are caused by the placement of the aromatic ring relative to the electrode.[7-8]

A similar phenomenon is likely occurring in the case of truncated menaquinones bound in the context of the liposome. Due to their limited solubility in water and increased solubility in liposomal solutions, as well as the data shown here in Chapter 3, it is likely that menaquinone analogues with the exception of MK1 are confined to a certain location in the bilayer, such as menaquinone-2 residing at the charged interface of a PC liposome. In addition to being confined to a certain location in the bilayer, it is also likely that they adopt a certain conformation based

on their surrounding environment, as evidenced here in Chapter 3 as well as in previous publications by our lab. This confinement in the liposome and preferred conformation of the menaquinone analogue may produce a similar effect to the odd-even effect observed on SAMS: a combination of conformation of the molecule itself and its interactions with the liposomal environment may result in a majority of the MK-*n* molecules displaying similar electronic characteristics, and resulting in the naphthoquinone head groups orientation being altered relative to the surface of the electrode. The reason that MK1 is likely not affected as strongly, or at all, is because of its increased water solubility: like the MK analogues studied in aprotic solvents, MK1 in an aqueous environment is likely not confined by the bilayer and is able to diffuse freely through aqueous solution to the electrode's surface. It is unclear, however, whether this odd-even effect affects the biological process of oxidation and reduction in those organisms which do use menaquinone in their electron transport system. The oxidation and reduction of menaquinone is typically carried out by enzymes which transfer electrons from a donor to the menaquinone, with another enzyme transferring the electrons from menaquinone to an electron acceptor. It is possible that the electrochemical differences observed here are overcome by the enzymes specific to the organisms which produce menaquinone as an electron transporter, and the observation that more or less extreme potentials are required for MK to undergo redox processes may have no difference to an enzyme which is simply transferring electrons to and from menaquinone and an electron donor or acceptor. However, due to the widely differing MK-*n* species which are produced by bacteria, even to the point that they are used for taxonomic purposes, it is advantageous to understand the behavior and electrochemical properties of this electron transporter in a bilayer.[9-11]

To further this project, though they have not yet been synthesized in our lab, longer chain

MK analogues with saturations in the side chain should be used for electrochemical studies of MK-*n* analogues in liposomes. Studies with alternating odd and even hydrocarbon lengths of molecules immobilized on a surface in SAMs show that an increase in chain length of the compound being studied shows greater differences between odd and even-length molecules.[7] Certainly, it would be interesting to see if the same odd-event trend here remains the same, but more pronounced, with longer isoprene chains attached to the naphthoquinone head group. In addition to determining whether the trend observed here with truncated analogues remains the same with longer MK-*n* analogues, it would also be of interest to study longer chain analogues simply because they are more likely to act as electron transporters for bacterial species, where shorter chain MK-*n* analogues do not.

5.2. The Utility of Model Membranes for Examining the Molecular Interactions and Placement of Menaquinone-2 Within a Liposome

Similar to work done with the electrochemical characterization of MK-*n* analogues, previous work done in our lab examined the conformation of menaquinone-2 in aprotic solvents as well as in the context of a reverse micelle. The work presented here in Chapter 3 builds on this previous work and characterizes the likely conformation of menaquinone-2 in the context of the more biologically relevant liposome. Unlike the work examining the electrochemistry of MK-*n* in solvents and reverse micelles, similar results were found here as in previous work. Previous work determined that, with the exception of minor conformational changes in the tail of MK-2 to minimize unfavorable solvent interactions, MK-2 in solution and in reverse micelles adopts a folded, U-like shape in which the tail folds itself over the naphthoquinone head group to one side of the ring's plane.[12] However, there were some minor differences in the placement of the molecule with respect to the surfactant or lipid head groups when moving from reverse

micelles to a liposomal bilayer. In this instance, lipid-MK-2 cross peak interactions indicated that MK-2 orients itself with the naphthoquinone head group oriented outwards towards the outer liposomal leaflet, rather than with the bend in MK-2 pointed towards the polar head groups of the AOT comprising reverse micelles. Additionally, at higher concentrations of MK2 relative to PC, MK2 appears to be pushed out of the bilayer, as evidenced by an emergent set of peaks in the 12 mg/mL MK2 liposomal spectrum which correspond directly to its peaks in D_2O. The conformation of liposome-bound and aqueous forms of MK2 are similar, in which the isoprene tail is folded over the naphthoquinone head group. However, the liposome bound form of MK2 is folded over itself more tightly, as evidenced by interactions between protons $H_{H,I}$ and protons $H_{C,D}$ which are not present in the liposomal spectra containing aqueous MK2 peaks.

While this work is interesting in that it determines the conformation of MK2 in the more biologically relevant context of a liposome, I think that this work could be pushed further by examining the placement of MK2(II-H_2) and MK2(H_4) within a liposomal bilayer and determine how the increasing saturations in the tail affect both the molecules placement in the bilayer as well as how their conformation may be affected by the lack of double bonds in the isoprene tail. MK2 is the ideal molecule for these preliminary studies because while the isoprene side chain is shortened, there are numerous rotational degrees of freedom which can complicate the data collected, particularly in the case of fully saturated MK2. MK-*n* molecules of longer chain length, while more biologically relevant, will prove difficult to study via 2D NMR or molecular modeling for these same reasons. However, in the case of MK2 with increasing saturations, the rotational degrees of freedom are manageable, and in Chapter 2 we see that with increasing saturations in the isoprenyl side chain of MK2 both half-wave potentials and reversibility ip_a/ip_c ratios change significantly. It is possible that this significant change in electrochemical

properties comes as a result of different conformations and placement in the liposomal bilayer due to the loss of the double bonds in the chain making the molecule more hydrophobic and potentially changing interactions of the isoprene tail with the head group for the same reason. Experiments should also be done with MK3 in a bilayer to determine if there are any significant differences in the placement and conformation of MK3 compared to MK2 which may also account for the odd-even effect observed in Chapter 2, however, again, this work may prove difficult due to the length of the isoprene side chain. Work with the truncated MK2 analogues mentioned here is being carried out currently in the lab. In all, the work presented in Chapter 3 on the placement and conformation of MK2 in a bilayer lays the foundation for the study of other MK analogues, or indeed, a number of other hydrophobic molecules for the lab.

5.3. Utility of model membranes for probing membrane interactions of polar molecules

As shown in Chapter 4, it is also possible to use model membranes to probe the interactions of molecules within a model membrane context using a reverse micelle. This chapter shows the use of a reverse micelle to probe interactions of short glycine peptides in the context of a membrane to determine what the placement of glycine and short glycine peptides are in the RM relative to glycine's function as a neurotransmitter as well as what effect glycine may have in antimicrobial peptides, or AMPs. This work found that the short glycine peptides GG, GGG and GGGG prefer to locate themselves at the reverse micellar interface rather than in the bulk water pool, where glycine prefers to reside. This work shows that glycine likely would not have much effect on a bacterial membrane as an AMP, and relative to its duties as a neurotransmitter, when it is released from the synaptic vesicle into the neuron, as it does not appear to have strong interactions with either the reverse micellar interface or with DPPC and DPPE monolayers.

5.4. Concluding remarks

The work shown in this thesis, particularly the work with menaquinones confined to liposomal bilayers, has helped to further our understanding of how the electron transporter menaquinone behaves in a more biologically relevant environment: a membrane bilayer. Though the liposomal bilayers used in this context are greatly simplified from what would be observed in an actual bacterial membrane as discussed in Chapter 1, we are still able to observe an odd-even effect with regards to the electrochemical properties of truncated MK analogues as well as the conformation that they are likely to adopt in such an environment. In addition to furthering our understanding of MKs confined to a bilayer this work can be applied to a number of other hydrophobic molecules, with potential applications such as determination of partitioning coefficients of relevant hydrophobic molecules such as cannabinoids for assessment of inebriation or the study of any number of other hydrophobic molecules whose study proves difficult/irrelevant outside of the context of a bilayer.

References

1. Liu, J.; Schüpbach, B.; Bashir, A.; Shekhah, O.; Nefedov, A.; Kind, M.; Terfort, A.; Wöll, C., Structural characterization of self-assembled monolayers of pyridine-terminated thiolates on gold. *Physical Chemistry Chemical Physics* **2010,** *12* (17), 4459-4472.
2. Duwez, A.-S., Exploiting electron spectroscopies to probe the structure and organization of self-assembled monolayers: a review. *Journal of Electron Spectroscopy and Related Phenomena* **2004,** *134* (2-3), 97-138.
3. Long, Y.-T.; Rong, H.-T.; Buck, M.; Grunze, M., Odd–even effects in the cyclic voltammetry of self-assembled monolayers of biphenyl based thiols. *Journal of Electroanalytical Chemistry* **2002,** *524*, 62-67.
4. Feng, Y.; Dionne, E. R.; Toader, V.; Beaudoin, G.; Badia, A., Odd–even effects in electroactive self-assembled monolayers investigated by electrochemical surface plasmon resonance and impedance spectroscopy. *The Journal of Physical Chemistry C* **2017,** *121* (44), 24626-24640.
5. Krzykawska, A.; Szwed, M.; Ossowski, J.; Cyganik, P., Odd–even effect in molecular packing of self-assembled monolayers of biphenyl-substituted fatty acid on Ag (111). *The Journal of Physical Chemistry C* **2018,** *122* (1), 919-928.
6. Toledano, T.; Sazan, H.; Mukhopadhyay, S.; Alon, H.; Lerman, K.; Bendikov, T.; Major, D. T.; Sukenik, C. N.; Vilan, A.; Cahen, D., Odd–even effect in molecular electronic transport via an aromatic ring. *Langmuir* **2014,** *30* (45), 13596-13605.
7. Jiang, L.; Sangeeth, C. S.; Nijhuis, C. A., The origin of the odd–even effect in the tunneling rates across EGaIn junctions with self-assembled monolayers (SAMs) of n-alkanethiolates. *Journal of the American Chemical Society* **2015,** *137* (33), 10659-10667.
8. Eckermann, A. L.; Feld, D. J.; Shaw, J. A.; Meade, T. J., Electrochemistry of redox-active self-assembled monolayers. *Coordination chemistry reviews* **2010,** *254* (15-16), 1769-1802.
9. Collins, M. D.; Jones, D., Distribution of isoprenoid quinone structural types in bacteria and their taxonomic implication. *Microbiological reviews* **1981,** *45* (2), 316.
10. Collins, M.; Pirouz, T.; Goodfellow, M.; Minnikin, D., Distribution of menaquinones in actinomycetes and corynebacteria. *Microbiology* **1977,** *100* (2), 221-230.
11. García-López, M.; Meier-Kolthoff, J. P.; Tindall, B.; Gronow, S.; Woyke, T.; Kyrpides, N. C.; Hahnke, R. L.; Göker, M., Analysis of 1,000 type-strain genomes improves taxonomic classification of Bacteroidetes. *Frontiers in microbiology* **2019,** *10*, 2083.
12. Koehn, J. T.; Magallanes, E. S.; Peters, B. J.; Beuning, C. N.; Haase, A. A.; Zhu, M. J.; Rithner, C. D.; Crick, D. C.; Crans, D. C., A synthetic isoprenoid lipoquinone, menaquinone-2, adopts a folded conformation in solution and at a model membrane interface. *The Journal of organic chemistry* **2017,** *83* (1), 275-288.

Appendix I: Contributions to works

The materials in Chapter 1 are largely review materials that were prepared for the purposes of this thesis. Figures in Chapter 1 are adapted from literature and referenced accordingly.

Work in Chapter 2 shows the electrochemical properties of truncated menaquinones in liposomal formulations. Liposomal formulations of MK-*n* compounds were made in triplicate either by Kaitlin Doucette or Brian Heritage. Data collection was performed by Kaitlin Doucette or by Brian Heritage. Data interpretation and workup was done by Kaitlin Doucette as well as the writing. In this work, both Debbie C. Crans and Dean C. Crick provided valuable insight to help with the interpretation of data and helped with the assembly of the story presented in several meetings which proved invaluable to the writing of this chapter. Cheryle N. Beuning provided training on this project and helped with initial set-up of the experiments.

Work in Chapter 3 shows the 1D and 2D ^{1}H NMR spectra of menaquinone-2 in a phosphatidylcholine liposome. MK-*n* compounds were synthesized in our lab previously by Jordan T. Koehn and Heide Murakami. Liposomal formulations were made either by Kaitlin Doucette or by Gaia Bublitz. Data collection was also carried out either by Kaitlin Doucette or Gaia Bublitz. Kate Kostenkova and Heide Murakami gave invaluable advice for working up the spectra obtained for interpretation. Data interpretation was carried out either by Kaitlin Doucette or Gaia Bublitz. As always, Debbie C. Crans and Dean C. Crick provided valuable advice on the interpretation of the results and creation of a story from the data.

Work in Chapter 4 explores the use of reverse micellar model membranes for the investigation of glycine and glycine peptides at an interface. Reverse micelles containing glycine and glycine peptides were prepared either by myself or Prangthong Chaiyasit. Kayli N.

Martinez collected data determining the pK_a of glycine in $w_0$30 reverse micelles. Mary Fisher provided general lab advice and training. Data interpretation was carried out by Kaitlin Doucette and Prangthong Chaiyasit. Writing and figure making was carried out by Kaitlin Doucette, Prangthong Chaiyasit, and Nuttaporn Samart. Useful advice on data interpretation and methodology was given by Debbie C. Crans.

The following appendices contain information about contributions to published works not discussed in this thesis as well as supplementary information for data contained in Chapters two, three and four.

Appendix II: P-values Obtained for MK-*n* $E_{1/2}$ Potentials, Reversibility and Diffusion Coefficients

Table A2.1. P-values Calculated for $E_{1/2}$ Values of Fully Saturated MK-*n* Analogues

MK-*n* comparison	P-value	Sig.
MK1-MK2	0.8428	
MK2-MK3	0.0513	
MK1-MK3	0.1022	
MK3-MK4	0.0800	
MK2-MK4	0.4110	
MK1-MK4	0.4441	

Table A2.2. P-values Calculated for $E_{1/2}$ Values Comparing Each MK-*n* to Itself with Increasing Saturations in Isoprenyl Chain

MK-*n* comparison	P-value	Sig.
MK1-MK1(H2)	0.2346	
MK2-MK2(II-H2)	0.0023	*
MK2(II-H2)-MK2(H4)	0.0679	
MK2-MK2(H4)	0.0039	*
MK3-MK3(II-H2)	0.0495	*
MK3(II-H2)-MK3(H6)	0.4137	
MK3-MK3(H6)	0.0487	*
MK4-MK4(II,III,IV-H6)	7.932E-05	*

Table A2.3. P-values Calculated for ip_a/ip_c Ratios of Fully Saturated Analogues

MK-*n* comparison	P-value	Sig
MK1-MK2	0.0295	*
MK2-MK3	0.0072	*
MK1-MK3	0.0287	*
MK3-MK4	0.1389	
MK2-MK4	0.0105	*
MK1-MK4	0.1093	

Table A2.4. P-values Calculated for ip_a/ip_c ratios Comparing Each MK-*n* to Itself with Increasing Saturations in Isoprenyl Chain

MK-*n* comparison	P-value	Sig.
MK1-MK1(H2)	0.4518	
MK2-MK2(II-H2)	0.0986	
MK2(II-H2)-MK2(H4)	0.3471	
MK2-MK2(H4)	0.0262	*
MK3-MK3(II-H2)	0.3330	
MK3(II-H2)-MK3(H6)	0.0730	
MK3-MK3(H6)	0.0182	*
MK4-MK4(II,III,IV-H6)	0.0234	*

Table A2.5. P-values calculated for D_O Comparing Fully Saturated Analogues

MK-*n* comparison	P-value	Sig.
MK1-MK2	0.017066	*
MK2-MK3	0.019201	*
MK1-MK3	0.014056	*
MK3-MK4	0.065338	
MK2-MK4	0.115372	
MK1-MK4	0.015221	*

Table A2.6. P-values Calculated for D_O Comparing Each MK-*n* to Itself with Increasing Saturations in Isoprenyl Chain

MK-*n* comparison	P-value	Sig.
MK1-MK1(H2)	0.0471	*
MK2-MK2(II-H2)	0.0107	*
MK2(II-H2)-MK2(H4)	0.0492	*
MK2-MK2(H4)	0.0244	*
MK3-MK3(II-H2)	0.2512	
MK3(II-H2)-MK3(H6)	0.8691	
MK3-MK3(H6)	0.3498	
MK4-MK4(II,III,IV-H6)	0.4863	

Appendix III: Cyclic Voltammograms of MK-*n* Analogues with Increasing Scan Rates

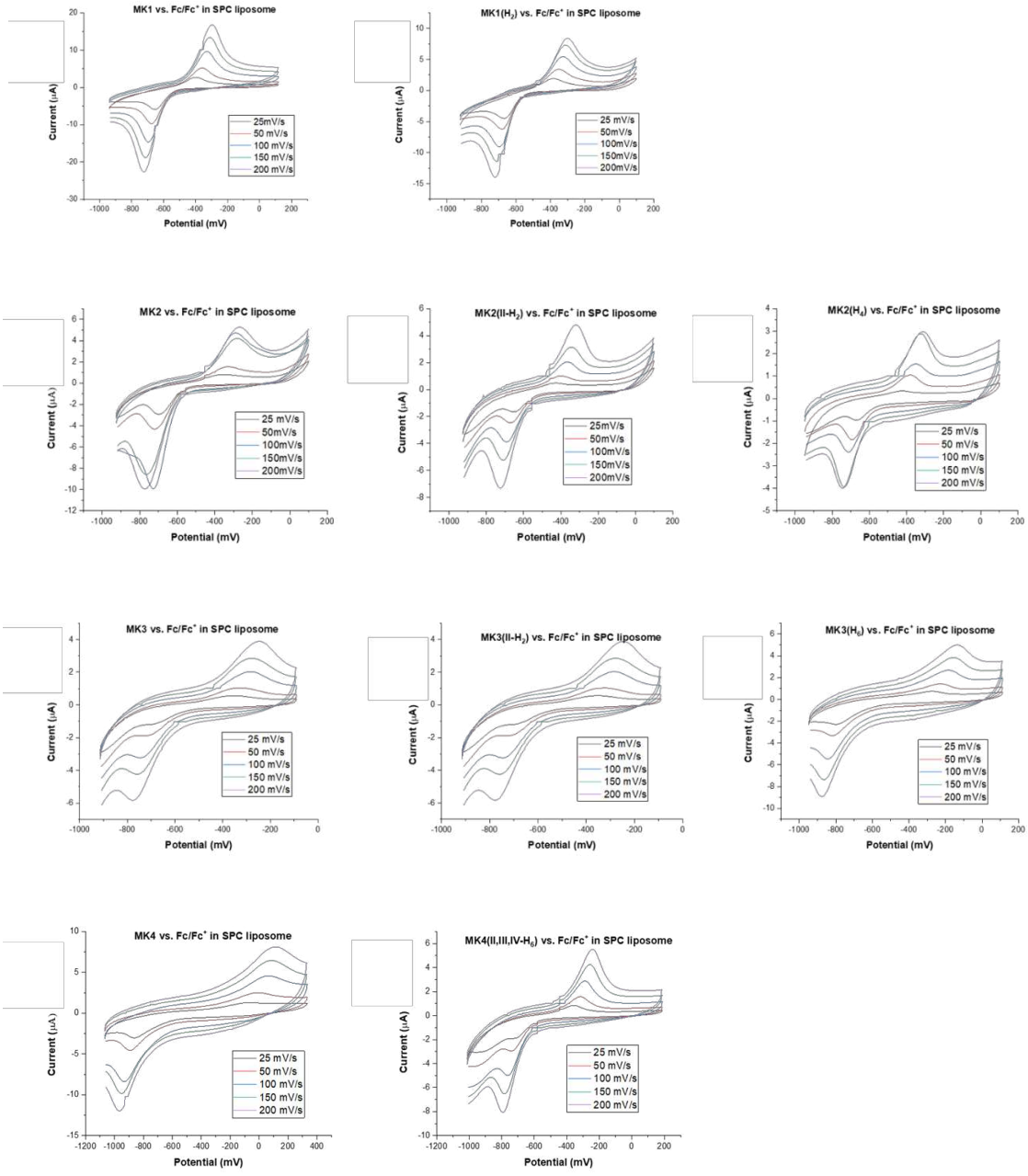

Figure A3.1. Cyclic voltammograms of each MK-*n* analogue studied at scan rates 25 mV/s, 50 mV/s, 100 mV/s, 150 mV/s, and 200 mV/s in soybean phosphatidylcholine liposomes.

Appendix IV. 2D ^{1}H-^{1}H ROESY NMR Spectra of MK-2 Confined in Egg Phosphatidylcholine Liposomes

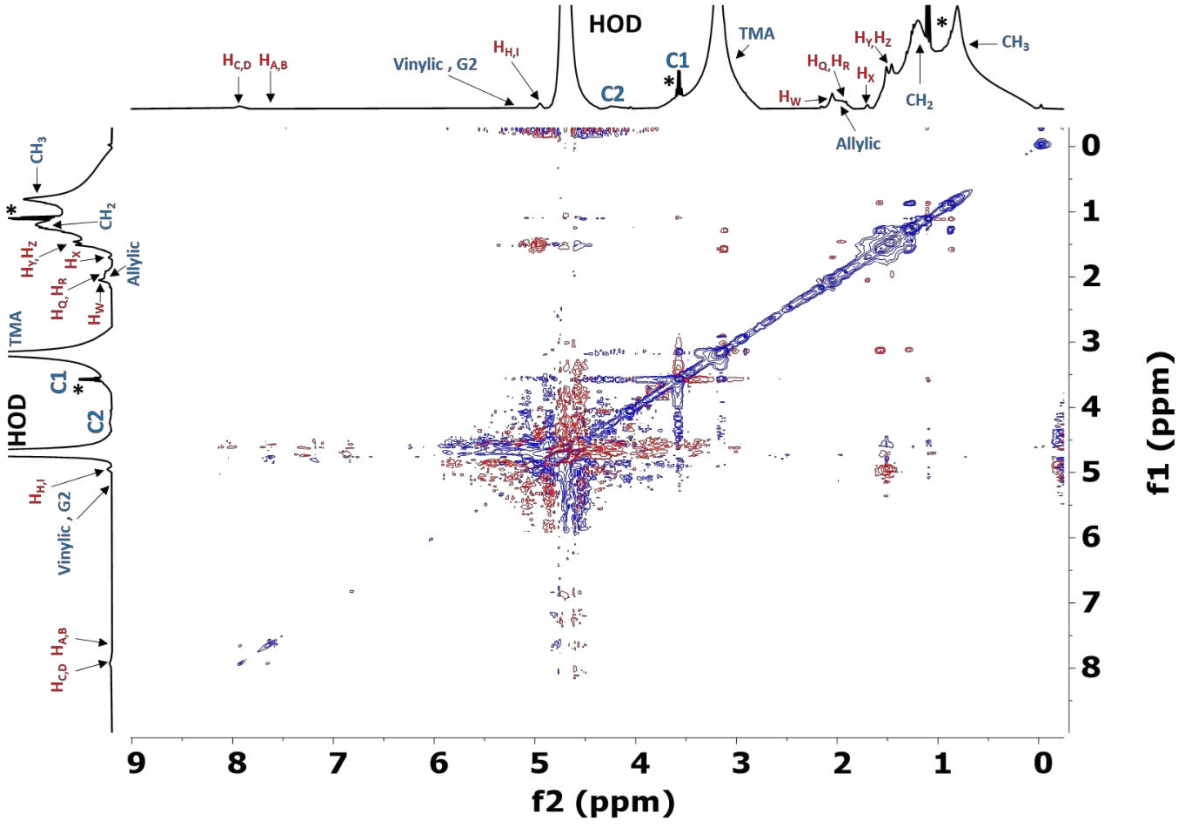

Figure A4.1. 2D ^{1}H-^{1}H ROESY NMR spectrum of 6 mg/mL MK-2 in PC liposomes.

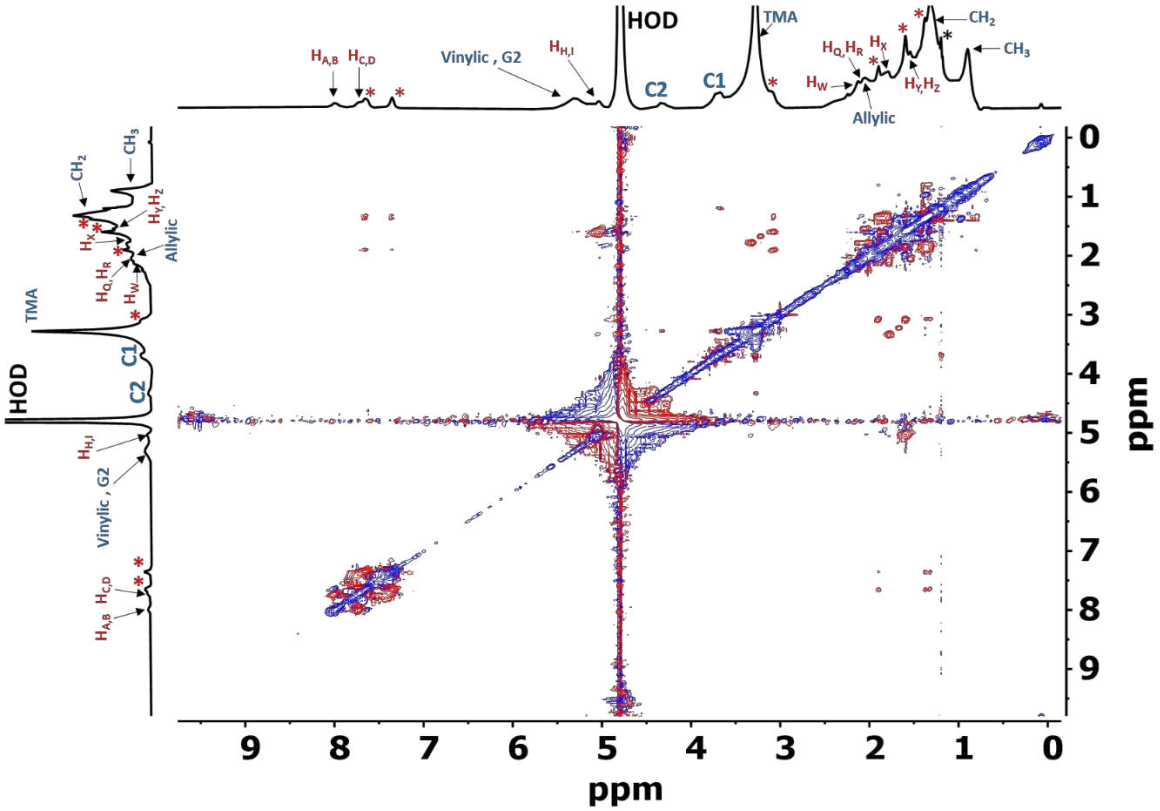

Figure A4.2. 2D ^{1}H-^{1}H ROESY NMR spectrum of 12 mg/mL MK-2 in PC liposomes.

Appendix V. ^{1}H NMR Spectra of Glycine in Aqueous and Reverse Micellar Solutions

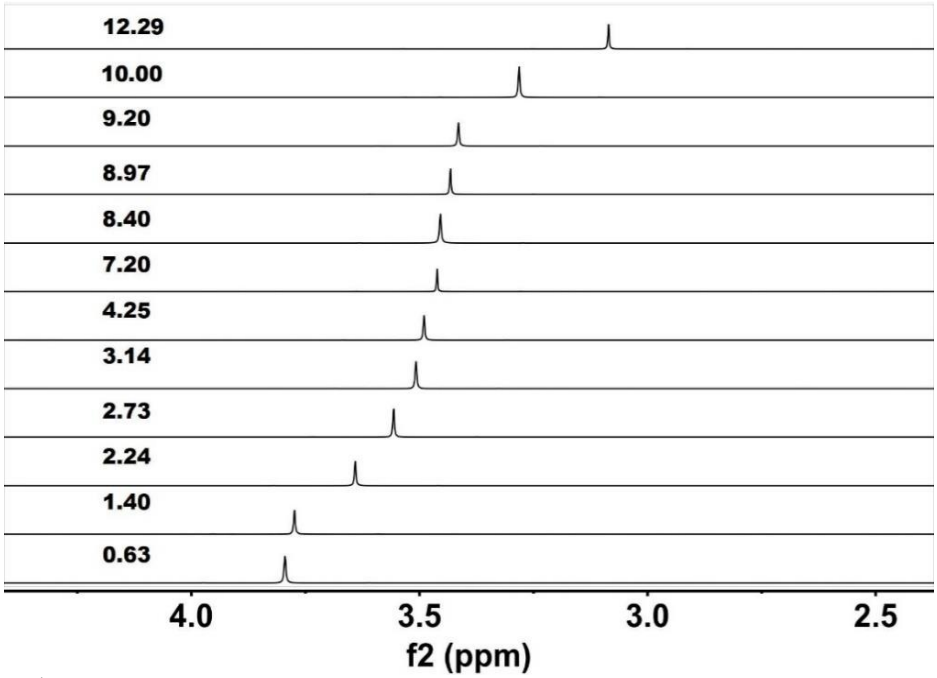

Figure A5.1. ^{1}H NMR of D_2O solutions containing G at varying pH values are shown. Spectra were run in triplicate and one representative series is shown.

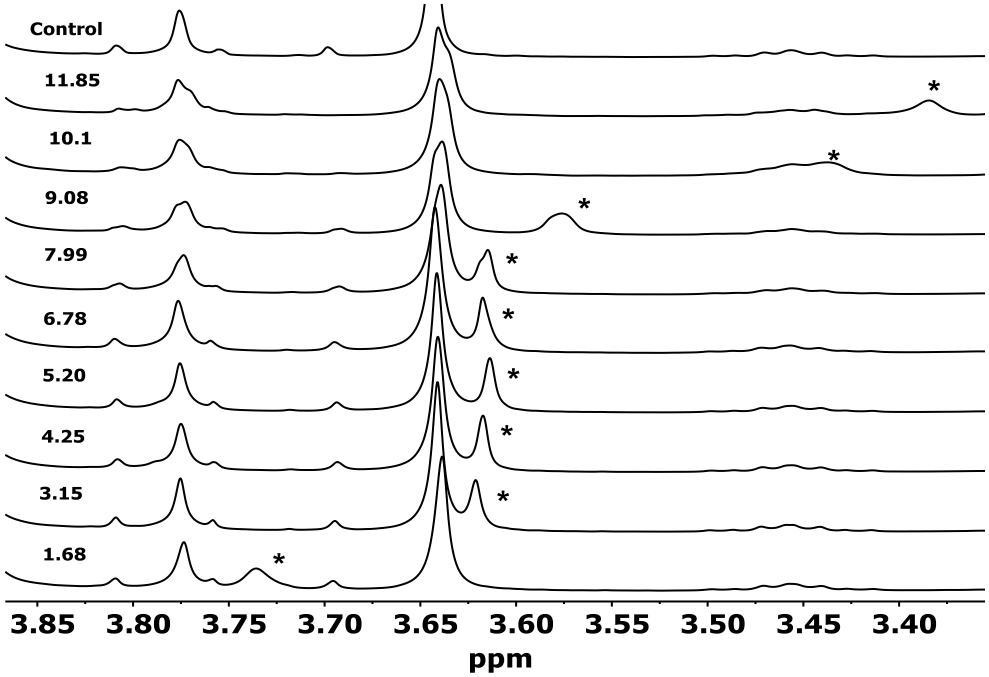

Figure A5.2. ^{1}H NMR of RM solutions containing G at varying pH values in the D_2O pool are shown. Samples are run in triplicate and one representative series is shown.

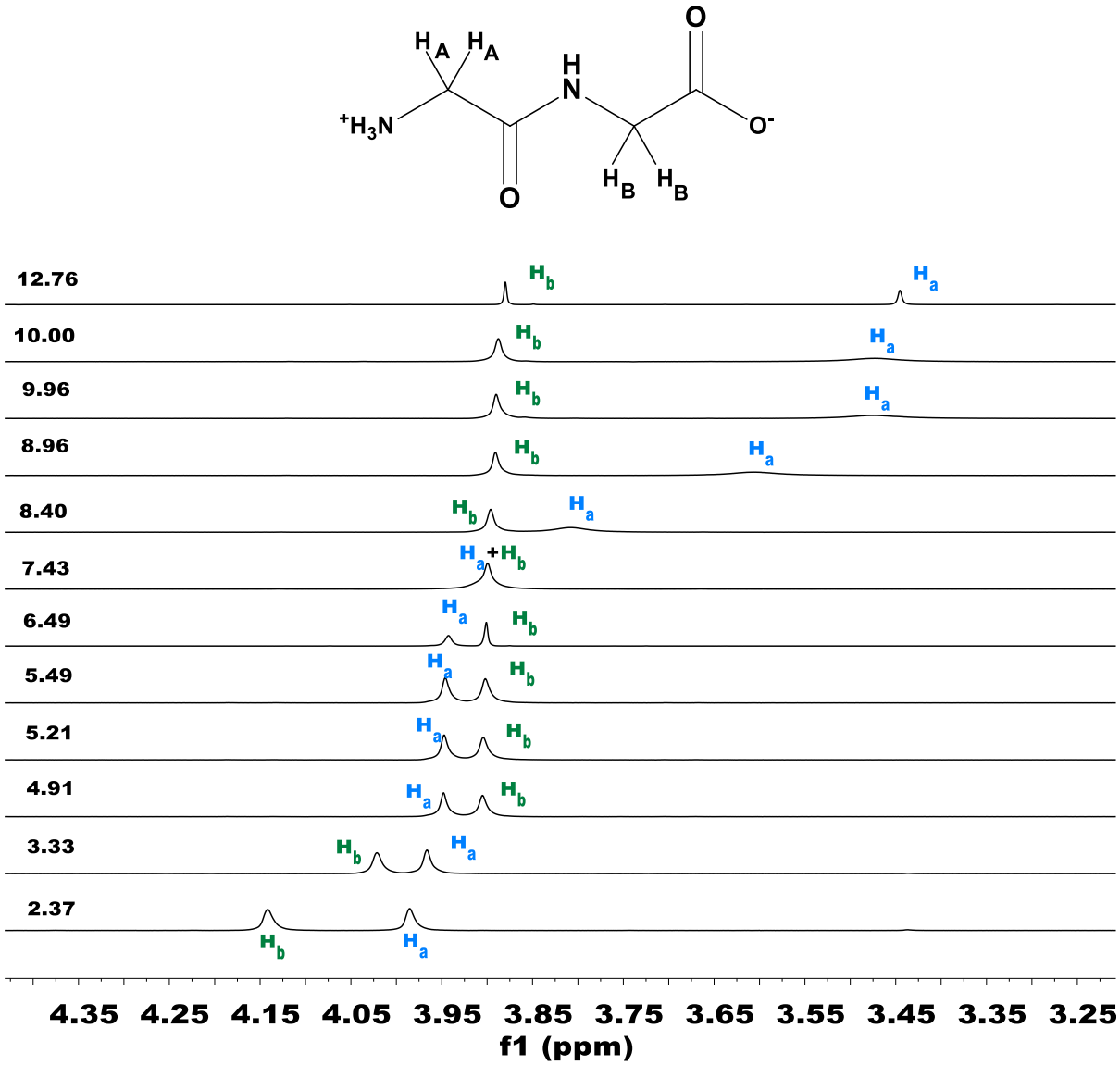

Figure A5.3. ^{1}H NMR of D_2O solutions containing GG at varying pH values. Spectra were run in triplicate and one representative series is shown. Protons are labeled according to the figure of GG shown above.

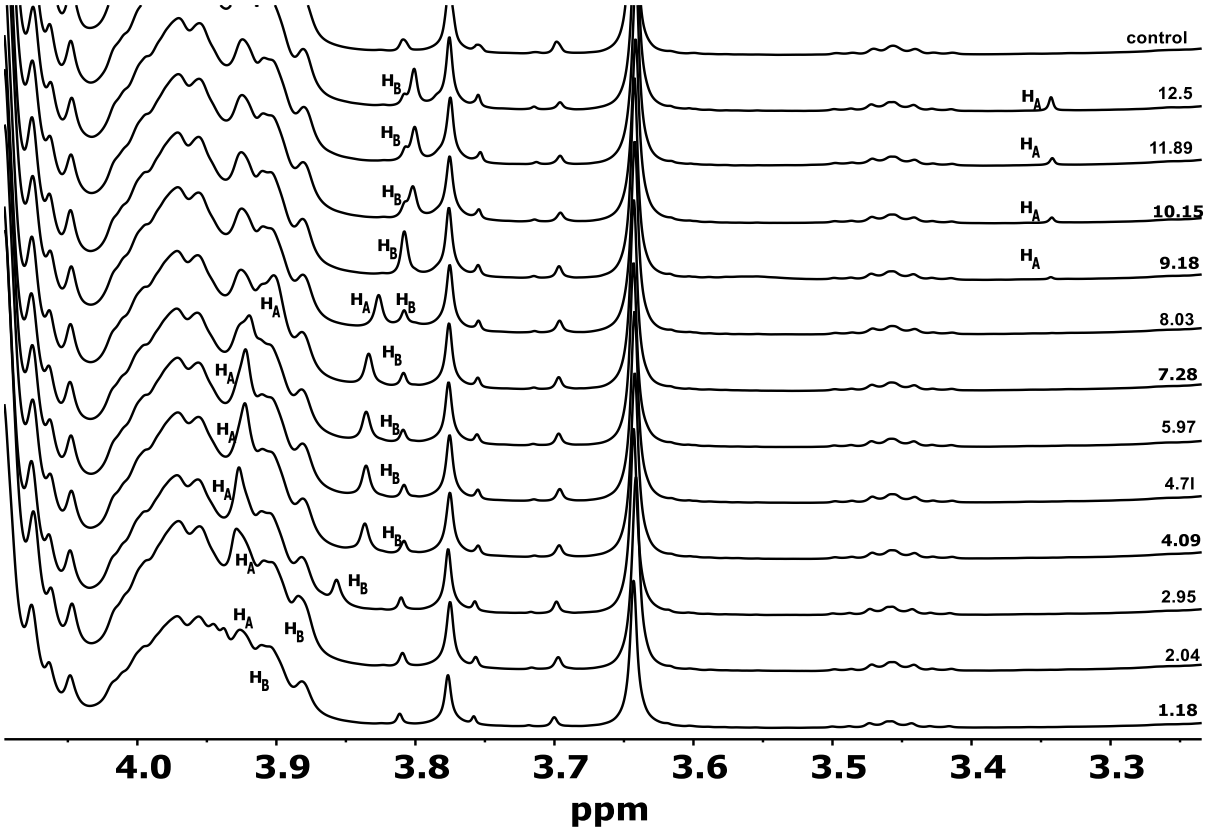

Figure A5.4. ^{1}H NMR of RM solutions containing GG at varying pH values in the D_2O pool are shown here. Spectra were run in triplicate and one representative series is shown. Peaks are labeled according to the structure of GG in Figure A3.3.

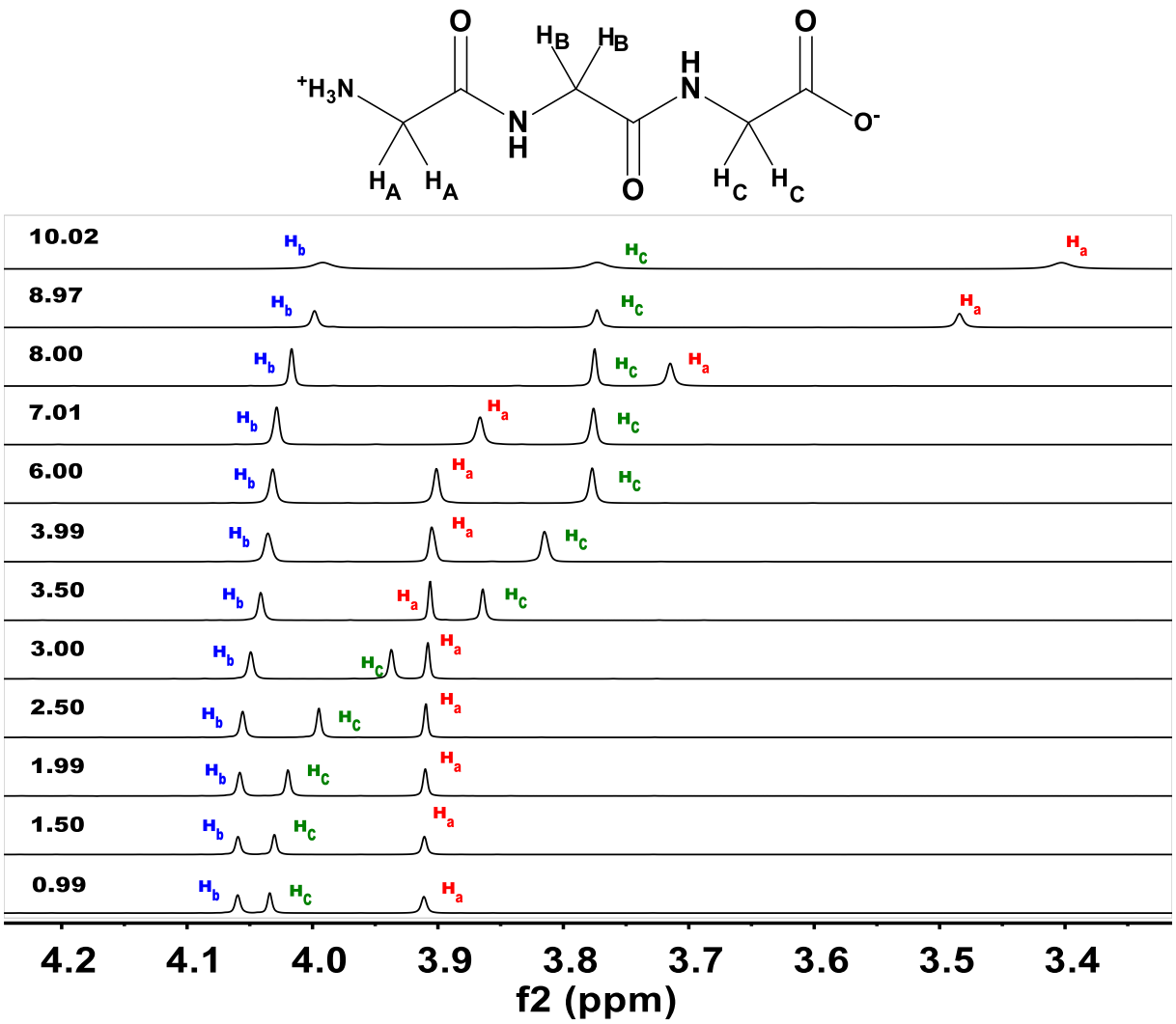

Figure A5.5. ^{1}H NMR of D_2O solutions containing GGG at varying pH values. Spectra were run in triplicate and one representative series is shown. Peaks are labeled according to the figure of GGG shown above.

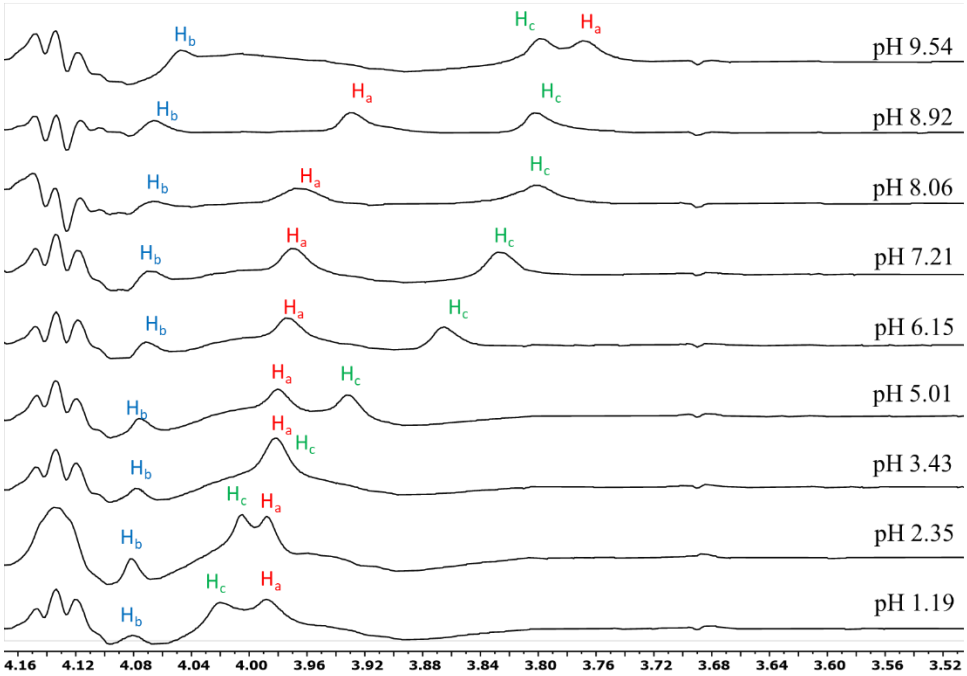

Figure A5.6. Representative spectrum showing subtraction technique utilized to elucidate GGG peaks overlapped by AOT peaks.

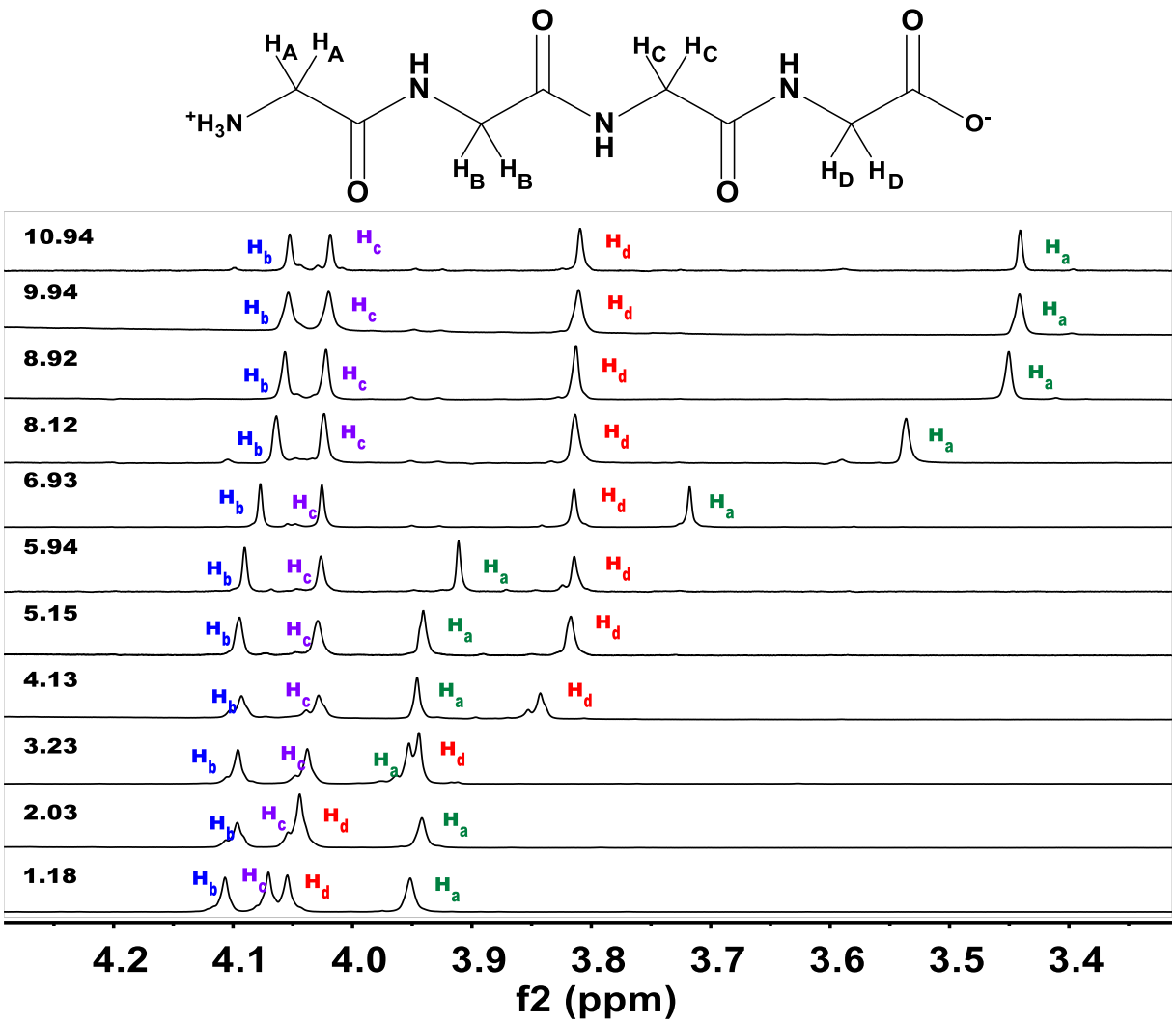

Figure A5.7. ^{1}H NMR solutions of D_2O containing GGGG at varying pH values. Spectra were run in triplicate and one representative series is shown here. Peaks are labeled according to the figure of GGGG shown above.

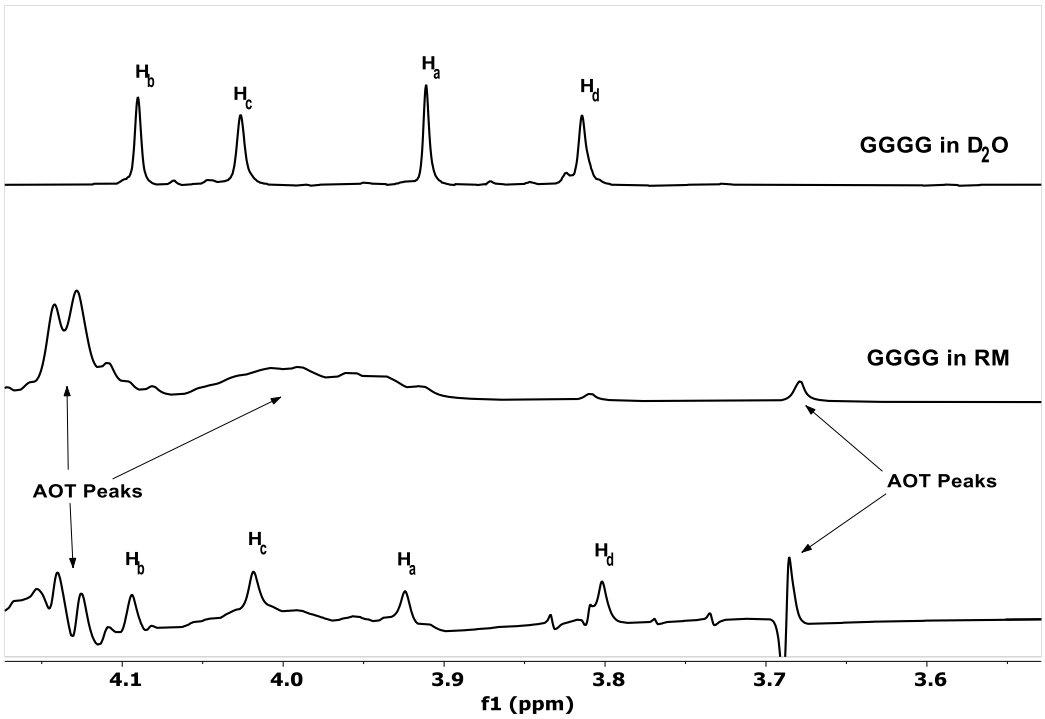

Figure A5.8. Representative spectrum showing subtraction technique utilized to elucidate GGGG peaks overlapped by AOT peaks.

Appendix VI: Selective Speciation Improves Efficacy and Lowers Toxicity of Platinum Anticancer and Vanadium Antidiabetic Drugs

This manuscript is published in the Journal of Inorganic Biochemistry with Kaitlin A. Doucette as the primary author. This work is a review article which focuses on the speciation of vanadium and platinum compounds as therapeutic compounds. Kelly N. Hassell prepared four figures within this manuscript and wrote sections on Lipoplatin. Debbie C. Crans helped greatly with preparation of the manuscript concerning vanadium, and Kaitlin A. Doucette prepared the sections on platinum speciation.[1]

Reference

1. Doucette, K. A.; Hassell, K. N.; Crans, D. C., Selective speciation improves efficacy and lowers toxicity of platinum anticancer and vanadium antidiabetic drugs. *Journal of Inorganic Biochemistry* **2016,** *165*, 56-70.

Journal of Inorganic Biochemistry 165 (2016) 56–70

Contents lists available at ScienceDirect

Journal of Inorganic Biochemistry

journal homepage: www.elsevier.com/locate/jinorgbio

Selective speciation improves efficacy and lowers toxicity of platinum anticancer and vanadium antidiabetic drugs

Kaitlin A. Doucette [a], Kelly N. Hassell [a], Debbie C. Crans [a,b,*]

[a] Cell and Molecular Biology Program, Colorado State University, Fort Collins, CO 80523, USA
[b] Dept. Chemistry, Colorado State University, Fort Collins, CO 80523, USA

ARTICLE INFO

Article history:
Received 21 April 2016
Received in revised form 22 September 2016
Accepted 29 September 2016
Available online 3 October 2016

Keywords:
Cisplatin
Anticancer
Speciation
Vanadium
Antidiabetes
Coordination chemistry

ABSTRACT

Improving efficacy and lowering resistance to metal-based drugs can be addressed by consideration of the coordination complex speciation and key reactions important to vanadium antidiabetic drugs or platinum anticancer drugs under biological conditions. The methods of analyses vary depending on the specific metal ion chemistry. The vanadium compounds interconvert readily, whereas the reactions of the platinum compounds are much slower and thus much easier to study. However, the vanadium species are readily differentiated due to vanadium complexes differing in color. For both vanadium and platinum systems, understanding the processes as the compounds, Lipoplatin and Satraplatin, enter cells is needed to better combat the disease; there are many cellular metabolites, which may affect processing and thus the efficacy of the drugs. Examples of two formulations of platinum compounds illustrate how changing the chemistry of the platinum will result in less toxic and better tolerated drugs. The consequence of the much lower toxicity of the drug, can be readily realized because cisplatin administration requires hospital stay whereas Lipoplatin can be done in an outpatient manner. Similarly, the properties of Satraplatin allow for development of an oral drug. These forms of platinum demonstrate that the direct consequence of more selective speciation is lower side effects and cheaper administration of the anticancer agent. Therefore we urge that as the community goes forward in development of new drugs, control of speciation chemistry will be considered as one of the key strategies in the future development of anticancer drugs.

1. Introduction

Metal-based drugs have continued to play an important role in combating a variety of diseases particularly in cancer. Cisplatin, for example, remains an effective platinum (Pt)-containing anticancer agent still used over 35 years after its introduction [1–10]. Because the processing of metal complexes is critical for the biological effects of metal-based drugs, it is important to consider their speciation [9–12]. In a number of different biological processes, hydrolytic, substitution and redox chemical reactions result in the conversion of the original, clinically administered metal complex, into new and distinct complexes with their own inherent and sometimes beneficial biological properties [9,10]. As a result of the coordination chemistry that takes place under biological conditions, many different forms of a metal species may exist in different environments and this can have advantageous consequences [12–17]. These different forms are often referred to as species, and the formation of these different compounds from one original species is referred to as speciation. The examination of speciation is the study of what specific species of a compound may exist under particular conditions [18]. In the present manuscript we will review the literature of anticancer drugs from the point of examining how speciation impact the effects of drugs and their efficacy [19–21]. Because speciation of vanadium-based drugs has been studied extensively and underline the importance of such studies by linking biological effects of specific vanadium species [22–25], we use vanadium-based drugs to draw parallels with platinum-based drugs and their speciation.

Previous work on V-based drugs has demonstrated the concept that one metal compound may result in several other compounds under different environmental circumstances [16,26]. Thus, one metal compound may also generate several forms in different biological matrices [11,12,16]. For example, vanadate, the simplest V(V)-containing salt, is found to exist in these different forms or species in aqueous and organic solvents [16,27–29]. We and others have also shown that vanadate interacts to form complexes with metabolites and buffer solutions [27,30–33], and that each of these V(V) species has different inherent chemical properties that generate different responses from enzymes [34–37], cells [38,39], and ultimately the animal or human system being treated as a whole [32,39–42]. Further illustrating that different forms of metal-based drugs may vary with their processing, it has been shown that the metal complexes formed in a pure aqueous solution will likely be different from those formed in a complex

* Corresponding author at: Dept. Chemistry and Cell and Molecular Biology Program, Colorado State University, Fort Collins, CO 80523, USA.
E-mail address: Debbie.Crans@ColoState.Edu (D.C. Crans).

http://dx.doi.org/10.1016/j.jinorgbio.2016.09.013
0162-0134/

biological system [43,44], see Fig. 1. We have recently reviewed the effects of oxidovanadiumdipicolinates as antidiabetic agents [16,17]. As part of this review, we have illustrated that the form of the compounds studied in solid state and aqueous solution are different as compared to the same compounds in a hydrophobic environment [16,17,27]. In fact, the properties of these compounds changed enough that even with limited characterization of the new systems formed, it was clear that the new structures were chemically distinct form of the parent compounds [16, 17]. Specifically in two cases, different oxidovanadiumdipicolinates derivatives were isolated in the solid state and characterized as having a peroxido- and hydroxylamine derivative [16]. The reactivity and the spectroscopic characterization of the species that exist in organic solution led to the identification of a derivative that was very reactive and acted as an oxidation catalyst [16,39,45]. Such changes in reactivity induced by the difference in the environment are likely to be important for the mode of action of these compounds [16,17]. Vanadium salts and some vanadium compounds have also shown potential as anticancer drugs [46, 47]. These examples testify to the importance of the speciation profile of the drug upon administration.

We have shown that different protonation and oligomeric forms of vanadate will exert different responses by enzymes. Specifically illustrating this example of diversity, enzymes such as phosphatases [23, 30,35,37,48,49] are known to be inhibited by the vanadate monomer ($H_2VO_4^-$, HVO_4^{2-}) while vanadate tetramer, an oxovanadate species with four V atoms, is found to be an inhibitor of 6-phosphogluconate dehydrogenase [50], glucose-6-dehydrogenase [22], glycerol-3-phosphate dehydrogenase [51] and aldolase [52]. A few studies have been reported of vanadium(IV) solutions and is found to be as potent an inhibitor as vanadate monomer with protein tyrosine phosphatase 1 B (PTP1B), *E. coli* and mammalian alkaline phosphatases. Similarly, organic V derivatives are more potent inhibitors for ribonucleases than the simple salts [53–56]. Because the environment plays a role in what species of metal complex are formed, the V species can change as they move across the cell and into different compartments. For example, the isolated V complex formed with triethanolamine (VO(tea)) was found to have the triethanolamine(3-) coordinated in a tetradentate manner to the V=O unit in the solid state and in organic solution [27]. By contrast, the structure in aqueous solution of the anionic complex (VO_2(tea)$^-$) has the triethanolamine (tea) coordinated in a tridentate manner to the VO_2^+ unit and had a free ethanol arm [27,37]. Indeed, it was found that using this amine as a cation that the V complex much more readily was taken up into Caco cells [57].

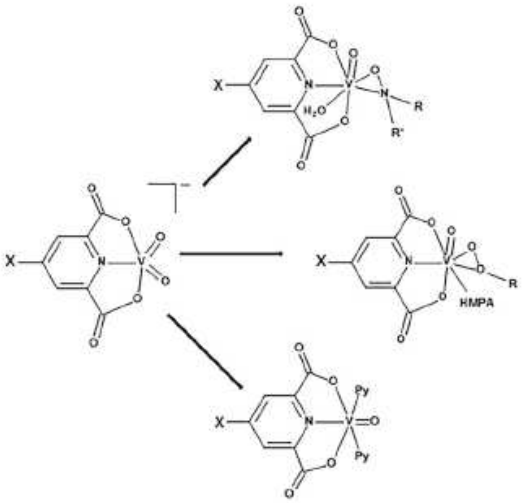

Fig. 1. The anionic [VO_2(dipic)]$^-$ existing in the aqueous solution and in the solid state when placed in different environments results in the formation of different compounds that have very different properties. The top resultant structure results from exposure to polar organic medium, middle structure results from exposure to very polar organic medium, and bottom is structure resulting from exposure to hydrophobic medium (Reviewed in Ref. [16]).

After these many studies have indicated that speciation of the V is an important factor in its biological action, we now turn our attention to platinum (Pt)-based antitumoral compounds where much less work has been carried out in the area of speciation [9,10,58–63]. There are currently three FDA-approved Pt-based drugs used for their anticancer properties: namely, cisplatin, carboplatin, and oxaliplatin as shown in Fig. 2 [4,7,64,65]. These drugs are used in the treatment of a variety of cancers such as bladder, testicular, lung and ovarian, among many others [66]. In addition, a few more Pt-compounds have been investigated and some are legalized in the clinics outside the USA. It is therefore important to, in a manner similar to the V-compounds, analyze speciation of the Pt-based compounds.

Approved by the FDA in 1978, cisplatin was the first small Pt-based antitumoral drug [3–7,67,68]. Clinical use of cisplatin was followed by the development of carboplatin and oxaliplatin, which were developed to minimize some of the undesirable side effects of cisplatin such as nephrotoxicity and ototoxicity, or toxicity to the kidneys and ears, respectively [62,69–71]. The generally accepted mechanism of action for this class of antitumoral drugs is the complexation of the Pt species with DNA, which leads to the bending of the DNA helical structure by a 35–40 degree angle. When DNA polymerase progression is inhibited as a result of this structural perturbation of the DNA chain, apoptosis of the cancer cell is induced [2,3,9,10,72]. In the case of Pt-containing antitumoral drugs like cisplatin, the administered compound is not the biologically active compound that exhibits these antitumoral effects. The Pt compound must first enter through the cell membrane, and upon reaching the cytoplasm, the chloride ligands are replaced by waters. It is generally believed that it is this aquated compound that is then able to bind to the DNA and induce apoptosis [3,73–75].

This biological conversion of the Pt-drug to its active form calls attention to the importance of speciation in understanding its full biological effects. Success with this class of drugs has demonstrated that there are a number of different Pt-based drugs that have been effective in treating cancer [1,7,76]. In the following, we have reviewed the information that is available on Pt speciation and placed it in context of the successful anticancer drugs. However, because of the increasing problems with development of drug resistance, it is important that scientists recognize how speciation impacts the complex problem of drug resistance. Currently, recognized issues in cancer resistance include changes in drug targets, development of alternative pathways for DNA repair, changes in cellular pharmacology such as increased drug efflux, changes in regulatory paths, and changes in the physiology of cancer [65]. Although these specific mechanisms are assisted by the intrinsic nature of cancer evolution, omitting the consideration that chemical and biotransformations of anticancer drugs may also contribute to this matter would leave out entirely another level at which we can combat cancer.

In this manuscript we will discuss how the biological speciation of Pt-complexes can be used to understand the anticancer effects of cisplatin and other platinum based compounds. This review will illustrate the importance species that may arise from the bioprocessing and chemical reactions within the cell in addition to the active form of the administered metal-based drug. The topic is introduced by first describing the more well-known speciation of V-based compounds and their biological activities. We point to the many V-containing products that are sold for many different purposes including management of glucose levels. Many different forms of V-containing products that are commercially available contain variable levels of V and a range of additives. Similarly, speciation of Pt-based anticancer drugs highlights the fact that speciation chemistry can explain the reported improved efficacy of Pt-drugs, and efficiency of the fight against cancer. It is our hypothesis

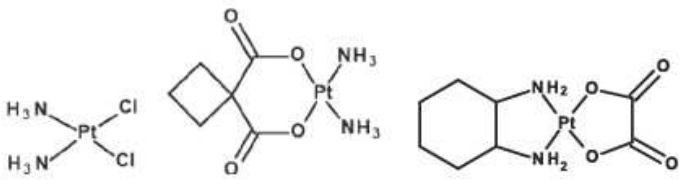

Fig. 2. From left to right: cisplatin, carboplatin, and oxaliplatin, the three platinum chemotherapeutics that have been approved by the FDA and are used in the clinic in the US for treatment of human beings.

that the speciation of Pt-containing drugs has considerable implications with regards to the efficacy of Pt-containing antitumoral drugs. We show that changes in speciation of the Pt-based compounds formed affects the Pt metabolism, biological efficacy, and drug resistance and can explain improved properties of second and third generation Pt-based drugs. In the following we describe the biological properties of the V- and Pt-containing drugs, and how this knowledge can improve biological efficacy. In consideration of the speciation chemistry involved, we recommend that the speciation chemistry be a factor considered when developing new anticancer drugs.

2. Definition of speciation

Speciation chemistry is a branch of chemistry that was historically developed in northern Europe and for decades had a home in the area of solution chemistry [14,18,77–82]. Because there are several discipline and area specific definitions for speciation [83–86], recent recommendations have been carried out within the International Union of Pure and Applied Chemistry (IUPAC) establishing a commission that developed several recommendations for the scientific community on the definition of speciation [18]. In addition to the classical areas of solution chemistry [79–82], bioinorganic chemistry and V chemistry have also embraced the principles of speciation and as a result [79–82,84,87] have used these for development within these disciplines [37,43,88]. Speciation studies have been done for a number of metals ions and systems [33,83,84,89–93], using a range of analytical methods for analysis [79,84,90,92,94,95]. The availability of the improved and high resolution analytical methods and powerful tools for data analysis have revolutionized the scientists' ability to measure different species under biological conditions [11,79,85,89,95] and environmental conditions [83,90,91]. However, regardless of the improved analytical methods available, the coordination chemistry of the target element dictates the processing and the potential of what can be observed. Such considerations are at the essence of chemical speciation [10,11], and the focus for can be observed.

For the purposes of this manuscript, we will here provide the classical solution chemistry definition of speciation, illustrated by Eqs. (1) and (2) [11,18]

$$pH^+ + qM + rL \rightleftharpoons (H^+)_p(M)_q(L)_r \quad (1)$$

$$\beta(p,q,r) = \frac{\left[(H^+)_p(M)_q(L)_r\right]}{[H^+]^p[M]^q[L]^r} \quad (2)$$

Eq. (1) shows H^+, a metal ion (M), and a ligand (L) forming a complex with the stoichiometry defined by p, q, and r respectively in an equilibrium reaction. The formation constant of the complex $\beta(p,q,r)$ is shown in Eq. (2), in which the concentration of the complex is divided by the multiplied concentrations of the individual constituents of H^+, M and L raised to their respective powers, p, q, and r [18]. The quotients values for p, q, and r are determined by a titration followed by the evaluation of the constants of the entire system using computations in an iterative process [11,80–82]. These potentiometric studies are most effective when an entire pH range is considered. Because hydrolysis reactions do not involve L, these complexes will be described as (p,q,0), where p and q are the coefficients for H^+ and the metal respectively, and the formation constant is defined by the concentration for the respective precursors [11,77]. Such speciation studies result in a series of constants that represent the system and allow for prediction of species distribution.

Several important limitations with the classical speciation approach include the types of reactions and specific species [11]. Only reactions with changes in H^+ give observable changes and indicate differences in the speciation. In addition the hydration number (i.e. the number of water molecules in the formula) in a complex cannot be measured because such addition does not add or take away a proton and thus is not detected. Furthermore, since this definition of speciation focuses on composition, it is important to recognize that stereochemistry is not taken into account. Stated differently, the classical definition of each species focuses on the atom composition rather than where the atoms are located in space. However, in this manuscript, we will point to both the differences in composition (that is, speciation) as well as how they are oriented in space.

3. Speciation case studies

3.1. Vanadium (abbreviated V)

The biological effects of the V salts and other V compounds are sensitive to their structure and composition [14,17,38,41–43,96–98]. As a result, speciation studies have played an important role in the development of new antidiabetic, anticancer, and other therapeutic compounds. The speciation of V compounds and salts are also sensitive to their conditions, or environment, and as a result the chemical bioprocessing is essential to their mode of action [16,32,48]. Additionally, the speciation of V is very sensitive to changes in oxidation state, thus similarly sensitive are the analytical techniques that are effective in monitoring them [32,97–105]. The routine methods used for measurement of speciation in aqueous solution include NMR and electron paramagnetic resonance (EPR) spectroscopy, UV–Vis spectroscopy, potentiometry and electrochemistry [29,106,107]. Less routine and instrumentally more demanding techniques include electron nuclear double resonance (ENDOR), high resolution magnetic resonance techniques and x-ray absorption spectrometry (XAS), and X-Ray absorbance near-edge spectroscopy (XANES) [108–112]. Some of these methods such as XAS offer advantages in that it can monitor several oxidation states at once. However, once the speciation is to be done in biological systems, fewer of these methods are available because of the complexity of the media investigated, and because it is difficult to monitor the low concentration of material in living beings. However, for the compounds with slower exchange rates isolation methods can be used as well. This however must be emphasized that it will not allow distinction of the faster exchanging materials [109–111]. Most of the methods listed are limited to one oxidation state of the V, since the V undergo redox chemistry, it is important that more than one method is used or a methods such as XAS is used that can measure different oxidation step [108–111].

3.1.1. Vanadium(V) (V(V)) speciation

The aqueous vanadium(V) (V(V)) metal can exist in both cationic and anionic forms, depending on the surrounding pH and the presence of other components. V in this oxidation state and its derivatives are readily monitored using ^{51}V NMR spectroscopy [29,32,113]. As a quadrupolar nucleus, its NMR properties are very favorable for analysis with fast relaxation time and large spectral window. In Table 1 we show the composition of a number of V(V) species in aqueous solution [114]. Detailed studies based on composition and classical speciation methods have characterized these species and the speciation is found to be sensitive to pH, concentration and electrochemical potential [114]. In addition, we show the species along with their chemical properties, such as pKa values that form in the presence of two simple buffers, diethanolamine and tricine. For these two simple buffers, only one complex forms, although it can exist in different protonation states [80]. However, for other interesting biological systems, many more species can form.

It is generally believed that the six-coordinate cationic species at low pH have properties analogous to metal ions and the anionic four-coordinate species at neutral and basic pH have properties more analogous to phosphorus [114–117]. Recent studies exploring the coordination environment of the solution species using extended X-ray absorption fine structure (EXAFS) and large-angle X-ray scattering (LAXS) and in the solid state by single-crystal X-ray diffraction and EXAFS suggest that the V in neutral and alkaline pH could also have coordination numbers higher than four, breaking the trend of phosphorous-like properties at the lower pH values [118]. However, generally the oligomeric oxovanadates are viewed as phosphate and pyrophosphate analogs, because monomeric vanadate is believed to be an excellent phosphate analog with regard to its structure, pKa values and the biological response that it exhibits [43,115] as shown in Table 1. The speciation of the V(V) ions is particularly complex as there are environments and situations in which some of these ions rapidly exchange ligands, whereas others may exchange more slowly [31,43,96]. In Fig. 3 we show the dramatic difference of the effect that mere pH can have on vanadate solutions, in which yellow decavanadate (the V species containing 10 V-atoms, see Table 1) is compared to the colorless oligomeric vanadates. Decavanadate readily forms from aqueous solution of colorless oligomeric vanadates in the presence of a couple of drops of acid as shown in Fig. 3. At neutral pH, the colorless oligomeric vanadates readily exchange, whereas the yellow decavanadate only exchanges slowly. Methods needed to explore the V chemistry containing both decavanadate and the oligomeric oxovanadates must be methods that can measure both fast exchanges and slow exchange processes [37,119].

Above describes the hydrolytic reactions that V(V) engages in and in the presence of buffers would show similar results. However, V also undergoes redox chemistry and accordingly more than one routine analytical method would be needed to properly describe the oxidation states in each system. In addition, powerful methods such as XAS require access to a synchrotron can provide detailed information on all oxidation states, however the available concentration ranges must be sufficiently high for detection [108–111]. In the sections below we briefly describe speciation of V in oxidation states IV and III.

3.1.2. Vanadium(IV) speciation

The aqueous V(IV) metal can also exist in both cationic and anionic forms [14,43,105,32]. The cationic forms are more common at a low pH, and the anionic forms at neutral and high pH. Less is known about the speciation of aqueous V(IV) compared to V(V), particularly at neutral pH, because at this pH there is no electron paramagnetic resonance (EPR) signal, presumably because of dimerization/oligomerization of the vanadyl species [32,105]. However, V(IV) forms tend to form more stable coordination complexes with ligands, and the equilibration of these systems is slower than for V(V) systems [28,97,105]. Dissolved $VOSO_4$ forms $[VO(H_2O)_5]^{2+}$ and is a bright turquoise color and will remain this color at acidic pH. However, when the pH of the solution is increased and approaches neutral and basic pH, the blue color of the solution disappears. However, the species with this form of V is dependent on preparation, at high pH the turquoise color change to colorless $VO(OH)_3^-$, which gives a strong EPR signal, or a different form of V depending on how the solution is prepared [32,105].

Chelated V(IV) is generally viewed as the most stable of the forms of V [28,32,105]. This is because for some ligands, such as maltolato, the speciation profile is shifted one pH unit in favor of neutral pH [28,33,97,120]. In addition, because the V(IV) complexes generally hydrolyze slower than their corresponding V(V) complexes, they are typically viewed as more desirable to work with. However, recent work has demonstrated that this perception does not hold for all types of ligands, and that there are V(V) complexes that are more potent antidiabetic agents than the corresponding V(IV) complexes [37,39,41,42]. Furthermore, more is known with regards to the interaction of V(V)-protein complexes and thus potential mode of action of the antidiabetic agents [37,49,98,117].

Although V(IV) is the most stable form of V in the reducing intracellular environment, it is prone to redox processes in the presence of oxidizing metabolites and in more oxidizing environments [121]. However, controversy has existed because ligand [26] and environments will change their redox state [16]. For example, dissolution of $VOSO_4$ into an aqueous solution at pH 7 in the presence of dissolved dioxygen will immediately oxidize about 30% of the solution to V(V) species [121]. Thus, maintaining the V(IV) in the lower oxidation state requires that the pH of the solution is acidic and/or that the samples must be prepared under an nitrogen or argon atmosphere at neutral pH [121]. The major routine method for measurement of V(IV) is EPR spectroscopy, but other methods such as UV–vis and IR spectroscopy can be helpful [28,122]. More specialized methods such as XAS and high field EPR spectroscopy can also be informative [123–125]. Many studies have addressed the issue of redox state of vanadium and difference have been observed depending on the study [126–129]. Studies with vanadium compounds as antidiabetic agents have demonstrated that there are efficacy differences with regard to the oxidation state [126] and different effects depending on oxidation state [127]. Feeding studies in rats have shown that both V(IV) and V(V) result [128]. The

Table 1
Formation constants for various species in the binary systems H^+-$H_2VO_4^-$, H^+-DEAE and H^+-Tricine (0.6 M Na(Cl), 25 °C [a,b]. Adapted from Refs. [80,114].

p,q,r	log β_{pqr}	pK_a	Formula/abbrev
H^+-vanadate			
1,0,0	–	–	H^+
−1,1,0	−7.92	–	HVO_4^{2-}, vanadate monomer
0,1,0	–	7.92	$H_2VO_4^-$, vanadate monomer
-2,2–0	−15.2	–	$V_2O_7^{4-}$, vanadate dimer
−1,2,0	−5.25	9.92	$HV_2O_7^{3-}$, vanadate dimer
0,2,0	2.77	8.02	$H_2V_2O_7^{2-}$, vanadate dimer
−2,4,0	−8.88	–	$V_4O_{13}^{6-}$, vanadate tetramer
−1,4,0	0.22	9.10	$HV_4O_{13}^{5-}$, vanadate tetramer
0,4,0	10.00	–	$V_4O_{12}^{4-}$, vanadate tetramer
0,5,0	12.38	–	$V_5O_{15}^{5-}$, vanadate pentamer
4,10,0	52.13	–	$V_{10}O_{28}^{6-}$, decamer
5,10,0	53.13	6.00	$HV_{10}O_{28}^{5-}$, decamer
6,10,0	61.87	3.74	$H_2V_{10}O_{28}^{4-}$, decamer
7,10,0	63.47	1.6	$H_3V_{10}O_{28}^{3-}$, decamer
2,1,0	6.96	–	VO_2^+, cis-dioxidovanadium(V)
H^+-diethanolamine (DEA)			
0,0,1	–	–	$C_4H_{11}O_2N$/DEA
1,0,1	9.072 ± 0.003	9.072	$C_4H_{12}O_2N^+$/HDEA$^+$
H^+- N-[tris(hydroxymethyl)-methylglycine (Tricine)			
−1,0,1	−7.929 ± 0.001	–	$C_6H_{12}O_5N^-$/Tricine$^-$
0,0,1	–	7.929	$C_6H_{13}O_5N$/Tricine
1,0,1	2.020 ± 0.004	2.02	$C_6H_{14}O_5N^+$/HTricine$^+$

[a]The results were obtained by use of the computer program LAKE.25 [b]Results taken from ref. [114] and recalculated with $H_2VO_4^-$ as the component in place of HVO_4^{2-}.

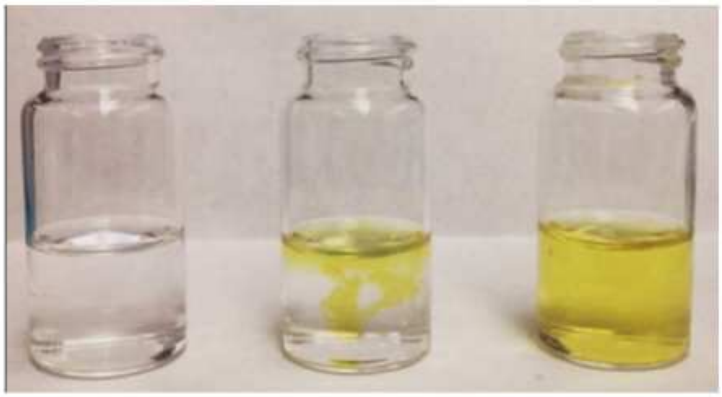

Fig. 3. Solutions of pH 2 yellow decavanadate (right) and pH 7 colorless oligomeric oxovanadates (left) approximately 500 mM in V-atoms. The middle image is a solution of oligomeric vanadates to which several drops of concentrated acid have been added to a vial (with no stirring) documenting the fast rate of formation of decavanadate when the local pH is acidic.

stability in serum of V(IV) and V(V) complexes also contribute to the distribution of the V [128]. Studies in yeast have shown that the addition of V(V) to the media will give both V(IV) and V(V) [130]. Undoubtedly there are significant differences depending on cell type. Recent studies using the powerful XANES technique from cells treated with both a V(IV) and V(V) complex have demonstrated some time dependent effects related to the nature of the intracellular V oxidation state. It was shown in mammalian cell culture that incubation of the cells with V(V) results in V(V) dominating in the early stages, and V(IV) dominating after about 16 h. However, interestingly at further timepoints the V(V) concentration increased thereafter. This is relatively independent of the oxidation state with which the cells are treated. The increase in V content and the proportion of V(V) with time after 16 h is consistent with the speciation showing that both V(IV) and V(V) species in the cell medium converge to the same ratio of V(V) to V(IV) after 24 h in a ratio of ~4:1 [131].

Considering more than one oxidation state is critical for an element like vanadium, because in biological systems V undergoes redox cycling between oxidation states IV and V and possibly also in some cases with oxidation state III, IV and V [101–103,132]. Interestingly, the biological response is not the same when compounds with different oxidation states are administered indicating that the redox processes are initiating other processes that are not reversible.

3.1.3. Vanadium(III) and lower oxidation states

There is less information on lower oxidation states of V, although V(III) may have an important role in V-containing nitrogenases [43] and in tunicates [133], and in the gastrointestinal tract when mammals are administered with V supplements [132]. Vanadium salts in the lower oxidation states are generally only stable at low pH at ambient temperatures and atmospheres unless the metal ion is complexes to strong ligand [43,101–103]. In the past, V(III) was considered very unstable, possibly because upon dissolution of salts, this oxidation state readily oxidizes. However, in the presence of a ligand, the V(III) compounds can be stable [43,101–103,132,134], and have even recently been reported to form in the presence of ascorbic acid [135]. The recent finding of V(III) under less rigorous conditions remains to be validated in biological studies in mammals, although XAS experiments have indicated the presence of V(III) in acidic gastric medium after addition of V(IV) or V(V) supplements [132]. Studies have been carried out using XAS of tunicates and there V(III) has been documented in a range of different organisms [133]. Unfortunately, the electronic properties of the V(III) compounds preclude observation with routine EPR spectroscopy and more specialized techniques such as high-frequency and high-field EPR spectroscopy [104,135] and XAS are necessary for detection [25]. Since mammalian biological samples are not commonly investigated using high-frequency and high-field EPR spectroscopy or XAS, how widely spread these compound are in biological systems is not known at this time.

3.1.4. The biological activities of specific V-species

Information on species distribution is important because different V species have different effects in biological systems. Although this topic is extensive we are only mentioning a few examples to illustrate that some V derivatives inhibit some enzymes and others are more readily taken up in cells. For example, phosphatases are generally inhibited by vanadate monomer [44,49,96,136], while vanadate dimer inhibit few enzymes such as glucose-6-dehydrogenase [22], aldolase [52], the prostatic acid [23], the Yersinia acid (YOPH) and the PTP1B phosphatases [25,49,137,138]. Vanadate tetramer is an inhibitor of 6-phosphogluconate dehydrogenase [22], glucose-6-dehydrogenase [22], glycerol-3-phosphate dehydrogenase [51] and aldolase [52]. Similarly, V-uridine is also found to be an inhibitor for this enzyme [139] and decavanadate has been found to be a potent inhibitor to RNases [139]. Less is known with regards to the specific effects of V(IV) species although the vanadyl cation is significantly faster taken up by yeast cells than its V(V) counterpart [39,130]. A study was carried out with V(V), V(IV) and V(III) complexes of dipicolinate [140] (and chlorodipicolinate) [103], and each oxidation state was found to interact differently with a model interface [140] correlating with the observed effects in animal studies [102,103]. However, the effects of V compounds in general are difficult to track because once administered to animals and cells, the compounds no longer remain in the form administered [17,32,39,41–43,96,103,134,136,141–143].

3.1.5. Comparison of V with Pt

V is an early transition metal and Pt is a late transition metal and as a result these metal ions have some similar and some different properties which are compiled in Table 2. As an early first row transition metal ion V can be more kinetically reactive in comparison with the less kinetically labile third row transition metal Pt. As a result the V compounds can exchange ligands rapidly, in contrast to the Pt compounds that do not convert readily. Therefore, it is much simpler to carry out speciation studies on the Pt-compounds, because it is possible to isolate and characterize them, whereas in the case of the V compounds there may be both rapidly converting and slowly converting species.

Table 2
The properties of the early transition metal V and late transition metal Pt are compared.

Property	Vanadium abbreviated V	Ref.	Platinum abbreviated Pt	Ref.
Atomic number	23	[144]	78	[144]
characteristic	Early transition metal	[144]	Late transition metal	[144]
Multiple accessible oxidation states	IV and V (less common III, II, 1 and 0)	[144]	II and IV	[12,64,144]
Common oxides	V_2O_5, $VOSO_4$	[144]	PtO, PtO_2	[12,64,144]
Chlorides	$VOCl_3$, $VOCl_2$	[144]	$[PtCl_4^{2-}]$	[12,64,144]
Chloride stability	Reactive; unstable in water	[144]	Stable and Stable in water	[12,64,144]
Oxido metalate aq. stability	High	[144]	High	[12,64,144]
Oxido metalate Exchange rates	High	[32]	Low	[12,64]
Isolation of species	Not likely	[32]	Likely	[12,145]
Reaction with glutathione	Redox; lability product	[32]	Substitution; stable Product	[12,64]
Enzyme inhibitor	Phosphatases Glycolytic enzymes	[32]		[146]
DNA binder	yes	[25]	Yes	[12,64,146]
Common speciation methods	Potentiometry, NMR, EPR, UV–vis, IR, MS	[11,105,115]	HPLC, LC, NMR, potentiometry, UV–Vis, MS	[62,147]
Non-routine methods	High field and high resonance EPR, XAS, ENDOR, XANES	[109–111]	XAS, ENDOR, XANES	[109–111]

4. Platinum

4.1. Platinum(II) drugs

The most common platinum (Pt) drugs and the three that are currently FDA-approved for clinical use in the US are Pt(II) drugs (cisplatin, carboplatin and oxaliplatin), Fig. 1 [4,7,64]. They are believed to follow the same general mode of action, in which the drug chelates DNA and results in cellular apoptosis [3,148–151]. The generally accepted mechanism shown below in Fig. 4 suggests that the neutral form (deprotonated hydrolysis product) of the cisplatin is the form that is traversing the nuclear membrane after having been formed in the cytoplasm, however, this mechanism is not accepted uniformly, because a positively charged Pt-compound would undergo Coulombic attraction to the membrane and are formed prior to formation of the neutral species. However the hydrolysis is likely to follow the steps shown in Fig. 5. This schematically underlines the fact that cisplatin by hydrolysis forms charged species, but that upon deprotonation the hydrolysis project(s) can be neutral or have one positive charge [3,5]. We will discuss several aspects of the species in this scheme and the speciation in greater detail below.

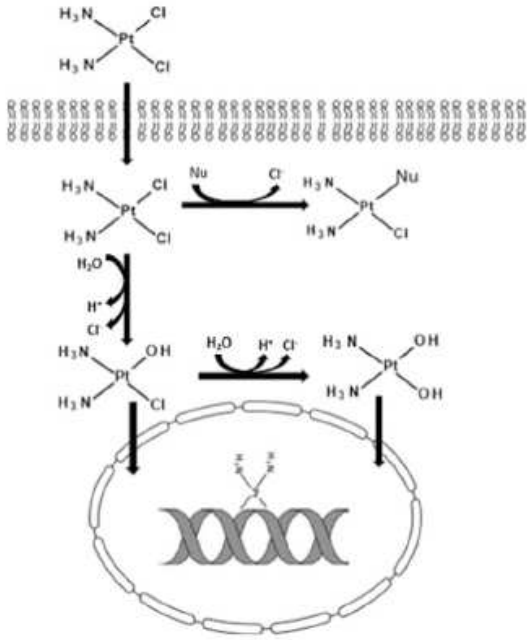

Fig. 4. Cellular uptake of cisplatin. Hydrolysis of one or two chloride ligands after penetrating into cell and potential deprotonation before uptake into the nucleus. Modified from Ref. [64].

Pt can also exist in oxidation state IV, and such Pt-compounds are even more inert than Pt(II) compounds. In general Pt(IV) compounds believed to undergo reduction forming Pt(II) complexes upon reaching the tumor, and their mode of action proceeds according to the mechanism for the other Pt(II) complexes [5,70,152]. Most of the reported processing of Pt(II) drugs generally involves hydrolytic reactions, thus keeping the Pt in oxidation state II, Fig. 5. Characterization of the chemical and biological processing of cisplatin and other Pt(II) compounds has been investigated using several analytical approaches including HPLC-ICP-MS, XAS, XANES, LC and potentiometry [62,73,109–111,147,153,154]. The fact that the Pt(II) compounds undergo slow ligand exchange reactions allows the isolation and characterization of the different species using a wide range of analytical methods [155–158]. In the following we will describe the fundamental speciation of the Pt-systems including the different processes that cisplatin and other Pt-drugs undergo under physiological conditions.

In addition to cisplatin the two other main FDA-approved Pt-drugs, carboplatin and oxaliplatin, were both developed to improve the properties of cisplatin so that it would be a more efficacious and less toxic drug to a wider range of cancers [69,70,159]. Specifically, carboplatin was developed as a more water soluble and have less nephrotoxic effects for treatment of a wide range of cancers, and oxaliplatin was developed similarly and is used for treatment of colorectal cancers [70,160,161].

4.1.1. Proposed mechanism of action for platinum(II) complexes and interaction of Pt with DNA

Because the Pt(II) compounds react upon entering cells [10,151], it is important to understand the products that it forms in a biological matrix. Cisplatin is administered intravenously and the focus here is therefore on the speciation that takes place as the Pt-drug is about to enter the cellular target. The more extensive processing leading to the ultimate speciation that occurs in the various different biological matrices including the GI tract, blood, cell media and cells are beyond the coverage in this review and the readers are referred elsewhere [132]. The specific reactions in the cytoplasm which we describe here will impact the mechanism of action of cisplatin and the other Pt(II) anticancer drugs. Generally it is expected that upon entrance through the cellular membrane into the cytoplasm, that the two chloride ligands are replaced

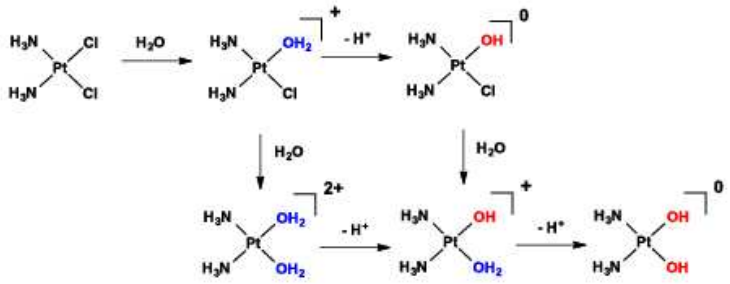

Fig. 5. Schematic illustration of the aquation reaction followed by deprotonation reactions. Aqua ligands that are bound to the Pt complex before they are deprotonated are acidic, with pKa values in the range of 5–8. Monoaquated cisplatin has a pKa of 6.6, while diaquated cisplatin (both chlorides replaced with aqua ligands) has a pKa of 5.5. Cisplatin with an aqua and hydroxide ligand (replacing the chloride ligands) has a pK_a of 7.3. Ref. [164].

by aqua ligands, see Fig. 6 [1,3,162,163], which because they are positively charged can deprotonate to form the neutral dihydroxy substituted Pt complex, see both Figs. 4 and 5. Aqua ligands that are bound to the Pt complex before they are deprotonated are acidic, with pK_a values in the range of 5–8 [164]. Monoaquated cisplatin has a pK_a of 6.6, while diaquated cisplatin (both chloride ligands replaced with aqua ligands) has a pK_a of 5.5. Cisplatin with an aqua and hydroxide ligand replacing the chloride ligands has a pK_a of 7.3 [164].

Which species enter the cell of the species shown in Fig. 4 is as far as we can tell tenuous. Many are convinced that it is the diaquated Pt-compound that enters the cell [9], but a number of researchers believe that it is the monoaqua derivative that penetrates the nucleus [70,149] and reacts with DNA. Stong arguments favor each position. The neutral diaquated Pt-compound, because of the neutral charge would seem to readily traverse the membranes and is the final hydrolysis product, see Fig. 6. However, the positively charged mono or diaquated Pt-derivatives are readily attracted to the membrane interface, and since more of this compound has been observed in speciation studies, this possibility seems like a viable alternative. Whether it is a monochlorido- or a dihydroxido-Pt complex that reacts with DNA, such a species will result in coordination of the two guanosine moieties on one DNA strand to the Pt atom, which will induce a 35–40 degree bend in the DNA, which will induce cellular apoptosis, as shown in Fig. 4 [3,5,10,75,162]. Cisplatin and oxaliplatin are found to form about 60–65% intrastrand adducts between two adjacent guanine bases (PtGG), 25–30% intrastrand adducts between adjacent adenine and guanine bases (PtAG), and 5–10% intrastrand adducts of the type PtGNG, where N is any of the four bases, and 1–3% interstrand adducts (G-Pt-G) [62,148]. These types of experiments distinguishing between these possibilities are nontrivial but would be very valuable for the community.

When used as an anticancer agent, the toxic nature of cisplatin does require that patients are carefully monitored when drug is administered. The cisplatin is administered by intravenous injection, and generally requires that the patient is checked in at an appropriate treatment facility for a couple of days [9]. The aquation and hydrolysis of cisplatin is decreased by administering the drug in saline solution because the higher concentration of Cl^- thermodynamically stabilizes the chloride complex, cisplatin, with respect to the aqua complexes and reduces hydrolysis [73,165]. Even after administration, cisplatin is reported to be relatively stable within the blood stream and extracellular fluid. We attributed these observations to slow ligand exchange allowing for use of analytical techniques that involve isolation of the compounds using HPLC and LC based methods [166,167].

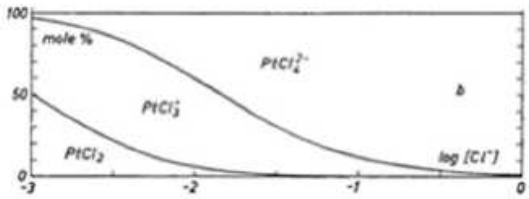

Fig. 6. Speciation of $[PtCl_4]^{2-}$ was measured at acidic pH and is shown as a function of Cl^- concentration. Adapted from Ref. [171] with permission.

4.1.2. Speciation of tetrachloridoplatinate(II) and its conversion to cisplatin

Because of the importance of hydrolysis and aquation of the chloride ligands, we turn to the substitution reaction, that is, aquation of the Pt—Cl bond. We therefore briefly summarize the preparation of cisplatin with the objective of giving the reader a sense of the chemistry involved in preparing this compound, and thus indirectly the first reactions taking place upon cellular uptake. Because the ligand exchange to Pt(II) is rather slow it is possible to isolate of both cis and trans forms of the compound with the formula $[PtCl_2(NH_3)_2]$ [151,168]. The preparation of cisplatin begins with potassium tetrachloridoplatinate(II), which is originally formed from treatment of Pt with Cl_2 at high temperatures (350 °C) [168]. Treatment of tetrachloridoplatinate(II) $[PtCl_4]^{2-}$ with KI results in tetraiodidoplatinate(II) ($[PtI_4]^{2-}$), which is treated with two equivalents of ammonia to form the yellow solid *cis*-diamminediiodidoplatinum(II) (*cis*-$[PtI_2(NH_3)_2]$) [76]. Treatment of this product with two equivalents of $AgNO_3$ results in the formation of *cis*-diamminediaquaplatinum(II) (*cis*-$[Pt(H_2O)_2(NH_3)_2]^{2+}$) [168,169]. The final product is formed after reacting this compound with excess KCl resulting in cisplatin (*cis*-$[PtCl_2(NH_3)_2]^{2-}$) [169]. It is interesting to note that these last two steps are the reverse reaction that takes place intracellularly upon uptake of the Pt-compound. Furthermore, the fact is that cisplatin is used and not the diaquated compound (*cis*-$[Pt(H_2O)_2(NH_3)_2]^{2-}$) because of the more favorable drug uptake properties.

The speciation of tetrachloridoplatinate(II) was reported in aqueous solution at basic pH [170] and in acidic solution [171,172]. These studies are important because this compound can be viewed as a reference compound to which the reactivity of Pt-based antitumoral drug compounds can be compared. The major species present in aqueous solutions is the original tetrachloridoplatinate(II) species, however, several additional hydrolysis products were also observed, see Fig. 6. The speciation of this compound as determined as a function of the chloride concentration at acidic pH and the equilibrium concentrations are shown in 6, [171–173]. As anticipated, in the presence of higher Cl^- concentration less of the aquation product is found. The kinetics of the hydrolysis reactions were also determined. The first and second aquation steps were found to be sufficiently different for each of the products to have a definite lifetime. The first aquation step, or replacement of one of the chloride ligands for an aqua ligand, was found to have a first order rate

constant of $3.69 \times 10^5\ s^{-1}$. Furthermore, this study reported a $\log \beta = 29.9 + 1.0$ for the double substituted product at high pH. This value measured for the stability of $[Pt(OH)_3]^-$ compares relatively well with a theoretically estimated value of 28.3 [174].

These results suggest that the predominant form of Pt in aqueous solution near neutral pH is not likely to be the charged monoaqua- or diaqua- species, but instead the Pt-species containing two chloride ligands and two ammine ligands [73,171,173]. Indeed some studies suggest, because in part that the predominant form is the monoaqua-species, that the species causing the biological activity may be the monoaqua-species instead of the diaqua-species that is generally depicted in many reviews [8,66,175]. Arguments are often made that a neutral species is best at penetration of the cell membrane, though it is well known that positively charged compounds readily penetrate cellular membranes [176].

4.1.3. Speciation of cisplatin in aqueous solution and in the presence of metabolites

In contrast to the V solutions discussed above, the aqueous solutions of cisplatin only slowly convert to form both the monoaqua- and diaqua- forms (*cis*-$[PtCl(H_2O)(NH_3)_2]^+$ and *cis*-$[Pt(H_2O)_2(NH_3)_2]^{2+}$) that after deprotonation, produce OH-analogs (*cis*-$[PtCl(HO)(NH_3)_2]$ and *cis*-$[Pt(HO)_2(NH_3)_2]$), illustrated in Fig. 5 [73,165]. These reactions lead to a derivative that can react and form adducts with the DNA. The production of these hydrolysis products was investigated by monitoring the reaction for days to assure that equilibrium was established [177]. The changes in cisplatin concentration (that is measuring the decay, disappearance or hydrolysis) were monitored for 50 h and the results are shown in Fig. 7. Despite the slow reactions, it was found that the reaction rates are sensitive to the surrounding environment. For example, in the presence of high concentrations of Cl^-, the rate of the first and second aquation steps will decrease by 10–20%. The first order rate constants k_1 of cisplatin aquation for three different chloride concentrations were $1.79 \times 10^{-5}\ s^{-1}$ (0 mg/L Cl^-), $1.68 \times 10^{-5}\ s^{-1}$ (50 mg/L Cl^-), and $2.06 \times 10^{-5}\ s^{-1}$ (100 mg/L Cl^-). For cisplatin second order reverse reaction, rate constants of $k_{-1} = 6.5 \times 10^{-3}\ M^{-1}\ s^{-1}$, $5.8 \times 10^{-3}\ M^{-1}\ s^{-1}$ and $4.1 \times 10^{-3}\ M^{-1}\ s^{-1}$ were measured [10,73]. Although the changes in the reaction kinetics are modest, the data in Fig. 7 show that there are some accumulation of unknown Pt-species after about 24 h in solution. Importantly, this data was used to justify the fact that cisplatin is administered in salt solutions in order to improve the speciation of cisplatin and its efficacy [12].

Since the speciation of cisplatin changes in the presence of the Cl^- anion, it follows that it will also change significantly if other, more nucleophilic metabolites, including protein or DNA that are present in solution or in the cell. As a late third row transition metal, Pt prefers soft ligands both in terms of thermodynamics and kinetics. That is, sulfur ligands are preferred over nitrogen, which again are preferred over oxygen ligand. Many studies have been done illustrating the reactivity of Pt(II) compounds, and the following example describe a case study. The reactions of cisplatin with S-based ligands have been investigated and in the case of methionine were also monitored at high (150 mM) and low (1.5 mM) chloride concentrations (using HPLC-ICP-DRCMS). The first order rate constant of cisplatin substitution in the presence of methionine at low chloride concentration was $k_1 = 2.28 \times 10^{-4}\ s^{-1}$, which is one order of magnitude higher than the rate constant observed for cisplatin aquation in water containing the equal amount of chloride and no methionine. At high chloride concentration, the first order rate constant of cisplatin aquation was $k_1 = 1.41 \times 10^{-4}\ s^{-1}$ in the presence of methionine and thus faster than the rate constant in water [178]. These results demonstrate that the environment is important and that cisplatin hydrolyzes faster in the presence of metabolites. Therefore, subtle changes in the reactivity and properties of the drug upon administration are likely. Presedent with V-compounds document different reactivities based on environment [16] and similarly a report with Co-compounds demonstrated a dramatic change in reactivity based on compound environment [179].

The cytoplasm contains metabolites including phosphate, citrate, glucose, amino acids as well as cellular components such as glutathione and ascorbate that maintain the redox environment of the cell [180–183]. Reduced drug accumulation of cisplatin has been reported in drug-resistant cell lines [65,184–186]. This reduced drug accumulation could be explained by a number of different mechanisms including reduced drug uptake from the culture media due to alterations in some specific membrane transporters, enhanced drug efflux, or changes in the metabolite concentrations in the resistant cell lines [65,187] or a combination of these factors. Once formed, the Pt-DNA adducts can be repaired by specific enzymes that recognize the DNA damage [188–190]. Another limiting factor is that once incorporated into the cells, the drug can be inactivated by binding to different biomolecules present within the cell cytosol such as glutathione and other sulfur-containing proteins [163,191]. Because of the high affinity of Pt for sulfur ligands, glutathione is likely to react with cisplatin [10,192,193]. Indeed glutathione adducts are reported upon administration of cisplatin, and, once formed, it is exported out of the cell. This is consistent with

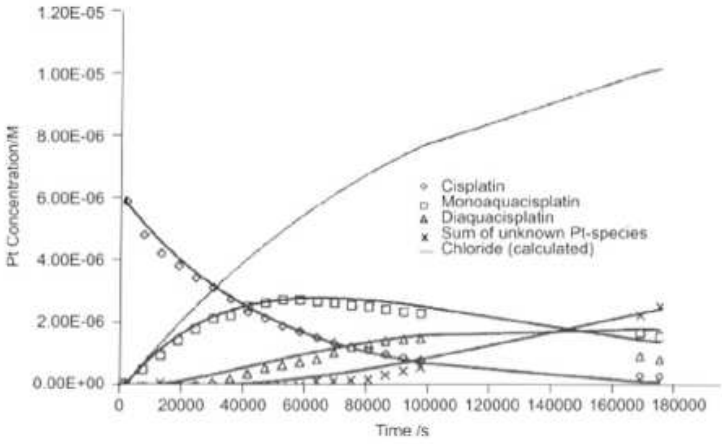

Fig. 7. Cisplatin decay at 0 mM Cl^- concentration. Adapted from Ref [10,73] with permission.

reduced drug accumulation cisplatin-resistant cell lines [194,195]. In contrast, studies done with carboplatin and glutathione have indicated that reactions between carboplatin and thiols such as glutathione are very slow, with only small amounts of Pt-thiolato complexes being detectable via ^{15}N NMR spectroscopy and HPLC in mice treated with ^{15}N carboplatin. This difference in reactivity with thiols between carboplatin and cisplatin may account for the decreased nephrotoxicity observed with carboplatin [196]. However, it is important to recognize that the identification of one pathway to reduce cisplatin accumulation does not preclude activity of other mechanisms.

Studies with amino acids and other metabolites are of interest because stability of the complexes is important with regard to understanding potential reactions that take place in the cytoplasm [197,198]. As shown in Table 3, the stability of Pt-complexes with peptides and the amino acid guanidinoacetic acid (GAA) with both chloride, ammine and hydroxide ligands demonstrate that the cisplatin complex has comparable stability with most except a few complexes [199]. It also shows that cisplatin complexing with guanidinoacetic acid in the place of its chloride ligands has a higher formation constant that does cisplatin itself, as do several other similar studied Pt complexes. Increased stability of these complexes can have a profound effect on the ability of these compounds to react with DNA. This study investigated the reaction with the unusual amino acid guanidinoacetic acid because is found at high concentrations in the kidney and liver, and thus complexes formed with it may have significance with regards to toxicity and development of resistance [199–201]. Since cisplatin accumulates in the kidney and the liver, the dramatic reduction in the levels of this amino acid is observed upon administration of cisplatin in urinary tract cancer patients. Guanidinoacetic acid is significantly involved in renal metabolism, since it is mainly synthesized in the kidneys and subsequently excreted in urine or methylated for creatine production [199,200]. The comparable stability of cisplatin in the presence of a sea of alternative nucleophiles including GAA thus explains why the original compound remains intact as long as it does.

In addition to cellular metabolites having the potential to inactivate these anticancer Pt complexes, other components in the administration liquid could potentially react similarly. This is an important fact, because dimethyl sulfoxide (DMSO) can be used by clinicians to solubilize Pt-drugs and it was recently reported that this practice has the potential to inactivate cisplatin and other anticancer Pt-complexes [63]. Because DMSO is commonly used as a solvent for solubilizing small molecules at high concentrations in biological studies, clinical Pt compounds are commonly dissolved in DMSO for biologic experiments as well [63, 202]. This is very important, because DMSO is nucleophilic, and will coordinate with the platinum, displacing its chloride ligands and thus changing the structure and reactivity of the anticancer agent by changing the speciation [203]. This change in the structure of the Pt compound has been reported to dramatically inhibit the cytotoxicity and ability to initiate apoptosis of Pt-drugs [63]. This recent report further underlines how necessary it is to take into consideration the administration fluid by the Pt-drug so that the efficacy of the drug is not decreased during drug administration [63].

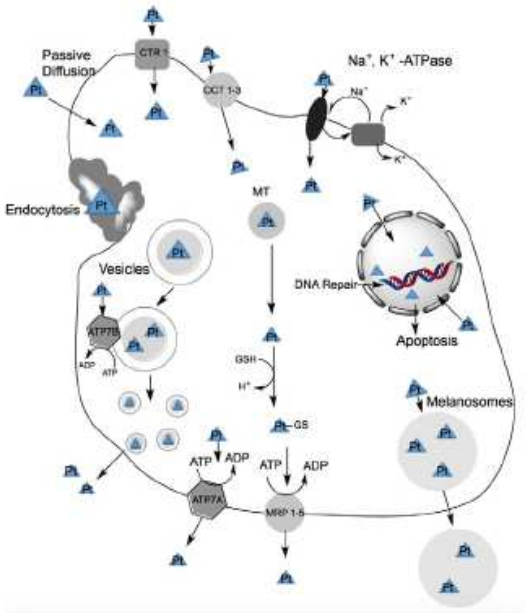

Fig. 8. The many possible pathways for influx and efflux for cisplatin are depicted. Ref. [149].

4.1.4. Uptake of cisplatin and interaction with proteins

The toxic nature of cisplatin requires that patients are carefully hydrated and monitored prior, during and following the drug administration [9,204]. The common mode of administration of Pt-based drugs is by intravenous injection, and generally requires that patient is checked in one additional day pre- and post-treatment at an appropriate outpatient facility [205]. It is the perception that cisplatin and other Pt-based anticancer drugs, as neutrally charged molecules, will enter the cell [7, 149] however, a reasonable potential exists that positively charged drugs enter as well [206–212] (or that a mechanism involving an initial pre-complex forms). This point is particularly important because only a small fraction of the administered Pt-drug will reach the nuclear DNA and produce the critical cytotoxic regions [10,213,214].

The many possible uptake pathways that are open to the Pt-drug are illustrated in Fig. 8. Such pathways include the copper influx transporter 1 and other transporters (Ctr1, ATP7A and ATP7B) [206,207], polyorganic specific cation transporters such as OCT1–3 [208,209,215] as well as a sodium dependent process that has yet to be fully characterized with regard to its role and interaction [210–212]. Melanosomes

Table 3
Formation constants of Pt-complexes with guanidinoacetic acid (G) and chloride, ammine, and hydroxide substituents, where GAA has a neutral charge. Adapted from Ref. [199].

Species	Log β	Species	Log β
$[HGAA]^+$	10.97 (0.01)/10.84[a]/10.85[b]	$[Pt_2(OH)_2(GAA)_2]^{2+}$	6.98 (0.03)
$[Pt Cl_4]^{2-}$	16.27 (0.05)	$[Pt Cl_2GAA]$	18.36 (0.02)
$[Pt Cl_2(OH)]^{2-}$	4.52 (0.03)	cis-$[Pt(NH_3)_2Cl_2]$	22.99 (0.01)
$[Pt Cl_3(OH)_1]^{2-}$	(−)22.24 (0.02)	$[Pt(OH)_2(NH_3)_2]$	(−)6.11 (0.03)
$[Pt_2Cl_4(OH)_2]^{2-}$	6.37 (0.05)	$[Pt(NH_3)_2GuAA]^{2+}$	22.09 (0.07)[c]
$[PtGAA]^{2+}$	12.1 (0.02)	$[Pt(OH)(NH_3)_2GAA]^+$	12.99 (0.02)
$[Pt GAA_2]^{2+}$	15.99 (0.01)	$[Pt_2(OH)_2(NH_3)_4]^{2+}$	14.60 (0.01)
$[Pt(HGAA)_2]^{4+}$	36.11 (0.01)	$[Pt(NH_3)_2(HGuAA)_2]^{4+}$	48.20 (0.05)
$[Pt(OH)_2(GAA)_2]$	(−) 4.83 (0.02)	$[Pt(NH_3)_2(HGuAA)GuAA]^{3+}$	39.46 (0.04)

provide another method for the transport of Pt-drugs through cells [216]. Finally, endocytosis and passive diffusion are common mechanisms for Pt-based drug entry of the cell. In contrast, reactions of the Pt-drug with glutathione can lead to their exportation via the multidrug resistant protein transporters, MRP 1–5 [217].

Protein systems are recognized as a principal contributor to the reduction in efficacy of Pt-drugs and the development of resistance, in addition to the transporters described above. The efficiency of the drugs in reaching and reacting with the DNA is dependent on its ability to produce active hydrolysis products once inside the cell and whether or not these hydrolysis products are inactivated by binding to serum proteins [218–220] and other proteins. Proteins such as HSA and γ-globulin, which make up about 80% of total plasma proteins, have been studied to explore how they bind and to determine how much Pt they bind [10,218]. Such studies with serum proteins have indicated that after administration, the largest percentage of the Pt-drugs are bound to extra and intracellular proteins, with as much as 80–85% of Pt-compound being bound after a 5 h incubation period [10,219,221–223]. In studies with human serum albumin (HSA) it was found that as a result of Pt-binding, disulfide bonds may break, and this is possibly accompanied by intramolecular cross-linking of the protein which may result in the partial unfolding of protein HSA at high drug concentrations [221,224]. Such changes may lead to a change in the protein's biological activity, as disulfide bonds play an important role in maintaining the shape of the protein, which may contribute to the observed toxicity of Pt-compounds [221]. More studies with HSA indicate that there is no saturation of the albumin with cisplatin, but rather that the bound metal-complex is influenced by the ratio between the drug and the protein, initial concentration of the protein, incubation time, and nature of the incubation medium [218]. A 14-day incubation of HSA with cisplatin in a 60-fold drug excess yielded as much as 20 Pt atoms bound to each protein. Generally, shorter incubation periods and lower cisplatin/albumin ratios lead to lower fractions of bound Pt to protein [218]. We refer the readers to more comprehensive coverage of the reactions with HSA, transferrin, γ-globulin and transporters with the Pt-drugs [65,146,215,217,219,220,225].

5. Examples where speciation has changed drug formulation and efficacy

5.1. Vanadium

Although the V salts (sodium metavanadate and vanadyl sulfate) and one coordination compound (BEOV, bis(ethylmaltolato) oxidovanadium(IV)) that have been in clinical trials for treatment of diabetes, none of these compounds are currently in the clinics in the US or worldwide. The effect of the BEOV compound on the human subjects in the type II clinical trial was variable, but since it went off patent Sept. 30, 2011 this compound is no longer being investigated for treatment of diabetes. However, both the salts and new compounds are continuously being investigated in cell and animal studies.

The V(IV) salt, vanadyl sulfate, is, however effectively, used for body builders and as a food additive to manage glucose levels [226]. However, the form of the V that can be purchased in stores varies dramatically. For example, in the three nutritional additives Vana Trace, Good sugar and Glu-pro VM, the V content varies from 15.5 mg, 7.75 mg and 1.55 mg in the pills with the vanadyl dosage of 50 mg, 25 mg and 5 mg, respectively. However, as shown in Fig. 9, many more formulations of vanadyl sulfate are available as found by searching the web and showing commercial products [219]. The abundance of different products is a testimony to the fact that such formulation even for nutritional additives is a profitable industry.

5.2. Platinum

Cisplatin was the first Pt-based-drug and remains an important anticancer drug [1–10]. We selected here two recent examples of Pt-based drugs [227–231], which are developed using fundamentally different approaches to treatment and delivery. The associated differences and thus resulting in placing these drugs in a different speciation space, one in which the cisplatin is wrapped in a liposome and a second one in which the Pt oxidation state is IV in place of II.

Fig. 9. Commercially different forms of vanadyl sulfate found on the internet in 2016 [219].

5.2.1. Lipoplatin – changes in speciation decrease toxicity of cisplatin and increase efficacy

We will first describe Lipoplatin, also known as liposomal cisplatin, which utilizes a liposomal delivery system for the intracellular deposit of cisplatin, Fig. 10 [227]. Lipoplatin was developed in an effort to circumnavigate the high nephrotoxicity levels patients experienced when using cisplatin as a primary line of treatment [196]. The lower toxicity presumably arises in part because of reduced glutathione or metallothionein mediated detoxification levels when treating some types of cancers. By targeting cisplatin resistant cell lines and specific cancerous organelles, the liposomal preparation permits the drug to enter the system through the vascular network tissue of the malignant tumor.

The lipids in the Lipoplatin capsule emulate the cellular membrane of the tumor cells they are targeted to, and consist of soy phosphatidyl choline, cholesterol, dipalmitoyl phosphatidyl glycerol (DPPG), and methoxyl-polyethylene glycerol diesteroyl phosphatidylethanolamine. This membrane composition allows for fusion with the phospholipid cellular membrane [232] of the targeted tumor, and is found to rapidly enter the targeted cell via endocytosis and direct fusion of the lipoplatin nanoparticles of the membrane due to the presence of fusogenic lipid DPPG on its shell [229]. Through direct fusion of nanoparticles that penetrate the leaky cell membranes of malignant tumors, illustrated in Fig. 10, lipoplatin represents a promising strategy to combat the cells resistant to Pt(II)-compounds [228–230]. Once inside the cell, the cisplatin is released, hydrolyzed as detailed in Figs. 4 and 5, and exhibits its anticancer activity by forming the cytotoxic intrastrand DNA adducts.

By utilizing this nanoparticle (110 nm) administration, cisplatin derived drugs exhibit increased specificity to the targeted cancer tumor [232–235] presumably because the method of liposomal uptake circumvents other methods of Pt resistance, such as up- or down-regulation of metal ion transporters [236]. In addition to preventing the decrease in cytotoxic Pt concentrations, the pharmacokinetic studies with lipoplatin indicated that this delivery method has resulted in a decrease in the distribution volume, shortened the half-life of the Pt-drug and has increased the plasma clearance in comparison to cisplatin [229]. These studies have shown that lipoplatin reached a higher plasma concentration while decreasing nephrotoxic side effects [227]. The direct consequences of these improved properties indicate that lipoplatin can be administered using an outpatient treatment facility [232], which is contrary to the intravenous treatment of cisplatin that requires constant monitoring and thus pre and post-administration overnight hospital stay [227].

Lipoplatin has been tested in clinical trials studies as both a primary course of action and secondary line of treatment for malignant tumors [227]. Previous studies have indicated that lipoplatin could be success as a secondary line of treatment for patients that had developed cisplatin resistance during the course of chemotherapy [237]. In clinical trials, drugs administered in concert with Lipoplatin include gemcitabine, used for treatment of pancreatic cancers [238], and Paclitaxel, used as an anti-microtubule agent given to treat Kaposi sarcomas [239]. Phase II clinical trials with lipoplatin administered in concert with gemcitabine as treatment for pancreatic cancer patients was also reported [240]. Additionally, phase III clinical trials have utilized lipoplatin in combination with gemcitabine or paclitaxel for patients with non-small cell lung cancer was also reported [241].

Combined, these studies demonstrate that the subtle change in the speciation chemistry of the cisplatin has a profound effect on the efficacy and toxicity of the drug. Although the fundamental mechanism of action remains the same, the changes in the stability and speciation allow administration of a systemic lower dose resulting in overall lower toxicity.

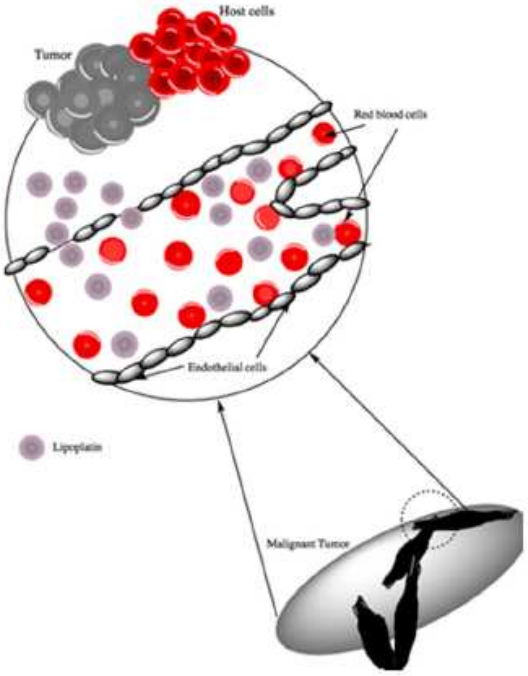

Fig. 10. Lipoplatin injected into malignant tumor, enter the blood via vascular tissue network (top). Lipoplatin fused with the phospholipid cellular membrane cisplatin intercellular delivery (bottom). Adapted with modification from Ref. [240].

5.2.2. Satraplatin – Pt(IV)-compounds modify uptake and speciation profiles

In addition to the Pt(II) based drugs, researchers have found that Pt(IV) compounds also exhibit desirable anticancer properties [231]. We here describe satraplatin (*trans,cis,cis* diacetatoamminedichlorido(cyclohexylamine)platinum(IV), JM216), the most successful orally active Pt(IV) antitumor drug to date, Fig. 11 [242, 243]. Satraplatin has a six-coordinate Pt(IV) with two ammine and two chloride ligands in the plane and two additional axial acetate groups, making this compound more lipophilic. Once in the bloodstream and intracellular, the satraplatin compound is metabolized. The Pt(IV) is reduced to Pt(II) in cells [244] and the Pt(IV) loses its acetato groups, forming a structure analogous to cisplatin (except for the replacement of one of the ammine groups with a cyclohexylammine group. This

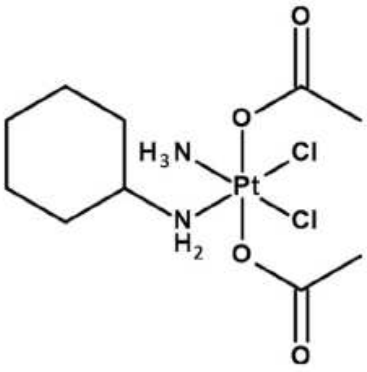

Fig. 11. Chemical structure of satraplatin.

new cisplatin-analog metabolite, referred to as JM 118 *cis*-amminedichlorido(cyclohexylamine)platinum(II) then follows a mechanism of action similar to that of cisplatin in that it enters the nucleus where it binds to DNA to form inter- and intrastrand cross-links, distorting the DNA. Because satraplatin is an orally active anticancer agent, exhaustive consideration of speciation for this compound would include examination of biological environments including the GI tract. Since this topic is beyond this manuscript, we are referring the readers to the elsewhere for information on such speciation as well for speciation *in vivo* [132,245]. We hypothesize that the speciation of this drug is contributing to the improved efficacy of this compound.

Satraplatin is low molecular weight, neutral, and kinetically inert in acidic media. The lower reactivity of the Pt(IV) compound allows oral administration because degradation in the gastric environment is not as problematic as with the Pt(II) compounds. Satraplatin is unstable in light and alkaline media, however, considering the oral administration its stability in acidic environments is much more important. Indeed, the half-live of reduction of satraplatin with 5 mM ascorbate is around 50 min, leaving adequate time for gastrointestinal absorption as parent Pt(IV) complex and allowing it to be administered orally [246]. The asymmetrical stable ligands, the ammine and cyclohexylammine, of satraplatin alter its DNA adduct profile such that inhibition of DNA synthesis is increased and likelihood of being recognized by DNA-mismatch repair is decreased [247,248], which contributes to the ability of satraplatin to overcome cisplatin resistance. In addition to increased efficacy as a result of its DNA binding and inhibition properties, satraplatin represents a distinct class of Pt-compounds that act very differently in uptake and during cellular processing than the Pt(II) compounds as a result of its increased lipophilicity and asymmetrical stable ligands. The effectiveness of satraplatin is related in part to the reduction of the Pt(IV) compound as it reaches the tumor sites and its ability to survive the uptake and the processing before entering the nucleus and reaching DNA [242,243]. Therefore, being hydrolytically inert, and considering the slow hydrolyzation of the Pt ligands, it is more likely to reach tumor DNA without reacting with other metabolites [249,250].

Although intraveneous injection cisplatin tends to be stable, there is the potential that in addition to reacting in the more reducing cellular environment in tumors that the Pt(IV)-drugs react and form the toxic Pt(II) prematurely before reaching the tumor. It is possible that in red blood cells (RBC) the reducing environment is responsible for forming the reactive Pt(II) form of the metal drug. Studies done with V(V) indicate that in the blood, the oxidation state of the metal is reduced to V(IV) [251] and similarly was observed in cell culture [252]. Such reaction may be occurring at least partly with Pt(IV) drugs as well, particularly in the reducing environments of the RBC before the drugs reach the tumor site. This possibility should be routinely be investigated in studies with Pt(IV) drugs.

Related to satraplatin is mitaplatin, Other examples of Pt(IV)-based drugs have been investigated including mitoplatin combining the cisplatin structure with two dichloroacetato groups in the axial positions [231]. Upon uptake in the tumor cells, this compound decomposes to form cisplatin by losing the two equivalents of dichloroacetato [253,254]. Dichloroacetate inhibits pyruvate dehydrogenase kinase involved in the glucose metabolism and found in excess in cancer cells and inhibition of PDK blocks the proliferation and survival of cancerous cells [255]. By inhibiting the phosphorylation of pyruvate dehydrogenase in the mitochondria, it primes the mitochondria of cancer cell for apoptosis, induced by the platination of nuclear DNA [231]. Although the design of this compound with cisplatin as a Trojan horse is conceptually interesting, mitaplatin was not found to be any more effective than cisplatin in animal and human studies [256] leaving satraplatin as a better Pt(IV)-compound [67].

Satraplatin on the other hand has shown success in Phase I, II, and III clinical trials. Satraplatin is given in concert with other anticancer agents, such as docetaxel for the treatment of prostate cancer, paclitaxel in the treatment of non-small cell lung cancer, and capecitabine for treatment of advanced solid tumors [67]. Positive results in clinical trials caused GPC biotech to file for the accelerated approval of satraplatin. However, this application was rejected by the FDA on the basis that satraplatin did not show convincing enough benefit in terms of overall survival, and concerns were raised that only 51% of patients in the trial had received prior docetaxel [67]. Recently, clinical trials with this drug have continued. In 2016, experiments were reported in which satraplatin was reformulated by encapsulation of cyclodextrin. This modification increased satraplatin's solubility, making it more suitable for medical treatments, while enhancing its stability in cellular environments by protecting against undesirable hydrolytic decomposition [257]. Time will show whether this or related approaches will be successfully lead to introduction of yet another Pt-agent to the clinic.

5.2.3. Current challenges

Consideration of speciation could point to efficient approaches for drug formulation in the future and would be an inexpensive way to probe the system. Topics needing characterization include basic chemistry, studies *in vivo* and consideration of the formulation used in administration of the drugs. Application of the range of routine methods that are available and are needed for speciation studies are readily done in aqueous solutions [28,119,123]. Similar studies are more difficult to carry out *in vivo*. That is, the biological matrices are very complex and the concentration of drug generally very low, essentially precluding studies identifying species *in vivo*. For example, potentiometry is not likely to be a method useful in complex systems but remains important in aqueous solutions and in the absence of many matric components [28]. However, non-routine methods have been developed such as high-frequency and field EPR spectroscopy and XAS and are found to be very informative even though such methods are generally not done *in vivo*, but of tissue samples that have been fixed and treated [123,124]. However, the many imaging techniques that are being developed could potentially be used for identification of key metabolite species [133,258], though most such methods have not been used for identification of small molecules. The overriding challenges in all such studies remains low concentration and the fact that most methods are not done *in vivo*. Additional challenges remain identification of systems and the metabolites that are condusive to such investigations.

The information described in this manuscript shows how Lipoplatin efficiently modifies the speciation of cisplatin and results in drugs that have lower toxicity and enhanced efficacy. It is important to recognize that details in the mode of action were not required for these considerations, although studies documenting the pharmacokinetic behavior of the compound was helpful to develop the hypothesis presented in this work. Further recommendations thus include speciation studies at all levels. Challenges in the area of metals in medicine and specifically anticancer compounds include difficulties in cases when kinetics is rapid and different species may not be isolated as well as the low concentrations of the drugs and their metabolites.

6. Conclusion

In this article we describe the fundamental speciation reactions and the role and importance of speciation with regard to the activity of V-compounds and Pt-drugs. The V-compounds have been extensively studied with regard to characterization of the speciation, and their biological effects. Less work in the area of speciation has been carried out with Pt-based anticancer agents even though they are among the most successful anticancer agents. The problems associated with Pt-treatment include high toxicity, lowered specificity and developing resistance and can be combated by developing new and improved strategies and systems.

Pt(II) and Pt(IV) both undergo slow ligand exchange reactions, which is why isolation of a range of species is possible. That is in contrast to a metal like vanadium, where the ligand exchanges on some of the systems are much faster. The inherent stability of the Pt-compounds

can readily be illustrated by description of the aquation and hydrolysis of the parent tetrachloridoplatinate(II) $[PtCl_4]^{2-}$, as well as cisplatin. Most of the administered cisplatin obtained from tissue samples from subjects treated with Pt-compounds from biological samples is in the form of the parent drug and only a small percentage is present as the monoaquated form and even less as the diaquated form. Some investigators favor the interpretation that the diaquated product of cisplatin reacts with DNA because these complexes are neutral, however, very little of this compound forms, so it is possible that the monoaquated hydrolysis product is a compound that reacts directly with DNA and is responsible for most of the Pt bound to DNA. This would imply a different mechanism of action than what is generally believed.

As we illustrate with the case of lipoplatin and satraplatin, speciation can be used to improve efficacy. Lipoplatin is prepared by enclosing cisplatin in a liposome and this modification of the cisplatin results in decreased toxicity. The lower toxicity of Lipoplatin is presumably because of the improved uptake and targeting and decreased systemic concentration of the drug. The practical consequence of the lower toxicity of the drug is that lipoplatin administration can be done in an outpatient manner, rather than requiring a hospital stay as in the case of cisplatin. Consideration of Pt chemistry also allows the administration of the inert nontoxic Pt(IV) compound, satraplatin, and the selectivity for tumor tissues even though it is administered orally. Importantly, both Lipoplatin and satraplatin have potential as a second line of treatment of tumors that have developed cisplatin resistance. In summary, we urge that as the community going forward in development of new drugs will consider speciation chemistry as one of the key strategies that will be considered in the future development of anticancer drugs. Indeed, minor reformulations or reconsiderations of Pt-based drug speciation can improve Pt's significance in targeted cancer treatment methodology; especially individualized medicine. The data presented here utilizing liposomes (that is nanoparticles) for Pt prodrug entry has promise as a low cytotoxic method for patients, as well as more cost effective for both the provider and insured.

Abbreviations

V	Vanadium
Pt	Platinum
NMR	Nuclear Magnetic Resonance
V(V)	Vanadate
FDA	Federal Drug Administration
PTP1B	protein tyrosine phosphatase 1 B
XAS	x-ray absorption spectroscopy
IUPAC	International Union of Pure and Applied Chemistry
EPR	electron paramagnetic resonance
KI	potassium iodine
$AgNO_3$	silver nitrate
ENDOR	electron nuclear double resonance
DEAE	diethylaminoethanol
EXAFS	extended x-ray absorption fine structure
LAXS	large angle x-ray scattering
YOPH	Yersinia acid phosphatase
GI	gastrointestinal
LC	liquid chromatography
HPLC	high performance liquid chromatography
HPLC-ICP-DRCMS	HPLC with inductively coupled plasma
GAA	guanidinoacetic acid
OCT	organic cation transporter
MRP	multidrug resistance protein transporter
HSA	human serum albumin
Ctr1	copper influx transporter
DPPG	dipalmitoyl phosphatidyl glycerol
GPC	German Biopharmaceutical Company
XANES	X-Ray absorption near-edge spectroscopy

Acknowledgements

DCC thanks the Arthur Cope Scholar Award Foundation for management of the Cope Scholar Award. KAD and KNH thank the GAANN foundation for a scholarship. We thank the National Institutes of Health and National Cancer Institute for grant 1R13CA200223-01A1 (Conference Organization support) supporting the 1st International Symposium on Clinical and Experimental Metallodrugs in Medicine: Cancer Chemotherapy, CEMM where this work was first presented and important discussions led to the current version of this work.

References

[1] Y. Jung, S.J. Lippard, Chem. Rev. 107 (2007) 1387–1407.
[2] E.R. Jamieson, S.J. Lippard, Chem. Rev. 99 (1999) 2467–2498.
[3] J. Reedijk, Pure Appl. Chem. 59 (1987) 181–192.
[4] I. Romero-Canelón, P.J. Sadler, Proc. Natl. Acad. Sci. 112 (2015) 4187–4188.
[5] P.J. Sadler, Z.J. Guo, Pure Appl. Chem. 70 (1998) 863–871.
[6] Z. Guo, P.J. Sadler, Angew. Chem. Int. Ed. 38 (1999) 1512–1531.
[7] N. Farrell, Cancer Investig. 11 (1993) 578–589.
[8] F. Muggia, N. Farrell, Crit. Rev. Oncol. Hematol. 53 (2005) 1–2.
[9] R.R. Barefoot, J. Chromatogr. B 751 (2001) 205–211.
[10] B. Michalke, J. Trace Elem. Med. Biol. 24 (2010) 69–77.
[11] D.C. Crans, K.A. Woll, K. Prusinskas, M.D. Johnson, E. Norkus, Inorg. Chem. 52 (2013) 12262–12275.
[12] S.J. Berners Price, P.J. Sadler, Coord. Chem. Rev. 151 (1996) 1–40.
[13] W.I. Mortada, M.M. Hassanien, A.A. El-Asmy, J. Trace Elem. Med. Biol. 27 (2013) 267–272.
[14] T. Kiss, T. Jakusch, D. Hollender, A. Dornyei, E.A. Enyedy, J.C. Pessoa, H. Sakurai, A. Sanz-Medel, Coord. Chem. Rev. 252 (2008) 1153–1162.
[15] T. Jakusch, J.C. Pessoa, T. Kiss, Coord. Chem. Rev. 255 (2011) 2218–2226.
[16] D.C. Crans, A.M. Trujillo, P.S. Pharazyn, M.D. Cohen, Coord. Chem. Rev. 255 (2011) 2178–2192.
[17] G.R. Willsky, L.-H. Chi, M. Godzala, P.J. Kostyniak, J.J. Smee, A.M. Trujillo, J.A. Alfano, W. Ding, Z. Hu, D.C. Crans, Coord. Chem. Rev. 255 (2011) 2258–2269.
[18] D.M. Templeton, F. Ariese, R. Cornelis, L.-G. Danielsson, H. Muntau, H.P. van Leeuwen, R. Lobinski, Pure Appl. Chem. 72 (2000) 1453–1470.
[19] C.F. Chin, Q. Tian, M.I. Setyawati, W. Fang, E.S.Q. Tan, D.T. Leong, W.H. Ang, J. Med. Chem. 55 (2012) 7571–7582.
[20] A. Herman, J.M. Tanski, M.F. Tibbetts, C.M. Anderson, Inorg. Chem. 47 (2008) 274–280.
[21] L. Cubo, A. Casini, C. Gabbiani, G. Mastrobuoni, L. Messori, J. Jiménez-Barbero, C. Navarro-Ranninger, A.G. Quiroga, Chem. Eur. J. 15 (2009) 9139–9146.
[22] D.C. Crans, S.M. Schelble, Biochemistry 29 (1990) 6698–6706.
[23] D.C. Crans, C.M. Simone, A.K. Saha, R.H. Glew, Biochem. Biophys. Res. Commun. 165 (1989) 246–250.
[24] D. Rehder, Inorg. Chem. Commun. 6 (2003) 604–617.
[25] A. Levina, P.A. Lay, Dalton Trans. 40 (2011) 11675–11686.
[26] D.C. Crans, B. Zhang, E. Gaidamauskas, A.D. Keramidas, G.R. Willsky, C.R. Roberts, Inorg. Chem. 49 (2010) 4245–4256.
[27] D.C. Crans, H. Chen, O.P. Anderson, M.M. Miller, J. Am. Chem. Soc. 115 (1993) 6769–6776.
[28] T. Jakusch, W.Z. Jin, L.Q. Yang, T. Kiss, D.C. Crans, J. Inorg. Biochem. 95 (2003) 1–13.
[29] X. Wu, B.J. Peters, C.D. Rithner, D.C. Crans, Polyhedron 114 (2016) 325–332.
[30] D.C. Crans, R.L. Bunch, L.A. Theisen, J. Am. Chem. Soc. 111 (1989) 7597–7607.
[31] D.C. Crans, C.D. Rithner, L.A. Theisen, J. Am. Chem. Soc. 112 (1990) 2901–2908.
[32] D.C. Crans, J.J. Smee, E. Gaidamauskas, L. Yang, Chem. Rev. 104 (2004) 849–902.
[33] T. Jakusch, É.A. Enyedy, K. Kozma, Z. Pasr, A. Bényei, T. Kiss, Inorg. Chim. Acta 420 (2014) 92–102.
[34] D.C. Crans, E.M. Willging, S.R. Butler, J. Am. Chem. Soc. 112 (1990) 427–432.
[35] G. Huyer, S. Liu, J. Kelly, J. Moffat, P. Payette, B. Kennedy, G. Tsaprailis, M.J. Gresser, C. Ramachandran, J. Biol. Chem. 272 (1997) 843–851.
[36] V. Lopez, T. Stevens, R. Lindquist, Arch. Biochem. Biophys. 175 (1976) 31–38.
[37] D.C. Crans, J. Org. Chem. 80 (2015) 11899–11915.
[38] D. Rehder, Future Med. Chem. 4 (2012) 1823–1837.
[39] G.R. Willsky, K. Halvorsen, M.E. Godzala III, L.-H. Chi, M.J. Most, P. Kaszynski, D.C. Crans, A.B. Goldfine, P.J. Kostyniak, Metallomics 5 (2013) 1491–1502.
[40] H. Sakurai, A. Katoh, T. Kiss, T. Jakusch, M. Hattori, Metallomics 2 (2010) 670–682.
[41] K.H. Thompson, J. Lichter, C. LeBel, M.C. Scaife, J.H. McNeill, C. Orvig, J. Inorg. Biochem. 103 (2009) 554–558.
[42] K.H. Thompson, C. Orvig, J. Inorg. Biochem. 100 (2006) 1925–1935.
[43] D.C. Crans, Pure Appl. Chem. 77 (2005) 1497–1527.
[44] M. Li, W. Ding, B. Baruah, D.C. Crans, R. Wang, J. Inorg. Biochem. 102 (2008) 1846–1853.
[45] S.K. Hanson, R.T. Baker, J.C. Gordon, B.L. Scott, D.L. Thorn, Inorg. Chem. 49 (2010) 5611–5618.
[46] A.M. Evangelou, Crit. Rev. Oncol. Hematol. 42 (2002) 249–265.
[47] E. Kioseoglou, S. Petanidis, C. Gabriel, A. Salifoglou, Coord. Chem. Rev. 301 (2015) 87–105.

[48] C.C. McLauchlan, J.D. Hooker, M.A. Jones, Z. Dymon, E.A. Backhus, B.A. Greiner, N.A. Dorner, M.A. Youkhana, L.M. Manus, J. Inorg. Biochem. 104 (2010) 274–281.
[49] C.C. McLauchlan, B.J. Peters, G.R. Willsky, D.C. Crans, Coord. Chem. Rev. 301 (2015) 163–199.
[50] L. Wittenkeller, A. Abraha, R. Ramasamy, D. Mota de Freitas, L.A. Theisen, D.C. Crans, J. Am. Chem. Soc. 113 (1991) 7872–7881.
[51] D.C. Crans, C.M. Simone, Biochemistry 30 (1991) 6734–6741.
[52] D.C. Crans, K. Sudhakar, T.J. Zamborelli, Biochemistry 31 (1992) 6812–6821.
[53] R.N. Lindquist, J.L. Lynn, G.E. Lienhard, J. Am. Chem. Soc. 95 (1973) 8762–8768.
[54] J.E. Ladner, B.D. Wladkowski, L.A. Svensson, L. Sjolin, G.L. Gilliland, Acta Crystallogr. D 53 (1997) 290–301.
[55] B. Borah, C.W. Chen, W. Egan, M. Miller, A. Wlodawer, J.S. Cohen, Biochemistry 24 (1985) 2058–2067.
[56] D.C. Crans, R.A. Felty, M.M. Miller, J. Am. Chem. Soc. 113 (1991) 265–269.
[57] Y. Zhang, X.D. Yang, K. Wang, D.C. Crans, J. Inorg. Biochem. 100 (2006) 80–87.
[58] W.A.J. Dewaal, J.C. Kraak, F. Maessen, Pharm. Weekblad. 7 (1985) 287.
[59] K. Polec-Pawlak, J.K. Abramski, O. Semenova, C.G. Hartinger, A.R. Timerbaev, B.K. Keppler, M. Jarosz, Electrophoresis 27 (2006) 1128–1135.
[60] D.G. Sar, M. Montes-Bayon, E.B. Gonzalez, A. Sanz-Medel, J. Anal. At. Spectrom. 21 (2006) 851–868.
[61] S. Thomas, M. Rivallan, M. Lepage, N. Takagi, H. Hirata, F. Thibault-Starzyk, Microporous Mesoporous Mater. 140 (2011) 103–107.
[62] A. Zayed, G.D.D. Jones, H.J. Reid, T. Shoeib, S.E. Taylor, A.L. Thomas, J.P. Wood, B.L. Sharp, Metallomics 3 (2011) 991–1000.
[63] M.D. Hall, K.A. Telma, K.-E. Chang, T.D. Lee, J.P. Madigan, J.R. Lloyd, I.S. Goldlust, J.D. Hoeschele, M.M. Gottesman, Cancer Res. 74 (2014) 3913–3922.
[64] W.I. Sundquist, S.J. Lippard, Coord. Chem. Rev. 100 (1990) 293–322.
[65] M.M. Gottesman, O. Lavi, M.D. Hall, J.-P. Gillet, in: P.A. Insel (Ed.) Annual Review of Pharmacology and Toxicology, Vol. 56, 2016, pp. 85–102.
[66] S. Dasari, P.B. Tchounwou, Eur. J. Pharmacol. 740 (2014) 364–378.
[67] N.J. Wheate, S. Walker, G.E. Craig, R. Oun, Dalton Trans. 39 (2010) 8113–8127.
[68] B. Rosenberg, Cancer 55 (1985) 2303–2316.
[69] A.H. Calvert, D.R. Newell, L.A. Gumbrell, S. O'reilly, M. Burnell, F.E. Boxall, Z.H. Siddik, I.R. Judson, M.E. Gore, E. Wiltshaw, J. Clin. Oncol. 7 (1989) 1748–1756.
[70] E. Raymond, S. Faivre, J.M. Woynarowski, S.G. Chaney, Proc. Semin. Oncol. 25 (1998) 4–12.
[71] G. Zhu, L. Song, S.J. Lippard, Cancer Res. 73 (2013) 4451–4460.
[72] S.M. Cohen, S.J. Lippard, Prog. Nucleic Acid Res. Mol. Biol. 67 (2001) 93–130.
[73] S. Hann, G. Koellensperger, Z. Stefanka, G. Stingeder, M. Furhacker, W. Buchberger, R.M. Mader, J. Anal. At. Spectrom. 18 (2003) 1391–1395.
[74] F. Liu, J. Suryadi, U. Bierbach, Chem. Res. Toxicol. 28 (2015) 2170–2178.
[75] R.C. Todd, S.J. Lippard, Metallomics 1 (2009) 280–291.
[76] M.J. Cleare, J. Hoeschele, Platin. Met. Rev. 17 (1973) 2–13.
[77] D. Rehder, J. Inorg. Biochem. 147 (2015) 25–31.
[78] A. Dornyei, S. Marcao, J. Costa Pessoa, T. Jakusch, T. Kiss, Eur. J. Inorg. Chem. 18 (2006) 3614–3621.
[79] T. Kiss, A. Odani, Bull. Chem. Soc. Jpn. 80 (2007) 1691–1702.
[80] D.C. Crans, P.M. Ehde, P.K. Shin, L. Pettersson, J. Am. Chem. Soc. 113 (1991) 3728–3736.
[81] K. Elvingson, D.C. Crans, L. Pettersson, J. Am. Chem. Soc. 119 (1997) 7005–7012.
[82] K. Elvingson, A.D. Keramidas, D.C. Crans, L. Pettersson, Inorg. Chem. 37 (1998) 6153–6160.
[83] V.M. Nurchi, G. Crisponi, I. Villaescusa, Coord. Chem. Rev. 254 (2010) 2181–2192.
[84] J. Szpunar, Analyst 130 (2005) 442–465.
[85] K.J. Powell, P.L. Brown, R.H. Byrne, T. Gajda, G. Hefter, S. Sjoberg, H. Wanner, Pure Appl. Chem. 79 (2007) 895–950.
[86] D. Schluter, Trends Ecol. Evol. 16 (2001) 372–380.
[87] L.C. Konigsberger, E. Konigsberger, P.M. May, G.T. Hefter, J. Inorg. Biochem. 78 (2000) 175–184.
[88] S. Caroli, Element Speciation in Bioinorganic Chemistry, 135 (1996), John Wiley & Sons, 1996 138–186.
[89] R.L. McNaughton, A.R. Reddi, M.H.S. Clement, A. Sharma, K. Barnese, L. Rosenfeld, E.B. Gralla, J.V. Valentine, V.C. Culotta, B.M. Hoffman, Proc. Nat Acad. Sci. 107 (2010) 15335–15339.
[90] Y. Kondo, S. Takeda, K. Furuya, Mar. Chem. 134 (2012) 18–28.
[91] C.D. Pereira, J.G. Techy, E.M. Ganzarolli, S.P. Quinaia, J. Environ. Monit. 14 (2012) 1559–1564.
[92] G. Crisponi, A. Dean, V. Di Marco, J.I. Lachowicz, V.M. Nurchi, M. Remelli, A. Tapparo, Anal. Bioanal. Chem. 405 (2013) 585–601.
[93] G. Crisponi, V.M. Nurchi, M. Crespo-Alonso, L. Toso, Curr. Med. Chem. 19 (2012) 2794–2815.
[94] P.M. May, D. Rowland, E. Konigsberger, G. Hefter, Talanta 81 (2010) 142–148.
[95] R. Lobinski, J.S. Becker, H. Haraguchi, B. Sarkar, Pure Appl. Chem. 82 (2010) 493–504.
[96] M. Aureliano, D.C. Crans, J. Inorg. Biochem. 103 (2009) 536–546.
[97] Y. Yoshikawa, H. Sakurai, D.C. Crans, G. Micera, E. Garribba, Dalton Trans. 43 (2014) 6965–6972.
[98] J.C. Pessoa, S. Etcheverry, D. Gambino, Coord. Chem. Rev. 301 (2015) 24–48.
[99] M. Hu, P.P. Coetzee, S. Afr. J. Chem. 60 (2015) 113–117.
[100] Z. Chen, G. Owens, R. Naidu, Anal. Chim. Acta 585 (2007) 32–37.
[101] M. Melchior, S. Rettig, B. Liboiron, K. Thompson, V. Yuen, J. McNeil, C. Orvig, Inorg. Chem. 40 (2009) 4686–4690.
[102] P. Buglyo, D.C. Crans, E.M. Nagy, R.L. Lindo, L.Q. Yang, J.J. Smee, W.Z. Jin, L.H. Chi, M.E. Godzala, G.R. Willsky, Inorg. Chem. 44 (2005) 5416–5427.
[103] M. Li, W. Ding, J.J. Smee, B. Baruah, G.R. Willsky, D.C. Crans, Biometals 22 (2009) 895–905.
[104] J. Krzystek, J. Telser, J. Li, M. Subramanian, Inorg. Chem. 54 (2015) 9040–9045.
[105] N.D. Chasteen, L. Berliner, J. Reuben (Eds.), Vanadyl(IV) EPR Spin Probes Inorganic and Biochemical Aspects, Biological Magnetic Resonance, Vol. 3, Plenum Press, New York 1981, pp. 53–119.
[106] Environmental Analysis by Electrochemical Sensors and Biosensors, Springer, (2015) 841–854.
[107] F. DSouza, P. Boulas, A.M. Aukauloo, R. Guilard, M. Kisters, E. Vogel, K.M. Kadish, J. Phys. Chem-US 98 (1994) 11885–11891.
[108] A. Levina, A.L. McLeod, P.A. Lay, Chem. Eur. J. 20 (2014) 12056–12060.
[109] R.W. Strange, M.C. Feiters, Curr. Opin. Struct. Biol. 18 (2008) 609–616.
[110] J.B. Aitken, A. Levina, P.A. Lay, Curr. Top. Med. Chem. 11 (2011) 553–571.
[111] Y. Wang, H. Wang, H. Li, H. Sun, Dalton Trans. 44 (2015) 437–447.
[112] J. Krzystek, A. Ozarowski, J. Telser, D.C. Crans, Coord. Chem. Rev. 301 (2015) 123–133.
[113] D. Rehder, Bull. Mag. Reson. 4 (1982) 33–83.
[114] L. Pettersson, B. Hedman, I. Andersson, N. Ingri, Chem. Scr. 22 (1983) 254–264.
[115] N.D. Chasteen, Copper, Molybdenum, and Vanadium in Biological Systems, Springer, (1983) 105–138.
[116] M.J. Gresser, A.S. Tracey, J. Am. Chem. Soc. 107 (1985) 4215–4220.
[117] D.C. Crans, M.L. Tarlton, C.C. McLauchlan, Eur. J. Inorg. Chem. 27 (2014) 4450–4468.
[118] J. Krakowiak, D. Lundberg, I. Persson, Inorg. Chem. 51 (2012) 9598–9609.
[119] N. Chasteen, Vanadium in Biological Systems: Physiology and Biochemistry, Springer, (1990) 53–119.
[120] P. Caravan, L. Gelmini, N. Glover, F.G. Herring, H. Li, J.H. McNeill, S.J. Rettig, I.A. Setyawati, E. Shuter, Y. Sun, A.S. Tracey, V.G. Yuen, C. Orvig, J. Am. Chem. Soc. 117 (1995) 12759–12770.
[121] D.C. Crans, M. Mahroof-Tahir, A.D. Keramidas, Vanadium Compounds: Biochemical and Therapeutic Applications, Springer, (1995) 17–24.
[122] R. Ramirez, B. Casal, L. Utrera, E. Ruiz-Hitzky, J. Phys. Chem. 94 (1990) 8960–8965.
[123] R. Renirie, J.M. Charnock, C.D. Garner, R. Wever, J. Inorg. Biochem. 104 (2010) 657–664.
[124] G. Hanson, L. Berliner, High Resolution EPR: Applications to Metalloenzymes and Metals in Medicine, Vol. 28, Springer Science & Business Media, 2009 507–533.
[125] M.J. Pushie, I.J. Pickering, M. Korbas, M.J. Hackett, G.N. George, Chem. Rev. 114 (2014) 8499–8541.
[126] I. Goldwaser, D. Gefel, E. Gershonov, M. Fridkin, Y. Shechter, J. Inorg. Biochem. 80 (2000) 21–25.
[127] J. Li, G. Elberg, D.C. Crans, Y. Shechter, Biochemistry 35 (1996) 8314–8318.
[128] N.D. Chasteen, J.K. Grady, C.E. Holloway, Inorg. Chem. 25 (1986) 2754–2760.
[129] H.J. Thompson, N.D. Chasteen, L.D. Meeker, Carcinogenesis 5 (1984) 849–851.
[130] G.R. Willsky, D.A. Preischel, B.C. McCabe, Biophys. J. 45 (1984) A76.
[131] A. Levina, A.L. McLeod, A. Pulte, J.B. Aitken, P.A. Lay, Inorg. Chem. 54 (2015) 6707–6718.
[132] A. Levina, A.L. McLeod, L.E. Kremer, J.B. Aitken, C.J. Glover, B. Johannessen, P.A. Lay, Metallomics 6 (2014) 1880–1888.
[133] P. Frank, E.J. Carlson, R.M. Carlson, B. Hedman, K.O. Hodgson, J. Inorg. Biochem. 102 (2008) 809–823.
[134] J.C. Pessoa, I. Tomaz, Curr. Med. Chem. 17 (2010) 3701–3738.
[135] D.C. Horton, D. VanDerveer, J. Krzystek, J. Telser, T. Pittman, D.C. Crans, A.A. Holder, Inorg. Chim. Acta 420 (2014) 112–119.
[136] D.C. Crans, Comments Inorg. Chem. 16 (1994) 35–76.
[137] T.A.S. Brandao, A.C. Hengge, S.J. Johnson, J. Biol. Chem. 285 (2010) 15874–15883.
[138] T.A.S. Brandao, H. Robinson, S.J. Johnson, A.C. Hengge, J. Am. Chem. Soc. 131 (2009) 778–786.
[139] J.M. Messmore, R.T. Raines, Arch. Biochem. Biophys. 381 (2000) 25–30.
[140] A.G. Sostarecz, E. Gaidamauskas, S. Distin, S.J. Bonetti, N.E. Levinger, D.C. Crans, Chem.-Eur. J. 20 (2014) 5149–5159.
[141] X.G. Yang, X.D. Yang, L. Yuan, K. Wang, D.C. Crans, Pharm. Res. 21 (2004) 1026–1033.
[142] D. Rehder, J.C. Pessoa, C. Geraldes, M. Castro, T. Kabanos, T. Kiss, B. Meier, G. Micera, L. Pettersson, M. Rangel, A. Salifoglou, I. Turel, D.R. Wang, J. Biol. Inorg. Chem. 7 (2002) 384–396.
[143] K. Li, W. Li, Y. Ding, Y. Ye, Z. You, Russ. J. Coord. Chem. 41 (2015) 549–554.
[144] F.A. Cotton, G. Wilkinson, Advanced Inorganic Chemistry, Vol. 594, Wiley, New York, 1988.
[145] C.F. Harrington, R.C. Le Pla, G.D.D. Jones, A.L. Thomas, P.B. Farmer, Chem. Res. Toxicol. 23 (2010) 1313–1321.
[146] R.N. Bose, Mini-Rev. Med. Chem. 2 (2002) 103–111.
[147] D. Vasilchenko, S. Tkachev, I. Baidina, S. Korenev, Inorg. Chem. 52 (2013) 10532–10541.
[148] F. Berruges, E. Holler, Nucleic Acids Res. 19 (1991) 1483–1489.
[149] D. Wang, S.J. Lippard, Nat. Rev. Drug Discov. 4 (2005) 307–320.
[150] T. Boulikas, M. Vougiouka, Oncol. Rep. 10 (2003) 1663–1682.
[151] J. Reedijk, P. Lohman, Pharm. Weekbl. 7 (1985) 173–180.
[152] E. Wexselblatt, D. Gibson, J. Inorg. Biochem. 117 (2012) 220–229.
[153] S. Hann, A. Zenker, M. Galanski, T.L. Bereuter, G. Stingeder, B.K. Keppler, Fresenius J. Anal. Chem. 370 (2001) 581–586.
[154] T. Tam, S. Sturup, J. Ostergaard, U. Franzen, B. Gammelgaard, J. Anal. At. Spectrom. 26 (2011) 1466–1473.
[155] M.S. Robillard, M. Bacac, H. van den Elst, A. Flamigni, G.A. van der Marel, J.H. van Boom, J. Reedijk, J. Comb. Chem. 5 (2003) 821–825.
[156] Z. Stefanka, S. Hann, K. Lenz, G. Koellensperger, M. Fuerhacker, G. Stingeder, in: G. Holland, D.R. Bandura (Eds.), Plasma Source Mass Spectrometry: Current Trends and Future Developments, Royal Society of Chemistry Special Publications 2005, pp. 235–241.

[157] S. Gil, A. Carmona, G. Martínez-Criado, A. Leon, Y. Prezado, M. Sabes, Biol. Trace Elem. Res. 163 (2015) 177–183.
[158] Z. Yang, X.D. Hou, B.T. Jones, Appl. Spectrosc. Rev. 37 (2002) 57–88.
[159] P. Perego, J. Robert, Cancer Chemother. Pharmacol. 77 (2016) 5–18.
[160] K.R. Harrap, Cancer Treat. Rev. 12 (1985) 21–33.
[161] A. Zaniboni, F. Meriggi, J. Chemother. 17 (2005) 656–662.
[162] M. Fuertes, J. Castilla, C. Alonso, J. Prez, Curr. Med. Chem. 10 (2003) 257–266.
[163] Z.H. Siddik, Oncogene 22 (2003) 7265–7279.
[164] I. Bertini, Biological Inorganic Chemistry: Structure and Reactivity, University Science Books, 2007.
[165] N. Nagai, R. Okuda, M. Kinoshita, H. Ogata, J. Pharm. Pharmacol. 48 (1996) 918–924.
[166] A. Eastman, Pharmacol. Ther. 34 (1987) 155–166.
[167] W.J. van der Vijgh, Clin. Pharmacokinet. 21 (1991) 242–261.
[168] C.G. Van Kralingen, Antitumor Platinum Compounds: Synthesis, Structure and Biological Activity, University of Leiden, 1979 PhD Thesis.
[169] R.A. Alderden, M.D. Hall, T.W. Hambley, J. Chem. Educ. 83 (2006) 728–734.
[170] S.A. Wood, Geochim. Cosmochim. Acta 55 (1991) 1759–1767.
[171] I.I. Elding, I. Leden, Acta Chem. Scand. 20 (1966) 706–715.
[172] L. Elding, Inorg. Chim. Acta 20 (1976) 65–69.
[173] I.I. Eld
ing, I. Leden, Acta Chem. Scand. 20 (1966).
[174] S.A. Wood, B.W. Mountain, B.J. Fenlon, Econ. Geol. 84 (1989) 2020–2028.
[175] C. Lepre, S. Lippard, Nucleic Acids and Molecular Biology 4, Springer, 1990 9–38.
[176] M. Vaara, Microbiol. Rev. 56 (1992) 395–411.
[177] H. Hohmann, B. Hellquist, R. Vaneldik, Inorg. Chim. Acta 188 (1991) 25–32.
[178] Z. Stefanka, S. Hann, G. Koellensperger, G. Stingeder, J. Anal. At. Spectrom. 19 (2004) 894–898.
[179] M.D. Johnson, B.B. Lorenz, P.C. Wilkins, B.G. Lemons, B. Baruah, N. Lamborn, M. Stahla, P.B. Chatterjee, D.T. Richens, D.C. Crans, Inorg. Chem. 51 (2012) 2757–2765.
[180] F. Rolland, J. Winderickx, J.M. Thevelein, Trends Biochem. Sci. 26 (2001) 310–317.
[181] D. Simpson, Am. J. Physiol. –Renal. 244 (1983) F223–F234.
[182] C.G. Davis, I. Van Driel, D. Russell, M.S. Brown, J.L. Goldstein, J. Biol. Chem. 262 (1987) 4075–4082.
[183] M. Gutscher, A.-L. Pauleau, L. Marty, T. Brach, G.H. Wabnitz, Y. Samstag, A.J. Meyer, T.P. Dick, Nat. Methods 5 (2008) 553–559.
[184] D. Zhou, Y. Cong, Y. Qi, S. He, H. Xiong, Y. Wu, Z. Xie, X. Chen, X. Jing, Y. Huang, Biomater. Sci. 3 (2015) 182–191.
[185] G. Giaccone, Drugs 59 (2000) 9–17.
[186] M. Corte-Rodríguez, M. Espina, L.M. Sierra, E. Blanco, T. Ames, M. Montes-Bayon, A. Sanz-Medel, Biochem. Pharmacol. 98 (2015) 69–77.
[187] L. Galluzzi, L. Senovilla, I. Vitale, J. Michels, I. Martins, O. Kepp, M. Castedo, G. Kroemer, Oncogene 31 (2012) 1869–1883.
[188] L.P. Martin, T.C. Hamilton, R.J. Schilder, Clin. Cancer Res. 14 (2008) 1291–1295.
[189] S.-L. Yasin, A.J. Rainbow, Int. J. Oncol. 39 (2011) 719–726.
[190] A. Sawant, A. Kothandapani, A. Zhitkovich, R.W. Sobol, S.M. Patrick, DNA Repair 35 (2015) 126–136.
[191] B. Lippert, Cisplatin: Chemistry and Biochemistry of a Leading Anticancer Drug, John Wiley & Sons, 1999.
[192] S. Goto, T. Iida, S. Cho, M. Oka, S. Kohno, T. Kondo, Free Radic. Res. 31 (1999) 549–558.
[193] E.L. Lempers, J. Reedijk, Inorg. Chem. 29 (1990) 217–222.
[194] R. Pratibha, R. Sameer, P.V. Rataboli, D.A. Bhiwgade, C.Y. Dhume, Eur. J. Pharmacol. 532 (2006) 290–293.
[195] A.K. Godwin, A. Meister, P.J. O'Dwyer, C.S. Huang, T.C. Hamilton, M.E. Anderson, Proc. Natl. Acad. Sci. 89 (1992) 3070–3074.
[196] K.J. Barnham, M.I. Djuran, P. del SocorroMurdoch, J.D. Ranford, P.J. Sadler, Inorg. Chem. 35 (1996) 1065–1072.
[197] P.T. Daley-Yates, D.C. McBrien, Biochem. Pharmacol. 33 (1984) 3063–3070.
[198] N.A.G. dos Santos, M.A.C. Rodrigues, N.M. Martins, A.C. dos Santos, Arch. Toxicol. 86 (2012) 1233–1250.
[199] J.L. Miranda, L.C. Moura, R.A.S. San Gil, M.T.M. Cruz, A.C.O. Silva, A.A. Barbosa, Polyhedron 102 (2015) 313–320.
[200] D.A. Bender, J.R. Soc, Health 113 (1993) 275.
[201] B. Marescau, D.R. Deshmukh, M. Kocks, I. Possemiers, I.A. Qureshi, P. Wiechert, P.P. De Deyn, Metabolism 41 (1992) 526–532.
[202] A. Peaston, J. Maddison, Aust. Vet. J. 72 (1995) 76–77.
[203] S.J.S. Kerrison, P.J. Sadler, J. Chem. Soc. Chem. Commun. 23 (1977) 861–863.
[204] N.E. Madias, J.T. Harrington, Am. J. Med. 65 (1978) 307–314.
[205] E.G. Jones, http://www.cisplatin.org/treat.htm.
[206] R. Safaei, S.B. Howell, Crit. Rev. Oncol. Hematol. 53 (2005) 13–23.
[207] S. Ishida, J. Lee, D.J. Thiele, I. Herskowitz, Proc. Natl. Acad. Sci. 99 (2002) 14298–14302.
[208] S. Zhang, K.S. Lovejoy, J.E. Shima, L.L. Lagpacan, Y. Shu, A. Lapuk, Y. Chen, T. Komori, J.W. Gray, X. Chen, Cancer Res. 66 (2006) 8847–8857.
[209] K.S. Lovejoy, R.C. Todd, S. Zhang, M.S. McCormick, J.A. D'Aquino, J.T. Reardon, A. Sancar, K.M. Giacomini, S.J. Lippard, Proc. Natl. Acad. Sci. 105 (2008) 8902–8907.
[210] K. Kasahara, M. Fujimura, T. Bando, K. Shibata, H. Shirasaki, T. Matsuda, Br. J. Cancer 74 (1996) 1553.
[211] P.A. Andrews, S.C. Mann, H.H. Huynh, K.D. Albright, Cancer Res. 51 (1991) 3677–3681.
[212] P.-W. Cheng, S.-H. Liu, C.-J. Hsu, S.-Y. Lin-Shiau, Hear. Res. 205 (2005) 102–109.
[213] V. Calderone, A. Casini, S. Mangani, L. Messori, P.L. Orioli, Angew. Chem. Int. Ed. 45 (2006) 1267–1269.
[214] D. Esteban-Fernández, M. Montes-Bayón, E.B. González, M.G. Gomez, M. Palacios, A. Sanz-Medel, J. Anal. At. Spectrom. 23 (2008) 378–384.
[215] J.W. Jonker, A.H. Schinkel, J. Pharmacol. Exp. Ther. 308 (2004) 2–9.
[216] K.G. Chen, R.D. Leapman, G. Zhang, B. Lai, J.C. Valencia, C.D. Cardarelli, W.D. Vieira, V.J. Hearing, M.M. Gottesman, J. Natl. Cancer Inst. 101 (2009) 1259–1271.
[217] U. Gradhand, R.B. Kim, Drug Metab. Rev. 40 (2008) 317–354.
[218] A.R. Timerbaev, K.S. Aleksenko, K. Polec-Pawlak, R. Ruzik, O. Semenova, C.G. Hartinger, S. Oszwaldowski, M. Galanski, M. Jarosz, B.K. Keppler, Electrophoresis 25 (2004) 1988–1995.
[219] J. Reedijk, Chem. Rev. 99 (1999) 2499–2510.
[220] O. Pinato, C. Musetti, N.P. Farrell, C. Sissi, J. Inorg. Biochem. 122 (2013) 27–37.
[221] J. Neault, H. Tajmir-Riahi, BBA-Protein Struct. M. 1384 (1998) 153–159.
[222] V.J. Da Silva, L.A.S. Costa, H.F. Dos Santos, Int. J. Quantum Chem. 108 (2008) 401–414.
[223] M. Hahn, M. Kleine, W.S. Sheldrick, J. Biol. Inorg. Chem. 6 (2001) 556–566.
[224] U. Kragh-Hansen, V.T.G. Chuang, M. Otagiri, Biol. Pharm. Bull. 25 (2002) 695–704.
[225] D. Hagrman, J. Goodisman, J.C. Dabrowiak, A.-K. Souid, Drug Metab. Dispos. 31 (2003) 916–923.
[226] P.M. Clarkson, E.S. Rawson, Crit. Rev. Food Sci. Nutr. 39 (1999) 317–328.
[227] T. Boulikas, Expert Opin. Investig. Drug 18 (2009) 1197–1218.
[228] M. Fantini, L. Gianni, C. Santelmo, F. Drudi, C. Castellani, A. Affatato, M. Nicolini, A. Ravaioli, Chemother. Res. Pract. 2011 (2010) 1–7.
[229] G.P. Stathopoulos, T. Boulikas, M. Vougiouka, G. Deliconstantinos, S. Rigatos, E. Darli, V. Viliotou, J.G. Stathopoulos, Oncol. Rep. 13 (2005) 589–595.
[230] N. Mylonakis, A. Athanasiou, N. Ziras, J. Angel, A. Rapti, S. Lampaki, N. Politis, C. Karanikas, C. Kosmas, Lung Cancer 68 (2010) 240–247.
[231] T.C. Johnstone, N. Kulak, E.M. Pridgen, O.C. Farokhzad, R. Langer, S.J. Lippard, ACS Nano 7 (2013) 5675–5683.
[232] G. Stathopoulos, T. Boulikas, J. Drug Deliv. 2012 (2011) 1–10.
[233] D.R. Gandara, W.A. Nahhas, M.D. Adelson, S.M. Lichtman, E.S. Podczaski, S. Yanovich, H.D. Homesley, P. Braly, P.S. Ritch, S.R. Weisberg, J. Clin. Oncol. 13 (1995) 490–496.
[234] C.M. Sorenson, A. Eastman, Cancer Res. 48 (1988) 4484–4488.
[235] I. Arany, R.L. Safirstein, Semin. Nephrol. 23 (2003) 460–464.
[236] K.J. Harrington, Expert Opin. Investig. Drug 10 (2001) 1045–1061.
[237] G. Karpathiou, E. Argiana, A. Koutsopoulos, M.E. Froudarakis, Oncology 73 (2008) 426–429.
[238] M.E. Froudarakis, A. Pataka, P. Pappas, S. Anevlavis, E. Argiana, M. Nikolaidou, G. Kouliatis, S. Pozova, M. Marselos, D. Bouros, Cancer 113 (2008) 2752–2760.
[239] T. Boulikas, Oncol. Rep. 12 (2004) 3–12.
[240] G.P. Stathopoulos, T. Boulikas, M. Vougiouka, S.K. Rigatos, J.G. Stathopoulos, Oncol. Rep. 15 (2006) 1201–1204.
[241] S. Anevlavis, A. Pataka, G. Kouliatsis, Eur. Respir. J. 32 (2008) 762s.
[242] H. Choy, Expert. Rev. Anticancer. Ther. 6 (2006) 973–982.
[243] A. Bhargava, U.N. Vaishampayan, Expert Opin. Investig. Drug 18 (2009) 1787–1797.
[244] M.D. Hall, H.L. Daly, J.Z. Zhang, M. Zhang, R.A. Alderden, D. Pursche, G.J. Foran, T.W. Hambley, Metallomics 4 (2012) 568–575.
[245] M.D. Hall, T.W. Hambley, Coord. Chem. Rev. 232 (2002) 49–67.
[246] L.R. Kelland, Expert Opin. Investig. Drug 9 (2000) 1373–1382.
[247] A. Vaisman, S.E. Lim, S.M. Patrick, W.C. Copeland, D.C. Hinkle, J.J. Turchi, S.G. Chaney, Biochemistry 38 (1999) 11026–11039.
[248] D. Fink, S. Nebel, S. Aebi, H. Zheng, B. Cenni, A. Nehmé, R.D. Christen, S.B. Howell, Cancer Res. 56 (1996) 4881–4886.
[249] J.A. Platts, G. Ermondi, G. Caron, M. Ravera, E. Gabano, L. Gaviglio, G. Pelosi, D. Osella, J. Biol. Inorg. Chem. 16 (2011) 361–372.
[250] P. Gramatica, E. Papa, M. Luini, E. Monti, M.B. Gariboldi, M. Ravera, E. Gabano, L. Gaviglio, D. Osella, J. Biol. Inorg. Chem. 15 (2010) 1157–1169.
[251] A. Levina, A.I. McLeod, S.J. Gasparini, A. Nguyen, W.M. De Silva, J.B. Aitken, H.H. Harris, C. Glover, B. Johannessen, P.A. Lay, Inorg. Chem. 54 (2015) 7753–7766.
[252] M. Garner, J. Reglinski, W.E. Smith, J. McMurray, I. Abdullah, R. Wilson, J. Biol. Inorg. Chem. 2 (1997) 235–241.
[253] D. Griffith, M.P. Morgan, C.J. Marmion, Chem. Commun. 44 (2009) 6735–6737.
[254] A. Coghlan, New Sci. 206 (2010) 6–7.
[255] W. Zhang, S.-L. Zhang, X. Hu, K.Y. Tam, Int. J. Biol. Sci. 11 (2015) 1390–1400.
[256] D. Gibson, Dalton Trans. 45 (2016) 12983–12991.
[257] J.-Q. Zhang, K. Li, K.-M. Jiang, Y.-W. Cong, S.-P. Pu, X.-G. Xie, Y. Jin, J. Lin, RSC Adv. 6 (2016) 17074–17082.
[258] A.V. Klein, T.W. Hambley, Chem. Rev. 109 (2009) 4911–4920.